2019

GPCR Activation of the G Protein-Gated Inward-Rectifier Potassium Channel

Kouki Touhara

GPCR ACTIVATION OF THE G PROTEIN-GATED INWARD-RECTIFIER POTASSIUM CHANNEL

A Thesis Presented to the Faculty of

The Rockefeller University

in Partial Fulfillment of the Requirements for

the degree of Doctor of Philosophy

by

Kouki Touhara

June 2019

GPCR ACTIVATION OF THE G PROTEIN-GATED INWARD-RECTIFIER POTASSIUM CHANNEL

Kouki Touhara, Ph.D.

The Rockefeller University 2019

Heart rate is tightly regulated by the combined effects of the sympathetic and parasympathetic branches of the autonomic nervous system. These two branches control heart rate by stimulating different G protein-coupled receptors (GPCRs), which in turn activate ion channels that modify the electrical properties of cardiac pacemaker cells. Sympathetic stimulation accelerates heart rate through activation of beta-adrenergic receptors (βARs), which open excitatory ion channels through the stimulatory G protein ($G\alpha_s$) pathway. Parasympathetic stimulation slows heart rate through activation of the muscarinic acetylcholine receptor M_2 (M2Rs), which inhibits the effect of sympathetic stimulation through the inhibitory G protein ($G\alpha_i$) pathway. M2Rs also release G protein beta-gamma subunits ($G\beta\gamma$), which slow heart rate by activating G protein-gated inward-rectifier potassium (GIRK) channels. Interestingly, βARs also release the very same free $G\beta\gamma$, but GIRK is not activated. The molecular mechanism underlying this specificity is poorly characterized.

What is the molecular basis behind signaling specificity? It has been proposed that GIRK channels form a macromolecular supercomplex with $G\alpha_i$-coupled receptors and G proteins, allowing released $G\beta\gamma$ to bind to and activate GIRK by proximity. However the evidence for the existence of the complex remains controversial. In the first part of my thesis, I challenge the supercomplex hypothesis by providing three experimental sets against the theory. First, GIRK

co-localization with GPCRs shows no preference for M2Rs over β2ARs. Second, β2ARs do not activate GIRK channels even when they are co-localized. Third, neither $G\alpha_{i1}$ nor G protein heterotrimers functionally interact with purified GIRK1/4 channels in the planar lipid bilayer system. I conclude that protein co-localization is not the underlying mechanism to explain why GIRK channels are specifically activated by $G\alpha_i$-coupled receptors.

I then set out to determine the molecular basis behind signaling specificity. Using electrophysiological technologies and bioluminescent resonance electron transfer (BRET) assays, I show that M2Rs catalyze release of Gβγ subunits at higher rates than β2ARs, generating higher Gβγ concentrations that activate GIRK and regulate other targets of Gβγ. The higher rate of Gβγ release is attributable to a faster GPCR-G protein association rate in M2Rs compared to β2ARs. I conclude that the activity of GIRK channels is simply determined by the efficiency of Gβγ release from GPCRs. Physiologically, only $G\alpha_i$-coupled receptors can provide sufficient concentration of Gβγ to activate GIRK channels.

In the second part of my thesis, I present my work on the functional characterization of Gβγ and Na^+ regulation of two cardiac GIRK channels, GIRK1/4 hetero-tetramers and GIRK4 homo-tetramers. It is known that cardiac GIRK channels are composed of GIRK1/4 hetero-tetramers and GIRK4 homo-tetramers. However little is known about the functional difference between the two channels. Using purified proteins and the planar lipid bilayer system, I find that Na^+ binding increases Gβγ affinity in GIRK4 homo-tetramers and thereby increases the GIRK4 responsiveness to G protein stimulation. GIRK1/4 hetero-tetramers are not activated by Na^+, but rather are in a permanent state of high responsiveness to Gβγ, suggesting that the GIRK1 subunit functions like a GIRK4 subunit with Na^+ permanently bound.

To my mentors, Roderick MacKinnon and David Gadsby.

ACKNOWLEDGEMENTS

Rod, I sincerely thank you for all that you have shared with me. You have always been supportive and allowed me to try anything I wanted. I have been always inspired by your ideas. These ideas are always crazy, and sound impossible. But you have been made the impossible possible, which led to great scientific discoveries. I was very fortunate that I could pursue science with you and with the greatest scientists in your lab.

I have learned electrophysiology in David Gadsby's lab in my first rotation. Since then David is my mentor and also the best friend. Friday night discussion with London Pride has been a lot of fun. Your oysters are the world's best oysters for sure. I sincerely thank you for everything you have done for me, and I hope you could give me another Ph.D. in shucking oysters.

Throughout my graduate life, I have been supported by many people in MacKinnon lab. I would like to thank Weiwei for working with me and sharing your ideas. It has been always fun and inspiring to discuss with you. Many thanks to Eunyong Park. Your harsh comments were extremely helpful. I would like to thank Chia-Hsueh Lee, Ji Sun, and Jon Whicher for advices on my manuscripts and thesis. I also enjoyed being your neighborhood in the lab. My thanks to Josefina for your advices as a graduate student in the lab. I would like to thank Xiao, Ernie, Emily, Ken, Steve, Rich, Zhenwei, and everyone who spent some time with me in the lab. Everyone contributed to my work and I greatly appreciate all of you.

I want to thank Jue Chen and Chen lab members for all your help and advices.

Thanks to Vanessa Ruta, Tarun Kapoor, and Andrew Kruse for their time and attention as members of my thesis committee.

I would like to thank Andrew Siliciano for assistance with BRET experiments.

Thanks to staffs in The Bio-Imaging Resource Center and The High-Throughput Screening Resource Centers.

Many thanks to RU Dean's Office. Especially I appreciate Marta for her help on my tax issues. If I were asked what was the toughest moment in my Ph.D., I would definitely say it was tax.

Thanks to my friends, especially members of Kant, and Team Radiators/Matsui.

I would like to thank Japan Student Services Organization (JASSO) for financial supports.

Lastly, I would like to greatly appreciate my family. Your supports have been extremely helpful.
ありがとう。これからもよろしく。

TABLE OF CONTENTS

LIST OF FIGURES

LIST OF TABLES

CHAPTER 1: INTRODUCTION

Our internal organs continuously function through the autonomous nervous system. The heart, one of the most important organs, pumps blood via the circulatory system, and supplies nutrition and oxygen to the tissues of the body. Loss of heart function for three minutes decreases patient survival rates by 50% and thus it is not surprising that the leading cause of death in North America and East Asia is cardiovascular disease (Lozano et al. 2012).

The heart is a muscular organ, which continuously contracts according to the spontaneous pacemaker activity of the sinoatrial node (SAN) cells. SAN cells are located in the wall of the right atrium and the generated electrical impulses travel down the electrical conduction system, causing heart contraction. Therefore, the spontaneous action potential frequency of SAN cells governs the rhythm of the heartbeat (Irisawa et al, 1993).

The action potential frequency of SAN cells is tightly regulated by the combined effects of two functional units of the autonomic nervous system, the sympathetic and parasympathetic nervous system (Anzola and Rushmer, 1956; Rayner and Weatherall, 1959; DiFrancesco, 1993). When we are mentally or physically excited, sympathetic neurons convey the electrical signal

from the brain to the sympathetic neuromuscular junction, and release a sympathetic neurotransmitter, norepinephrine. On the other hand when we are at rest, parasympathetic neurons convey the electrical signal from the brain to the parasympathetic neuromuscular junction, and release a parasympathetic neurotransmitter, acetylcholine. Released norepinephrine and acetylcholine bind to and activate different subtypes of G protein-coupled receptors (GPCRs) expressed on the plasma membrane of SAN cells. The subtype of GPCRs stimulated by norepinephrine accelerate the spontaneous action potential frequency of SAN cells, and the subtype of GPCRs stimulated by acetylcholine slow it down by activating or inhibiting distinct kinds of cardiac ion channels (Brodde and Michel, 1999).

In this chapter, I will first discuss how cardiac ion channels generate spontaneous action potentials. I will introduce G protein-coupled receptors and how they regulate cardiac ion channels upon sympathetic and parasympathetic stimulation. Then I will introduce the G protein-gated inward-rectifier potassium (GIRK) channel from a biophysical and cell biological perspective. Finally, I will introduce the aims of my research on the cardiac GIRK channel.

1.1 CARDIAC ION CHANNELS AND SPONTANEOUS ACTION POTENTIALS

The interior of cells is separated from the outside environment by the cell membrane, which consists of a lipid bilayer with embedded membrane proteins. The cell membrane is selectively permeable. Hydrophobic molecules can diffuse through the lipid bilayer whereas large polar molecules and ions cannot. In the cardiac cell membrane, activities of Na^+/K^+-ATPase, Ca^{2+}-pumps, and Na^+/Ca^{2+} exchangers form an electrochemical gradient where high extracellular Na^+ (~145 mM outside vs ~20 mM inside the cell), high intracellular K^+ (~5.4 mM outside vs ~150 mM inside the cell), and high extracellular Ca^{2+} (~2 mM outside vs 0.1 μM inside) are present (Albers et al, 1967; Barry and Bridge, 1993; Bers et al, 2003). Ion channels are pore forming membrane proteins, allowing those ions to pass through the membrane according to the ionic concentration gradient. The cell membrane potentials are determined by the concentrations of ions inside and outside the cell, and the permeability of the cell membrane to ions through ion channels (Hodgkin and Huxley, 1952).

Pacemaker action potentials are divided into three phases, and four major subtypes of ion channels, hyperpolarization-activated nucleotide-gated channels (HCN channels), voltage-gated calcium channels (Cav channels), delayed rectifier potassium channels (Kv channels), and inward rectifier-potassium channels (Kir channels) play central roles in each phase of an action potential (Fig 1.1). During Phase 4, HCN channels are activated by membrane hyperpolarization, which increases Na^+ conductance of the membrane and hence causes membrane depolarization (Brown et al, 1979). Upon membrane depolarization Cav channels are activated, which rapidly increases Ca^{2+} conductance of the membrane and causes acute depolarization (Phase 0) (Irisawa et al, 1993). Kv channels are also activated by membrane depolarization, however, their activation is slower than that of Cav channels. Therefore, Kv channels slowly start to increase K^+

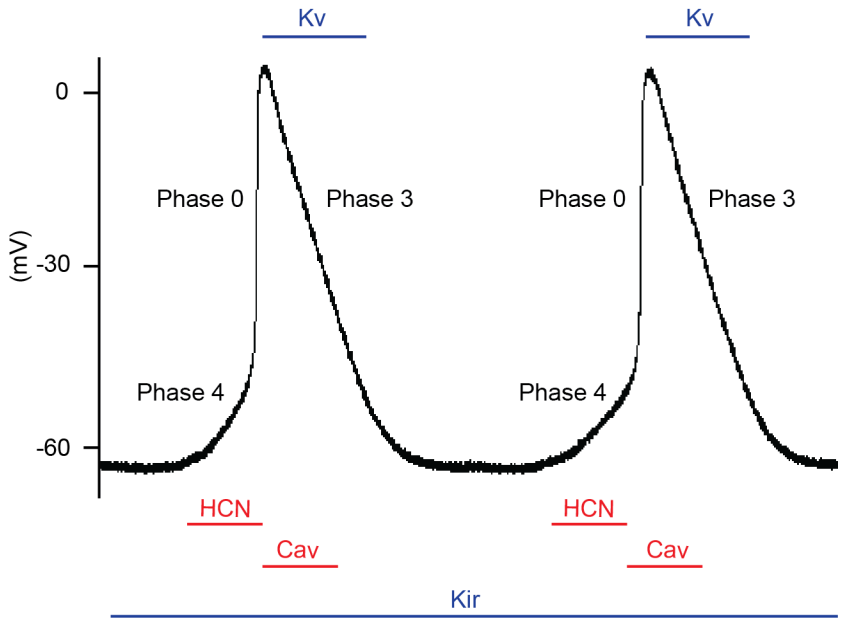

Figure 1.1. Schematic of cardiac pacemaker action potentials. Ion channels contributing to membrane depolarization are represented as red, and those contributing to the membrane hyperpolarization are represented as blue. Pacemaker action potentials can be divided into three phases. At Phase 4, hyperpolarization-activated nucleotide channels (HCN) are activated due to the low membrane potential, which increases Na^+ conductance of the membrane and hence causes membrane depolarization. Membrane depolarization activates voltage-gated calcium channels (Cav), which rapidly depolarize the membrane at Phase 0. Membrane depolarization also causes delayed activation of voltage-gated potassium channels (Kv), which repolarize the membrane at Phase 3. Membrane repolarization activates HCN channels again, and cycle is spontaneously repeated. There is a background K^+ conductance due to the presence of inward-rectifier potassium channels (Kir), which controls the baseline membrane potential.

conductance and repolarize the membrane (Phase 3) (Schmitt et al, 2014). Once the cell membrane is completely repolarized, HCN channels are again activated and the cycle is spontaneously repeated. There is a prominent background K^+ conductance due to the presence of Kir channels (Ito et al, 1994; Schmitt et al, 2014). Increase of the background Kir current lowers the baseline membrane potential, lengthening the interval between spontaneous action potentials (Irisawa et al, 1993; Schmitt et al, 2014).

1.2 G PROTEIN-COUPLED RECEPTORS

G protein-coupled receptors (GPCRs), also known as seven-transmembrane domain receptors, convert an extracellular hormonal signal into intracellular G protein signaling, which directs specific cellular responses. G proteins are composed of three subunits, G protein alpha subunits (Gα), G protein beta subunits (Gβ), and G protein gamma subunits (Gγ). Gβ and Gγ tightly bind to each other and function as a Gβγ subunit. Free Gβγ attaches to the inner surface of the membrane with its lipid anchor, and targets downstream messengers (Wedegaertner et al, 1995). Gα contains the GTPbinding domain. When bound to GDP, Gα associates with Gβγ to form the G protein heterotrimer (Wall et al, 1995; Lambright et al, 1996; Hillenbrand et al, 2015). When bound to GTP, Gα becomes active, diffuses on the membrane with its lipid anchor, and targets downstream messengers (Wedegaertner et al, 1995, Oldham and Hamm, 2006; Sprang et al, 2007; Cabrera-vera et al, 2008).

GPCRs catalyze GDP/GTP exchange to promote G protein activation. The resting state of GPCRs and GDP-bound G protein heterotrimers (Gα(GDP)βγ) randomly interact with each other on the membrane (Sungkaworn et al, 2017). Agonist binding to GPCRs induces a

conformational change in the receptor that promotes binding of Gα(GDP)βγ (Rasmussen et al, 2011; Hilger et al, 2018). The receptor accelerates removal of GDP from the Gα, which allows intracellular GTP to bind. The GTP-bound Gα (Gα(GTP)) and Gβγ then dissociate from the receptor (Fig 1.2A). Dissociated Gα(GTP) and Gβγ diffuse on the inner surface of the membrane and bind to their effectors. While at the same time, dissociated Gα(GTP) hydrolyzes GTP, which allows it to re-associate with Gβγ and thus convert back to Gα(GDP)βγ.

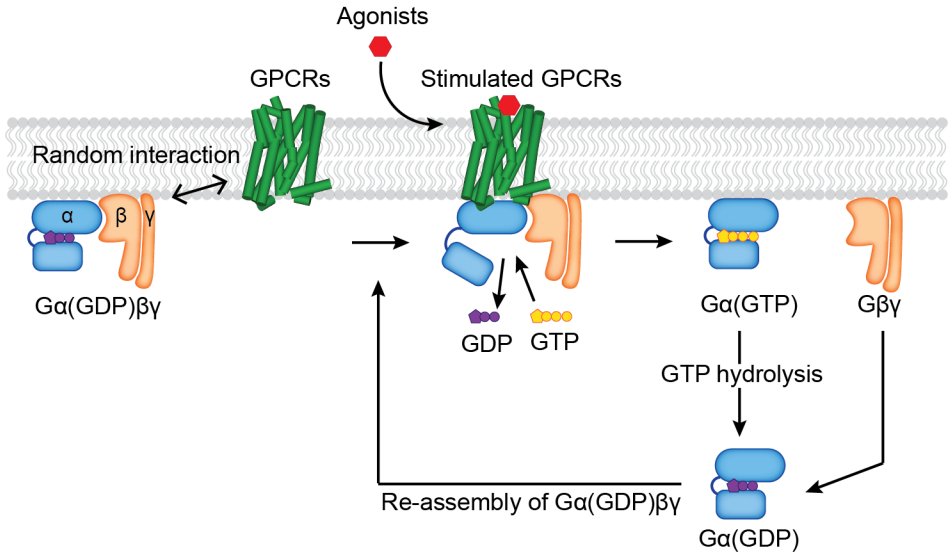

Figure 1.2. Schematic representation of GPCR signal transduction. The resting state of GPCRs and G protein heterotrimers, (Gα(GDP)βγ), diffuse in the membrane and randomly interact with each other. Upon agonist stimulation, activated receptor couples to Gα(GDP)βγ, which triggers nucleotide exchange followed by dissociation of Gα(GTP) and Gβγ subunits. Dissociated Gα(GTP) and Gβγ diffuse on the inner surface of the membrane with their lipid anchors and bind to their effectors. Dissociated Gα(GTP) hydrolyzes GTP, and re-associates with Gβγ to form a Gα(GDP)βγ again.

1.3 AUTONOMIC REGULATION OF CARDIAC SPONTANEOUS ACTION POTENTIALS

Different GPCRs preferentially couple to different G proteins, which are classified into four families: $G\alpha_s$, $G\alpha_i$, $G\alpha_q$, and $G\alpha_{12}$ (Syrovatkina et al, 2017). In cardiac pacemaker cells, $G\alpha_s$-coupled beta-adrenergic receptors (βARs) and $G\alpha_i$-coupled muscarinic acetylcholine receptors M2 (M2Rs) control cardiac ion channel activity and thus play central roles in autonomic regulation of the heart (Fig 1.3 and 1.4) (Breitwieser and Szabo, 1985; Irisawa et al, 1993; Brodde and Michel, 1999; Gordon et al, 2015).

Upon sympathetic stimulation, released norepinephrine binds to βARs. Activated βARs couple to stimulatory G protein heterotrimers, and $G\alpha_s$(GTP) and Gβγ are released. Released $G\alpha_s$(GTP) binds to adenylyl cyclase (AC), which catalyzes the conversion of ATP to cAMP, which directly binds to and activates HCN channels (DiFrancesco and Tortora, 1991; Simonds, 1999). Activation of HCN channels increases the pacemaker action potential frequency by accelerating the Phase 4 (Fig 1.1). cAMP also activates protein kinase A (PKA), which phosphorylates and thereby activates Cav channels, resulting in further acceleration of the pacemaker spontaneous action potential frequency (Fig 1.3) (Harvey and Hell, 2013).

Upon parasympathetic stimulation, released acetylcholine binds to M2Rs. Activated M2Rs couple to inhibitory G protein heterotrimers, and $G\alpha_i$(GTP) and Gβγ are released. Released $G\alpha_i$(GTP) inhibits ACs, slowing down the spontaneous action potential frequency (Taussig et al, 1993; Simonds, 1999; Harvey and Belevych, 2003). Furthermore, released Gβγ directly binds to and activates G protein-gated inward-rectifier potassium (GIRK) channels (Sakmann et al, 1983; Soejima and Noma, 1984; Logothetis et al, 1987; Wickman et al, 1994; Krapavinsky et al, 1995). Activation of GIRK channels shifts the resting membrane potential of

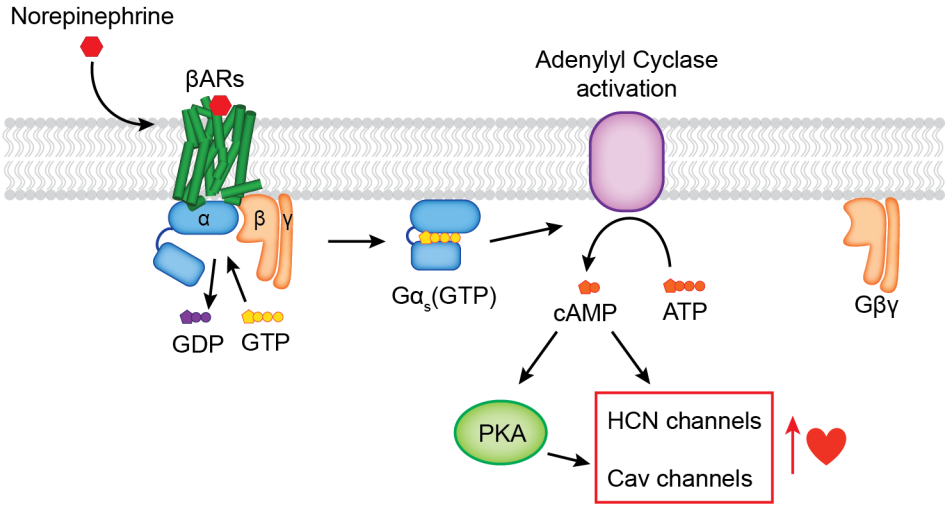

Figure 1.3. Schematic representation of adrenergic GPCR signal transduction in cardiac pacemaker cells. Upon sympathetic stimulation, norepinephrine is released and binds to beta-adrenergic receptors (βARs) expressing on the surface of the pacemaker cell membrane. βARs preferentially couple to stimulatory G protein heterotrimers ($G\alpha_s(GDP)\beta\gamma$), and $G\alpha_s(GTP)$ and $G\beta\gamma$ are released from the βAR-$G\alpha_s(GDP)\beta\gamma$ complex. Released $G\alpha_s(GTP)$ directly binds to and activates adenylyl cyclase (AC). Activated ACs catalyze conversion of ATP to cAMP, which directly binds to and activates HCN channels. Activation of HCN channels increases Na^+ conductance of the membrane, resulting in acceleration of the heart. Intracellular cAMP also activates the protein kinase A (PKA), which phosphorylates and activates Cav channels, resulting in further acceleration of the heart.

pacemaker cells toward the equilibrium potential for K^+, lengthening the interval between pacemaker action potentials and thereby slowing the heartbeat (Fig 1.4) (Noma et al, 1979; DiFrancesco, 1993).

Of note, however, upon sympathetic stimulation βARs do not activate GIRK channels in cardiac pacemaker cells, even though they are known to liberate free Gβγ (Hein et al, 2006; Digby et al, 2009). Furthermore, in heterologous expression systems $G\alpha_i$-coupled GPCRs such as M2Rs can activate GIRK, whereas $G\alpha_s$-coupled GPCRs such as βARs do not (Lim et al, 1995; Leaney et al, 2000). Thus, GIRK channels seem to be able to differentiate free Gβγ based on its source and are only affected by those released from $G\alpha_i$-coupled GPCRs. The reason why GIRK channel opening is specific to $G\alpha_i$-coupled GPCR stimulation and not to $G\alpha_s$-coupled GPCR stimulation has remained a long-standing unsolved question in the field.

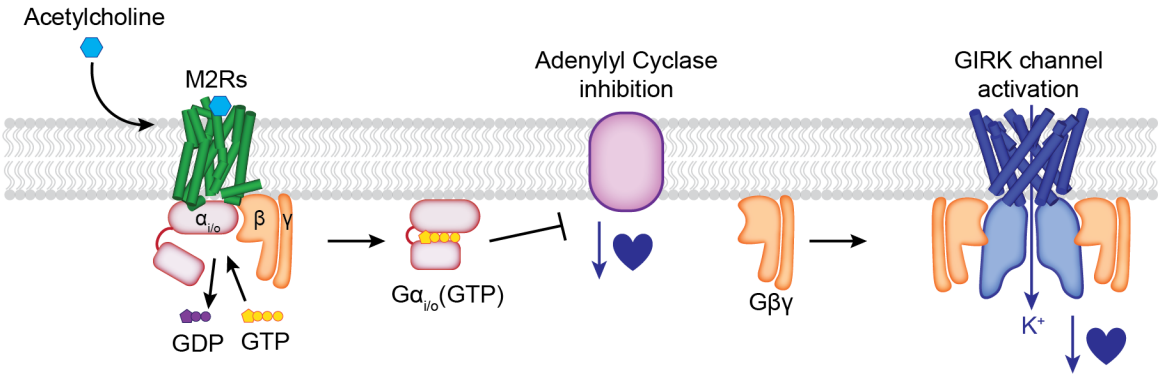

Figure 1.4. Schematic representation of cholinergic GPCR signal transduction in cardiac pacemaker cells. Upon parasympathetic stimulation, acetylcholine is released and binds to muscarinic 2 receptors (M2Rs) expressing on the surface of the pacemaker cell membrane. M2Rs preferentially couple to inhibitory G protein heterotrimers ($G\alpha_i(GDP)\beta\gamma$), and $G\alpha_i(GTP)$ and $G\beta\gamma$ are released from the M2R-$G\alpha_i(GDP)\beta\gamma$ complex. Released $G\alpha_i(GTP)$ directly binds to and inhibits adenylyl cyclase (AC), thereby competes with the adrenergic pathway. Released $G\beta\gamma$ directly binds to and activates G protein-activated inward-rectifier potassium channels (GIRK channels). Activation of GIRK channels shifts the resting membrane potential toward the equilibrium potential for K^+, lengthening the interval between pacemaker action potentials and thereby slowing the heart.

1.4 G PROTEIN-GATED INWARD-RECTIFIER POTASSIUM CHANNELS

GIRK channels are gated by direct binding of Gβγ, signaling lipids, and intracellular Na^+ (Huang et al., 1998; Sui et al., 1998; Logothetis and Zhang, 1999; Ho and Murrell-Lagnado, 1999a). As discussed above, $G\alpha_i$-coupled GPCRs release Gβγ and activate GIRK. Our lab has previously demonstrated that Gβγ and phosphatidylinositol 4,5-bisophosphate (PIP_2) are absolutely required to activate GIRK (Wang et al, 2014). Na^+ is not required but further activates the channel in the presence of both Gβγ and PIP_2 (Wang et al, 2014). Structural studies of GIRK2 channels have revealed these ligand-binding sites (Whorton and MacKinnon, 2011; Whorton and MacKinnon, 2013). Overall, four Gβγ, four PIP_2, and four Na^+ are able to bind to a single GIRK channel (Fig 1.5A and 1.5B). Gβγ binds at the interface between two GIRK subunits (Fig 1.5C) and induces a rotation of the cytoplasmic domains relative to the transmembrane domain, splaying the inner helices to open the channel. PIP_2 binds at the interface between the transmembrane and cytoplasmic domains, and Na^+ binds to the cytoplasmic domains (Fig 1.5D). Although these ligand-binding sites have been well characterized, there are several important unsolved questions. First, how many Gβγ are required to open the channel? Second, what is the affinity of Gβγ to GIRK? This affinity value has yet to be measured due to the difficulty in controlling G protein signaling in cells. Third, are the binding of Gβγ, PIP_2, and Na^+ thermodynamically coupled?

A final unsolved question regards the stoichiometry of GIRK channels. All GIRK channels are tetramers with each monomer containing one pore-forming domain. Mammals express four GIRK channel subunits (GIRK1-4), forming various homo-tetramers and hetero-tetramers. However, little is known about the functional differences between these homo-tetrameric and hetero-tetrameric GIRK channels.

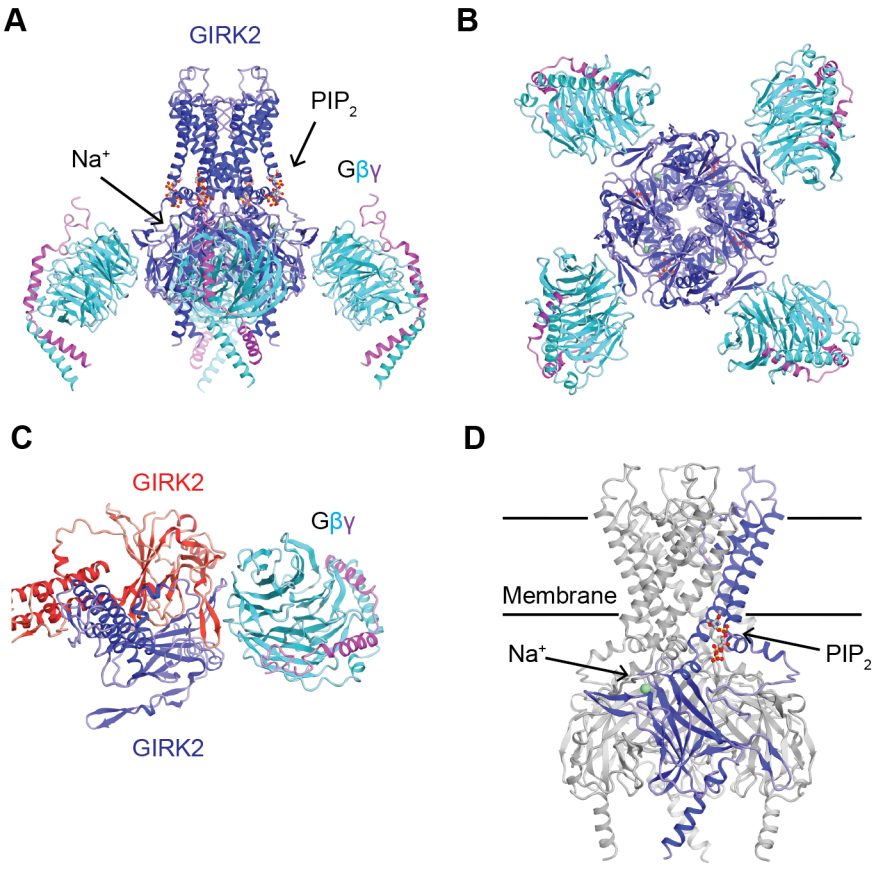

Figure 1.5. Crystal structures of the GIRK2 channel in complex with its physiological ligands. (A)(B) The side view (A) and bottom view (B) of the crystal structure of the GIRK2 channel in complex with Gβγ, PIP_2, and Na^+. Four Gβγ, PIP_2, and Na^+ are bound to a single GIRK2 homo-tetramer. (C) Gβγ binds to an interface between two cytoplasmic domains of GIRK2 subunits. Two different GIRK2 subunits are represented as red and blue, respectively. (D) The crystal structure of the GIRK2 channel in complex with PIP_2 and Na^+. One GIRK2 subunit is highlighted as blue, and the rest of them are represented as grey. PIP_2 and Na^+ are represented as spherical models. PIP_2 binds to the interface between the transmembrane domains and cytoplasmic domains. Na^+ binds to the cytoplasmic domains.

1.5 AIMS OF THESIS RESEARCH

GIRK activity is tightly regulated by GPCRs and their intracellular downstream signaling pathways. Although cellular electrophysiology experiments, biochemical analyses, and structural studies have yielded a rich understanding of GIRK channel function, there are two fundamental unsolved questions as to its mechanism of activation and regulation. First, why can $G\alpha_i$-coupled GPCRs activate the channel whereas $G\alpha_s$-coupled GPCRs cannot under physiological conditions? Second, what are the functional differences between two cardiac GIRK channels, GIRK1/4 hetero-tetramers and GIRK4 homo-tetramers? The aim of my thesis research is to answer these two questions.

Functional investigation of GIRK channels in living cells has many limitations, as it is difficult to control intracellular G protein signaling. Indeed, it took more than 20 years since the cloning of the *GIRK1* gene to reveal that GIRK channels require both $G\beta\gamma$ and PIP_2 for their activation (Kubo et al, 1993; Wang et al, 2014). A number of recent advances in biophysical and cell biological techniques allowed the investigation of G protein activation of GIRK channels in a more quantitative manner. First, our lab has established a method to reconstitute purified GIRK channels and G proteins into the isolated planar lipid bilayer system (Wang et al, 2014). This allows us to quantitatively describe the relationship between GIRK activity and ligand concentrations. Second, a new mammalian expression system has enabled us to work on wide ranges of mammalian membrane proteins (Goehring et al, 2014). Third, the super-resolution microscopy technique has been developed to localize the proteins in a cell with 20-100 nm resolution (Jones et al, 2011). Fourth, the bioluminescence resonance energy transfer (BRET) technique has been developed and applied to the field of GPCRs and G proteins, which enabled us to study GPCR-G protein interaction at higher sensitivity and time-resolution (Masuho et al,

2015). In my doctoral studies, I combined these state-of-the-art techniques and cellular electrophysiological techniques to investigate G protein activation of cardiac GIRK channels. From Chapter 2 to 4 I describe my work on signaling specificity between GPCRs and GIRK, and propose a simple kinetic explanation for specificity.

In Chapter 2, I re-evaluate signaling specificity between GPCRs and GIRK channels. I demonstrate that a single isolated cardiac pacemaker cell functionally expresses both M2Rs and β2ARs, however, only M2Rs can activate GIRK channels. Furthermore, I find that signaling specificity can be reconstituted in various heterologous expression systems including HEK, CHO, and insect Sf9 cells.

What is the molecular basis behind signaling specificity? It has been suggested that GIRK channels directly interact with inhibitory Gα and G protein heterotrimers, which led to the hypothesis that GIRK channels, G proteins, and $G\alpha_i$-coupled GPCRs form a macromolecular supercomplex (Peleg et al, 2002; Clancy et al, 2005). Such a supercomplex would allow Gβγ released from $G\alpha_i$-coupled GPCRs to immediately access and activate GIRK channels. In Chapter 3, I challenge this hypothesis with three experiments. First, I compare co-localization of GIRK channels with M2Rs or β2ARs by using super-resolution microcopy and find no difference in the degree of co-localization. Second I find that the proximity between GIRK channels and GPCRs does not explain signaling specificity. Third, I demonstrate that GIRK channels do not functionally interact with inhibitory Gα and G protein heterotrimers by using purified proteins and the planar lipid bilayer system.

In Chapter 4, I propose a new model explaining signaling specificity between GPCRs and GIRK channels. By combining electrophysiological and BRET techniques, I demonstrate that GIRK activity simply depends on Gβγ concentration in the membrane, and that $G\alpha_i$-coupled

GPCRs catalyze release of Gβγ at higher rates compared to $G\alpha_s$-coupled GPCRs. Therefore physiologically only $G\alpha_i$-coupled GPCRs can generate a high enough concentration of Gβγ to activate the channel.

In Chapter 5, I describe my work on quantitative analyses of ligand activation of two cardiac GIRK channels, GIRK1/4 hetero-tetramers and GIRK4 homo-tetramers. I first describe the purification and functional reconstitution of GIRK1/4 hetero-tetramers using a tandem affinity purification strategy. I then, in collaboration with postdoctoral fellow Weiwei Wang, develope a method to quantitatively study Gβγ activation of GIRK in the bilayer system. With this technique I demonstrate that the GIRK1 subunit potentiates Gβγ activation of GIRK1/4 channels. Finally, using mouse embryonic stem cell-derived cardiac myocytes, I show that cardiac GIRK channels are mostly composed of GIRK1/4 channels, not GIRK4 channels.

There has been major progress in understanding GPCR-activation of GIRK channels. However the molecular basis behind GPCR-GIRK signaling specificity has been controversial, and quantitative description of the relationship between GIRK activity and each ligand concentration has been lacking. My work has redefined the GPCR activation of GIRK channels in both cell biological and biophysical contexts and has provided a better understanding of ligand activation of homo-tetrameric and hetero-tetrameric GIRK. My work will contribute to our understanding of both GPCR-activation of GIRK and activation of the Gβγ pathway in general.

CHAPTER 2: SPECIFIC ACTIVATION OF GIRK CHANNELS BY $G\alpha_i$-COUPLED GPCRs BUT NOT BY $G\alpha_s$-COUPLED GPCRs

Extensive research on cardiac pacemaker cells identified two major GPCRs that regulate their electrical properties, M2Rs and βAR. M2Rs activate GIRK channels whereas βARs do not (DiFrancesco, 1993). However, somewhat surprisingly, there is no published demonstration of both autonomic responses in the same cardiac pacemaker cell.

In this chapter, I discuss my work on functional characterization of cardiac GIRK channels using acutely isolated murine SAN cells. I found that a single pacemaker cell exhibits both cholinergic and adrenergic responses, however GIRK channels are activated only by M2Rs. Furthermore, I successfully reconstituted signaling specificity between GPCRs and GIRK channels in various heterologous expression systems including mammalian and Sf9 insect cells.

2.1 Gβγ SPECIFICITY IN NATIVELY EXPRESSED GIRK CHANNELS

I isolated murine sinoatrial node (SAN) cells from adult mice and performed whole-cell patch-clamp recordings to test whether a single pacemaker cell exhibits both cholinergic and adrenergic responses. I first recorded spontaneous action potentials in current-clamp mode (Fig 2.1A). Isoprenaline (Iso) activated βARs and increased action potential frequency from ~1 Hz to ~3 Hz. On the other hand, ACh activated M2Rs, which hyperpolarized the cell membrane by ~15 mV and ceased spontaneous action potentials. I subsequently performed the voltage-clamp recording on the exact same cell, and observed robust GIRK currents during ACh application, which is the origin of action potential cessation in Figure 2.1A (Fig 2.1B). However, Iso did not activate GIRK channels even though βARs stimulated the $G\alpha_s$ signaling pathway in Figure 2.1A (Fig 2.1B). These experiments demonstrate the co-existence of functional M2Rs, βARs, and GIRK channels in a single pacemaker cell. Interestingly, while both M2Rs and βARs release free Gβγ in the SAN cells GIRK channels are only activated by M2Rs.

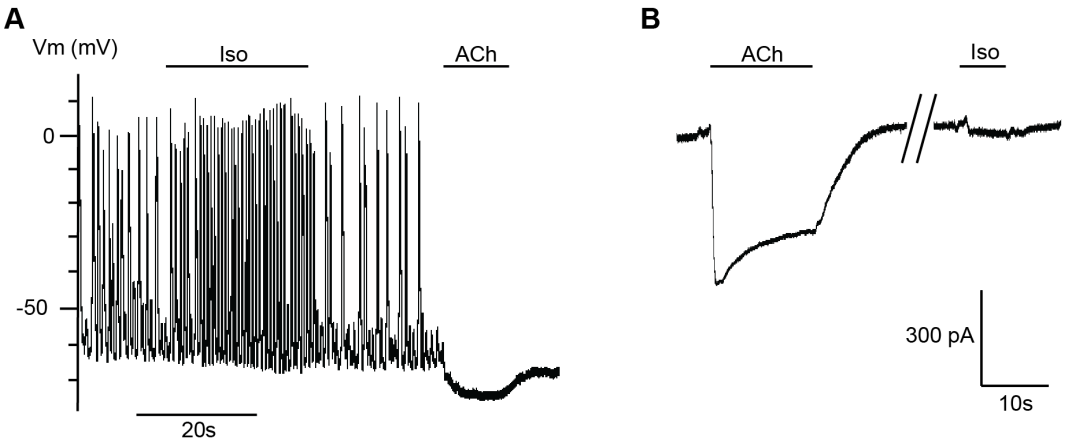

Figure 2.1. Gβγ specificity in natively expressed GIRK channels. (A) A representative current-clamp recording of spontaneous action potentials from acutely isolated murine sinoatrial node (SAN) cells. 1 μM Isoprenaline (Iso) or Acetylcholine (ACh) was applied as indicated above the signal. (B) A representative voltage-clamp recording from SAN cells. Membrane potential was held at -80 mV, and 10 μM Iso or ACh was applied as indicated above the signal

2.2 Gβγ SPECIFICITY IN HETEROLOGOUSLY EXPRESSED GIRK CHANNELS

Figure 2.2A shows voltage clamp experiments in HEK cells (a human-derived cell line) in which GIRK channels and GPCRs were heterologously expressed. M2R is a $G\alpha_i$-coupled GPCR stimulated by ACh and β1AR and β2AR are both $G\alpha_s$-coupled GPCRs stimulated by Iso. In each experiment, agonist (ACh or Iso) is applied to reveal the level of stimulated K^+ current. Only M2R receptor stimulation activates GIRK to a large extent. A difference in surface expression levels of the GPCRs does not explain this result, as Alexa Fluor 488-labeled M2Rs and β2ARs show similar fluorescence intensity at the plasma membrane (Fig 2.2E and 2.2F). To ensure that β1AR and β2AR are indeed functional in the cells and capable of initiating the $G\alpha_s$ pathway, a separate assay was used to measure Iso-stimulated increases in cAMP concentration (Fig 2.2D). Similar experiments were carried out in CHO cells (also mammal-derived) and Sf9 cells (insect-derived) (Fig 2.2B-2.2D). In each cell line only M2R receptor stimulation activates GIRK channels. These data demonstrate that specificity persists across mammalian and insect cells and is therefore a robust property of these signaling pathways.

Figure 2.2. Gβγ specificity in heterologously expressed GIRK channels. (A) HEK293T or (B) CHO cells were transiently transfected with GIRK4 channels, and either M2Rs, β2ARs or β1ARs. Whole-cell voltage-clamp recordings were performed. Membrane potential was held at -80 mV in the presence of extracellular 100 mM K^+. 10 μM ACh or Iso was applied as indicated above signals. (C) Sf9 cells were infected with baculovirus of the GIRK4, and either M2Rs, β2ARs or β1ARs. Whole-cell voltage-clamp recordings were performed. (D) Validation of the function of overexpressed βARs. HEK293T, CHO, or Sf9 cells expressing β1ARs or β2ARs were treated with 10 μM Propranolol (Pro) or Iso for 10 min. Cells were lysed and the intracellular cAMP levels were quantified (N = 3, ± SD). (E)(F) Confocal images of HEK293T cells expressing M2Rs or β2ARs. HEK293T cells were transiently transfected with (E) SNAP-M2Rs or (F) SNAP-β2ARs. Receptors were stained using Alexa Fluor 488 conjugate to a SNAP-ligand. Three representative images are shown for each receptor.

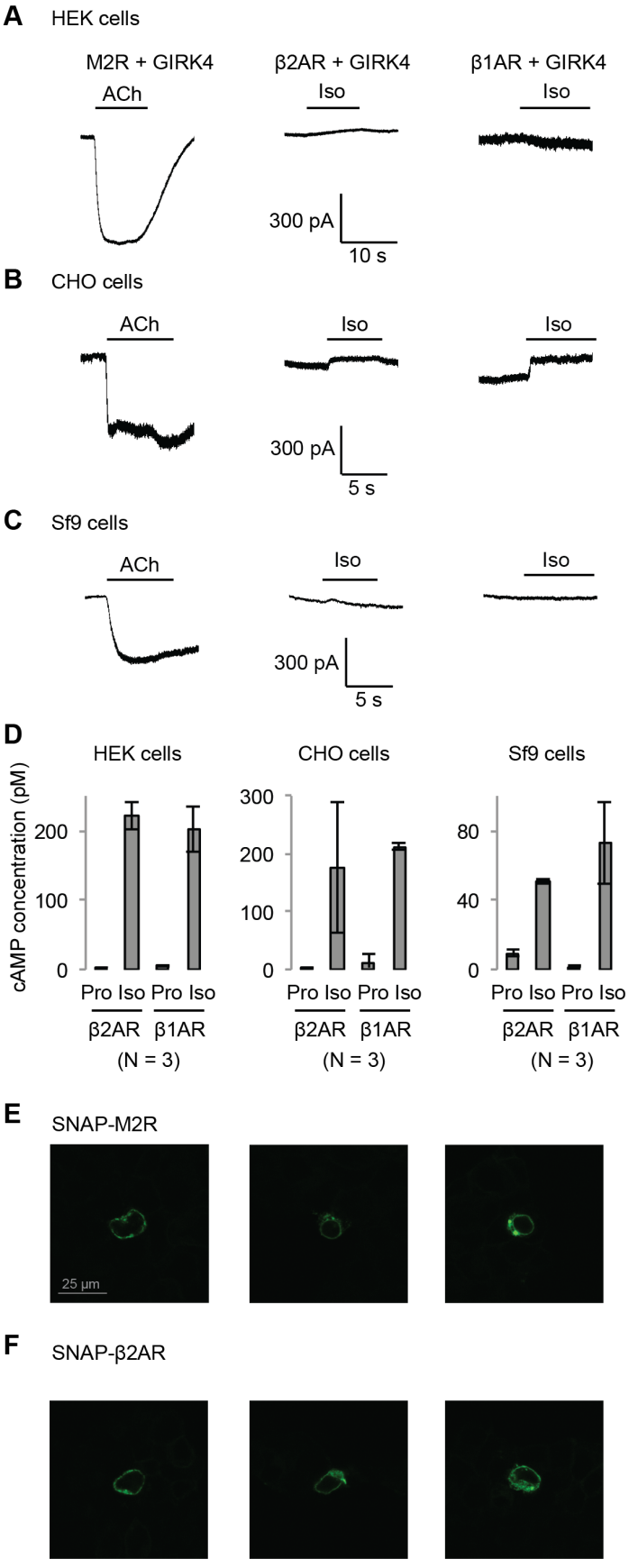
A
HEK cells
M2R + GIRK4
ACh
β2AR + GIRK4
Iso
β1AR + GIRK4
Iso
300 pA
10 s
B
CHO cells
ACh
Iso
Iso
300 pA
5 s
C
Sf9 cells
ACh
Iso
Iso
300 pA
5 s
D
HEK cells
CHO cells
Sf9 cells
cAMP concentration (pM)
0
100
200
300
80
40
Pro Iso Pro Iso
β2AR β1AR
(N = 3)
E
SNAP-M2R
25 µm
F
SNAP-β2AR

2.3 DISCUSSION

In this chapter, I demonstrated that cardiac pacemaker cells responded to both cholinergic and adrenergic stimulations, but only $G\alpha_i$-coupled M2Rs activated GIRK channels. Furthermore, I demonstrated that signaling specificity persists across various heterologous expression systems including insect Sf9 cells. βARs were functional and able to increase the intracellular cAMP concentration in these systems, but failed to activate GIRK channels. These experiments clearly demonstrated that physiologically there is a signaling specificity between GPCRs and GIRK channels, and that signaling specificity is conserved among wide ranges of cell types. It is interesting to note that GIRK channels are found only in vertebrates (Bargmann, 1998; Döring et al, 2002), but signaling specificity persists in insect cells, implying that the molecular basis behind the specificity is conserved in both vertebrates and invertebrates.

CHAPTER 3: CO-LOCALIZATION OF GIRK CHANNELS AND GPCRs IS NOT REQUIRED FOR SPECIFIC ACTIVATION OF GIRK CHANNELS BY $G\alpha_i$-COUPLED GPCRS

I have shown in Chapter 2 that physiologically there is a signaling specificity between GPCRs and GIRK channels. What is the molecular mechanism behind the specificity? It has been suggested that GIRK channels directly interact with inhibitory Gα and GDP-bound G protein heterotrimers (Gα(GDP)βγ), which led to the hypothesis that GIRK channels form a macromolecular supercomplex with inhibitory G proteins and GPCRs (Clancy et al, 2002; Rubinstein et al, 2007; Geng et al, 2009; Rubinstein et al, 2009; Berlin et al, 2010). In a macromolecular supercomplex, Gβγ released from $G\alpha_i$-coupled receptors can immediately bind to and activate GIRK channels. Further supporting this hypothesis, electrophysiological experiments demonstrated that $G\alpha_i$ regulates the activity of GIRK and the kinetics of GPCR activation of GIRK channels (Schreibmayer et al, 1996; Peleg et al, 2002; Ivanina et al, 2004; Clancy et al, 2005). In addition, fluorescent resonance electron transfer (FRET) and bioluminescence resonance energy transfer (BRET) assays suggested possible pre-coupling

between GIRK and G proteins (Riven et al, 2006), adenylyl cyclase (Lavine et al, 2002), β2ARs (Lavine et al, 2002), $GABA_B$ receptors (Fowler et al, 2007), and regulators of G protein signaling (RGS) (Fowler et al, 2007). However, it is puzzling that adenylyl cyclase and β2ARs, which are components of $G\alpha_s$ signaling, associate with GIRK channels.

Recently, the macromolecular supercomplex hypothesis has been challenged by a growing body of evidence. For example, in the resting state of GPCRs and G protein heterotrimers do not pre-couple to each other (Yao et al, 2008; Rasmussen et al, 2011; Sungkaworn et al, 2017; Gregorio et al, 2017; Hilger et al., 2018). Additionally, a study from our lab showed that GIRK2 channels do not functionally interact with $G\alpha_{i1}$ (Wang et al, 2014). In this chapter, I provided three additional lines of evidence against the macromolecular supercomplex hypothesis. First, I directly compared the degree of co-localization of GPCRs and GIRK4 channels using the stochastic optical reconstruction microscopy (STORM), and found that GIRK showed similar degree of co-localization with M2Rs and β2ARs. Second, a β2AR-GIRK4 concatemer construct which forces co-localization of β2ARs and GIRK4 channels failed to activate the channel. This along with the co-localization experiments indicate that the proximity of GPCRs and GIRK channels does not explain the specific activation of GIRK channels by $G\alpha_i$-coupled receptors. Third, I show that $G\alpha_{i1}$(GTP) and G protein heterotrimers do not functionally interact with GIRK1/4 channels in the planar lipid bilayer system. Taken together these experiments indicate that $G\alpha_{i1}$ and G proteins are unlikely to interact with GIRK prior to GPCR activation to form a macromolecular supercomplex.

3.1 GIRK CO-LOCALIZATION WITH GPCRs SHOWS NO PREFERENCE FOR M2Rs OVER β2ARs

To directly compare the degree of co-localization of GPCRs and GIRK channels, I established stabsle HEK cell lines expressing the C-terminus SNAP-tagged GIRK4 channels and the N-terminus Halo-tagged M2Rs or β2ARs (Fig 3.1A). Both GIRK4-SNAP and Halo-GPCR were expressed under the same tetracycline-inducible CMV promoter separated by an internal ribosome entry site (IRES) sequence. To confirm the expression of GIRK4 channels and GPCRs, we induced protein expression using different concentrations of doxycycline (Dox), a stable tetracycline analogue. GIRK4-SNAP and Halo-GPCR were then fluorescently labeled using SNAP and Halo-tag protein labeling systems, and cells were imaged under a confocal microscope. Between the two stable cell lines, I observed increasing protein expression with increased Dox concentration and similar expression levels of GIRK4 channels and the two different GPCRs, M2Rs and β2ARs (Fig 3.2A). I then performed whole-cell voltage-clamp recordings on M2R-GIRK4 stable cells, and found that the averaged amplitude of the acetylcholine (ACh)-activated currents increased with increased Dox concentration (Fig 3.1B and 3.2B). However, β2ARs did not activate GIRK4 channels even when the expression was induced with a high concentration of Dox (Fig 3.1C). This absence of currents may be because the β2AR downstream pathway is incapable of activating GIRK or because overexpressed β2ARs were not functional. However, I found that agonist stimulation of β2ARs increased intracellular cAMP concentration, suggesting that overexpressed β2ARs functionally coupled to

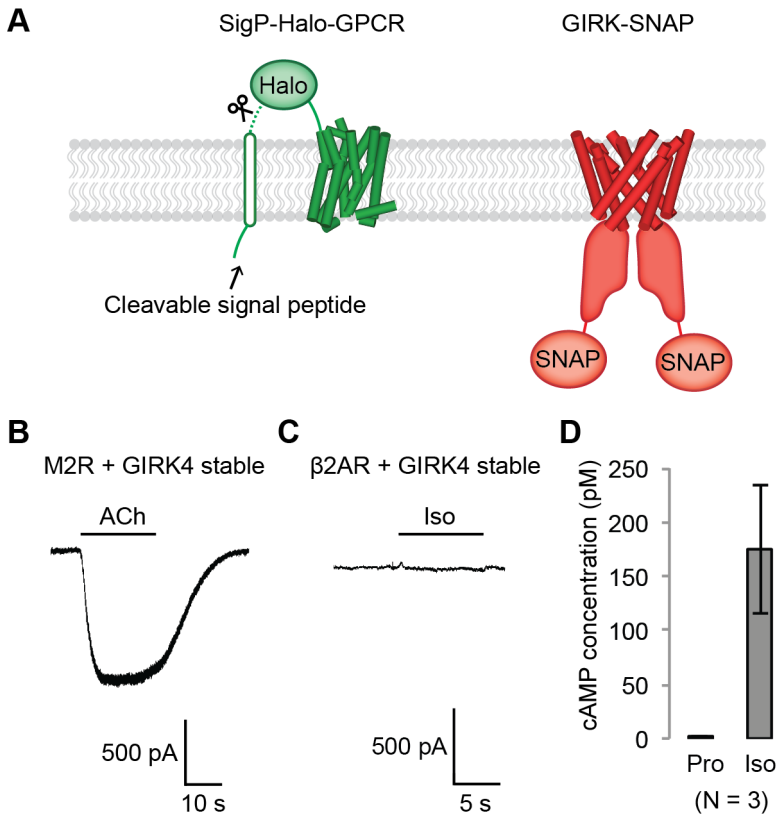

Figure 3.1. Gβγ specificity in stable HEK cell lines expressing GPCRs and GIRK4 channels. (A) Schematic representation of GPCR and GIRK4 constructs used in stable HEK cell lines. A serotonin 5HT signal and a Halo-tag were added to the N-terminus of GPCRs (Halo-GPCR). A SNAP-tag was added to the C-terminus of the GIRK4 (GIRK4-SNAP). Both Halo-GPCR and GIRK4-SNAP were expressed under the same tetracycline-inducible CMV promoter using an internal ribosome entry site (IRES) sequence. (B)(C) A representative voltage-clamp recording from stable HEK cells. Protein expression was induced with 1000 ng/mL doxycycline (Dox) for 20-24 h, and whole-cell voltage-clamp recordings were performed. Membrane potential was held at -80 mV in the presence of 100 mM extracellular KCl. (B) 10 μM acetylcholine (ACh) or (C) isoprenaline (Iso) was applied as indicated above signals. (D) Validation of the function of overexpressed β2ARs. β2AR-GIRK4 stable HEK cells were treated with 1000 ng/mL Dox for 20-24 h to induce protein expression. Then β2ARs were stimulated with an antagonist, propranolol (Pro), or an agonist, isoprenaline (Iso) for 10 min, and intracellular cAMP concentration levels were quantified (N = 3, ± SD).

the endogenous $G\alpha_s$ pathway (Fig 3.1D). Taken together, my experiments demonstrate that GIRK channels are specifically activated by M2Rs, but not by β2ARs in HEK cells even in the presence of roughly equivalent amounts of M2Rs and β2ARs.

Next I investigated whether M2Rs and GIRK channels form a macromolecular supercomplex. If co-localization of M2Rs and GIRK channels is required for the specificity, then M2Rs should co-localize with GIRK to a higher degree than β2ARs. Therefore, I directly compared the degree of co-localization of M2Rs and β2ARs with GIRK channels using Halo-GPCR/GIRK-SNAP stable HEK cell lines and the super-resolution microscopy technique. Protein expression was induced with 6 ng/mL Dox, which produces optimal expression levels of GIRK4 channels and GPCRs for imaging (Fig 3.2). After 20-24 h induction, Halo-GPCRs were labeled with HaloTag-TMR. Then cells were fixed and permeabilized, and GIRK4-SNAP was labeled with SNAP-Surface Alexa Fluor 647. Subsequently, I performed the STORM analysis to localize individual molecules in the membrane (Fig 3.3A and 3.3B) (Jones et al, 2011; Dempsey et al, 2011). Each GPCR and channel was identified according to the coordinates of the fluorophore blinking events (See Methods and Fig 3.4 for details). I identified 5 ± 1 M2Rs and 12 ± 2 GIRK4 channels per μm^2 from the M2R-GIRK4 stable cells, and 4 ± 1 β2ARs and 11 ± 3 GIRK4 channels per μm^2 from the β2AR-GIRK4 stable cells (N = 4, ± SD). I then calculated the fraction of GPCRs co-localized (localized within 100 nm) with GIRK channels. I found that 25 ± 7% of M2Rs co-localized with GIRK4 channels, and 26 ± 4% of β2ARs co-localized with GIRK4 channels (N = 4, ± SD) (Fig 3.3C). This result demonstrates that the degree of co-localization with GIRK channels is similar between M2Rs and β2ARs.

Figure 3.2. M2R-GIRK4 and β2AR-GIRK4 stable HEK cells express similar levels of GPCRs and GIRK4 channels. (A) M2R-GIRK4 or β2AR-GIRK4 stable HEK cells were treated with different concentrations of Dox (0-500 ng/mL), and receptors and channels were stained with Alexa Fluor 488 and TMR, respectively. Images were taken under a confocal microscope. Microscope and software settings were the same for all images acquired. (B) M2R-GIRK4 stable HEK cells were treated with different concentrations of Dox (0-1000 ng/mL), and whole-cell voltage-clamp recordings were performed. ACh-activated GIRK currents were normalized to the capacitance of the cells. (N = 3-16, ± SEM).

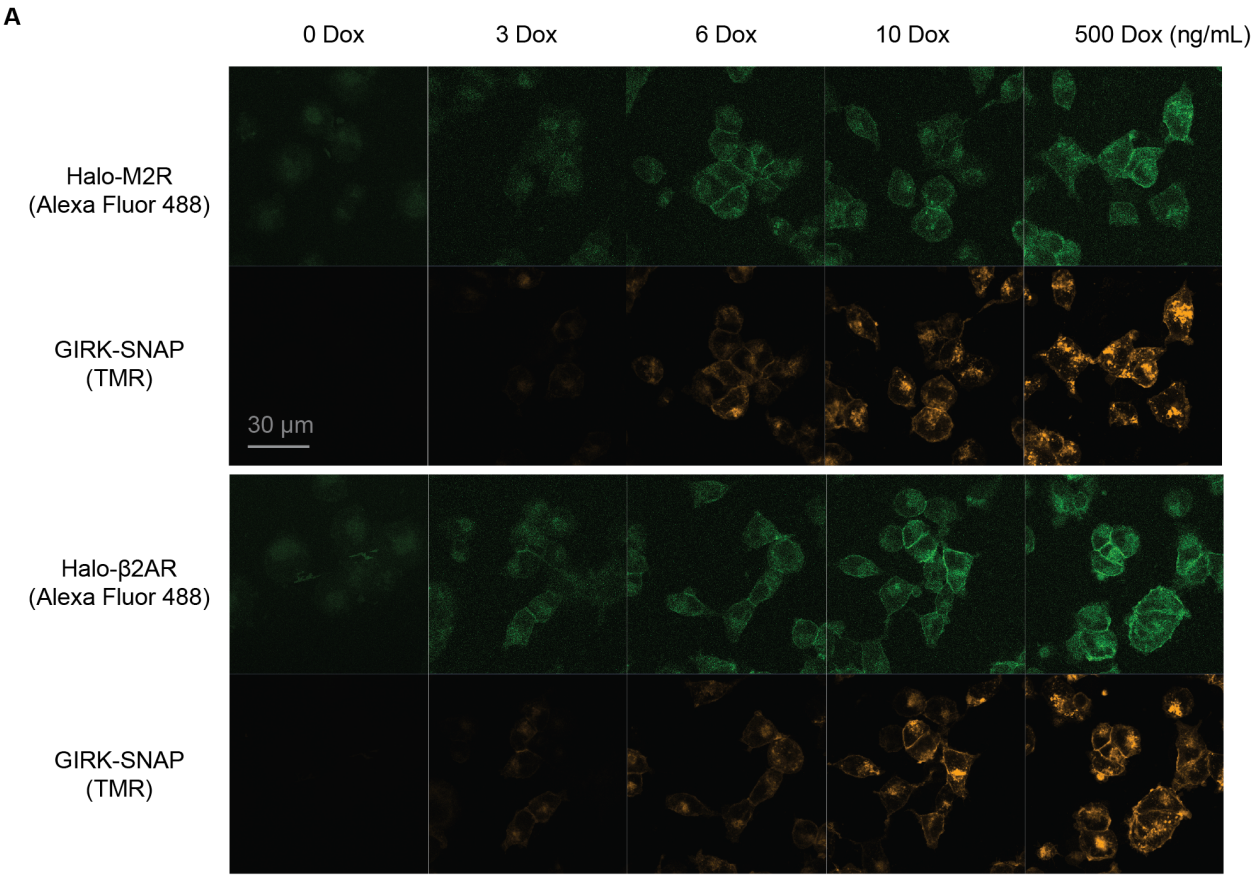
A
0 Dox
3 Dox
6 Dox
10 Dox
500 Dox (ng/mL)
Halo-M2R
(Alexa Fluor 488)
GIRK-SNAP
(TMR)
30 µm
Halo-β2AR
(Alexa Fluor 488)
GIRK-SNAP
(TMR)

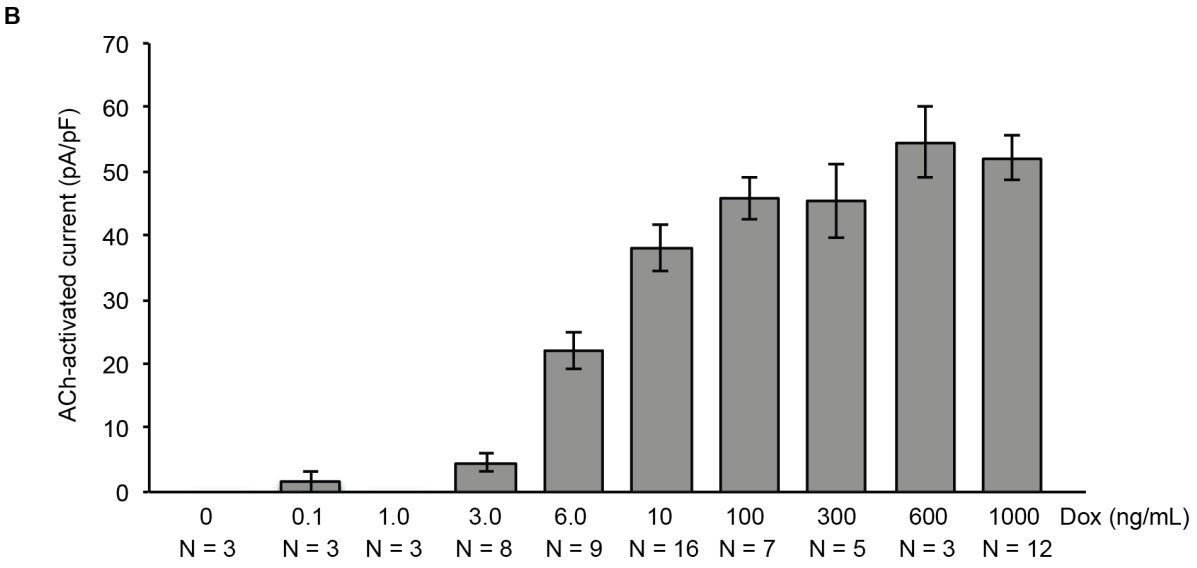
B
ACh-activated current (pA/pF)
70
60
50
40
30
20
10
0
0
N = 3
0.1
N = 3
1.0
N = 3
3.0
N = 8
6.0
N = 9
10
N = 16
100
N = 7
300
N = 5
600
N = 3
1000
N = 12
Dox (ng/mL)

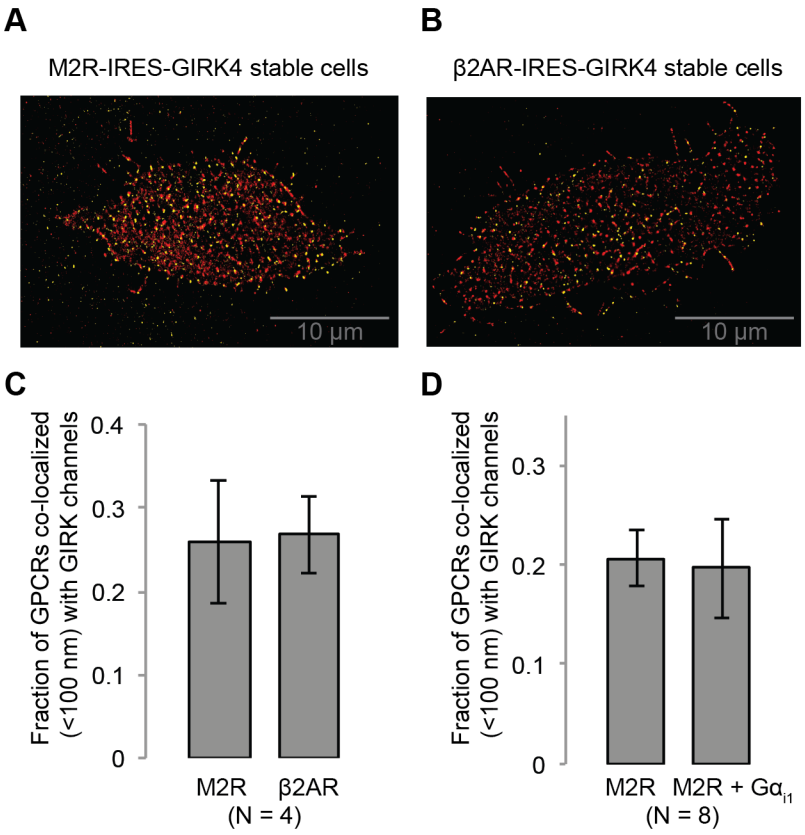

Figure 3.3. M2Rs do not co-localize with GIRK4 channels more than β2ARs do.
(A)(B) Representative STORM images obtained from stable HEK cells expressing (A) M2Rs and GIRK4 channels, and (B) β2ARs and GIRK4 channels. Halo-GPCRs were labeled with TMR (yellow), and GIRK4-SNAP channels were labeled with Alexa Fluor 647 (red). (C) There is no difference in the degree of co-localization between M2Rs or β2ARs with GIRK4 channels. The coordinates of GPCRs and GIRK4 channels were determined, and the number of GPCRs within 100 nm from GIRK4 channels was divided by the total number of GPCRs (N = 4, ± SD). (D) Overexpression of $G\alpha_{i1}$ did not alter the degree of co-localization of M2Rs and GIRK4 channels. A control plasmid expressing GFP or $G\alpha_{i1}$ was overexpressed in M2R-GIRK4 stable HEK cells, and STORM analysis was performed. The coordinates of M2Rs and GIRK4 channels were determined, and the number of M2Rs within 100 nm from GIRK4 channels was divided by the total number of M2Rs (N = 8, ± SD)

I further investigated whether overexpression of $G\alpha_{i1}$, which is reported to play a role as a bridge between GIRK and GPCR, alters the co-localization between GIRK4 channels and M2Rs. I transiently transfected a control vector expressing GFP or $G\alpha_{i1}$ to M2R-GIRK4 stable HEK cells, and at the same time induced the GPCR and channel expression with 6 ng/mL Dox. I found that overexpression of $G\alpha_{i1}$ did not alter the degree of co-localization of M2Rs and GIRK4 channels (Fig 3.3D). Taken together, my STORM analysis shows that GIRK4 does not display a preferential co-localization with M2Rs over β2ARs, and that $G\alpha_{i1}$ does not affect the degree of co-localization between M2Rs and GIRK channels. These results are inconsistent with the macromolecular supercomplex theory.

In the STORM data analysis, I determined the coordinates of GPCRs and GIRK channels based on the coordinates of fluorophore blinking events. A fluorophore attached to a single GPCR or GIRK subunit blinked several times before it bleached. Therefore, I regarded two blinking events that happened within 100 pixels (90 nm) in two different frames as the same molecule. As a result, I could not distinguish two different molecules localized within 90 nm with this method. Thus the number of GPCRs and GIRK channels identified may not be accurate and the method could not identify potential hot spots in the membrane where receptors and channels reside in a specialized region. However, the average number of fluorophore blinking events observed from a single GPCR molecule was similar between M2Rs and β2ARs (5.5 ± 1.1 for M2Rs and 4.8 ± 1.2 for β2ARs) (N = 4, ± SD), excluding the possibility that M2Rs cluster more than β2ARs in the membrane.

Figure 3.4. Summary of coordinate determination procedures for STORM analysis. (A) Schematic representation of an example of the coordinate determination procedure. At the frame 1, three dyes in the fluorescent state were observed (red stars), and they were assigned as distinct dyes. At the frame 2, the dyes in the frame 1 switched to the dark state, and a new dye in the fluorescent state was observed. However it was not within 100 pixels (90 nm) from any of dyes observed in the previous frames. Therefore, it was assigned as a new dye. A new dye in the fluorescent state in in the frame 3 was within 100 pixels from a previously determined dye. Therefore, they were regarded as the same molecule, and the coordinate of the dye was replaced by that of the new event in the fluorescent state (frame 4). These procedures continued over 1000 frames, and coordinates of GPCRs or GIRK4 channels were determined. (B) A representative STORM image obtained from β2AR-GIRK4 stable HEK cells. Halo-β2ARs were labeled with TMR (yellow), and GIRK4-SNAP channels were labeled with Alexa Fluor 647 (red). (C) The result of coordinate determination of β2ARs in the STORM image shown in Figure S2B. Each circle represents a single β2AR. (D) The result of coordinate determination of GIRK4 channels in the STORM image shown in Figure S2B. Each circle represents a single GIRK channel. (E) The region in the red box in Figure S2C was magnified. The center of the blue circle, whose radius is 100 pixels, represents the coordinate of β2ARs. Single dots represent single blinking events, and blinking events belong to different molecules were colored differently.

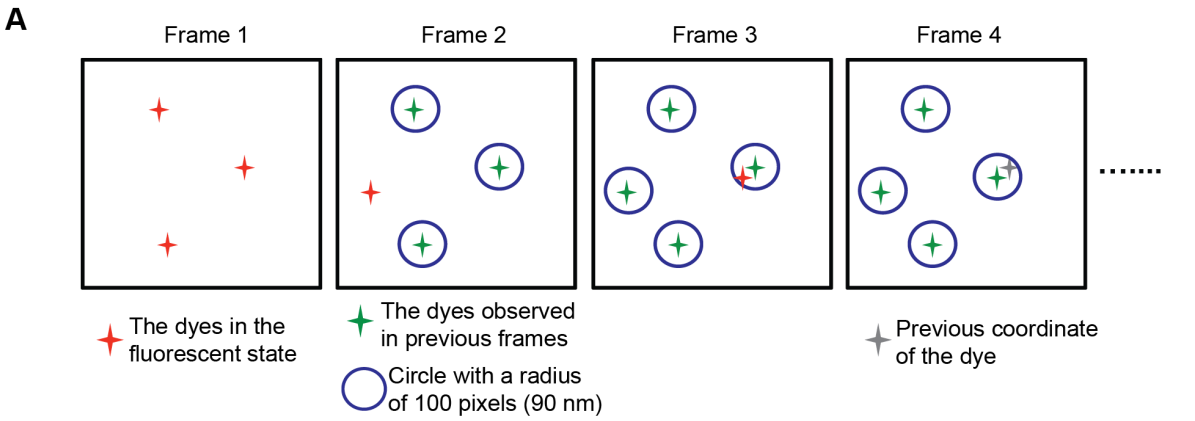
A
Frame 1
Frame 2
Frame 3
Frame 4
.....
The dyes in the fluorescent state
The dyes observed in previous frames
Previous coordinate of the dye
Circle with a radius of 100 pixels (90 nm)

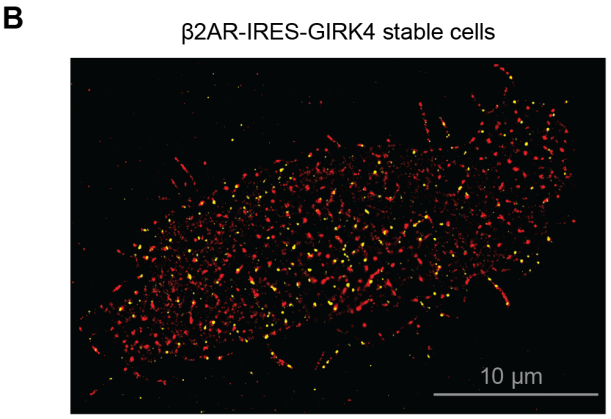
B
β2AR-IRES-GIRK4 stable cells
10 μm

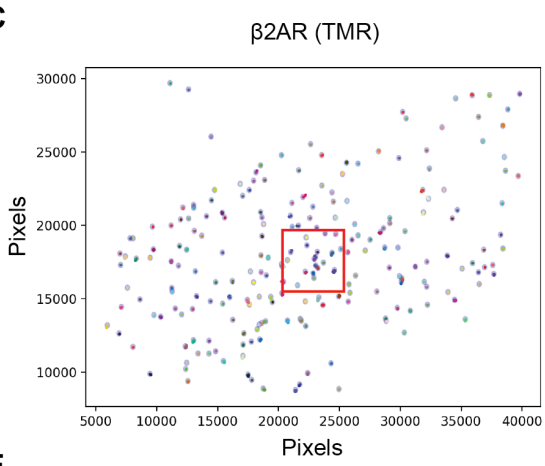
C
β2AR (TMR)
Pixels
Pixels
30000
25000
20000
15000
10000
5000
10000
15000
20000
25000
30000
35000
40000

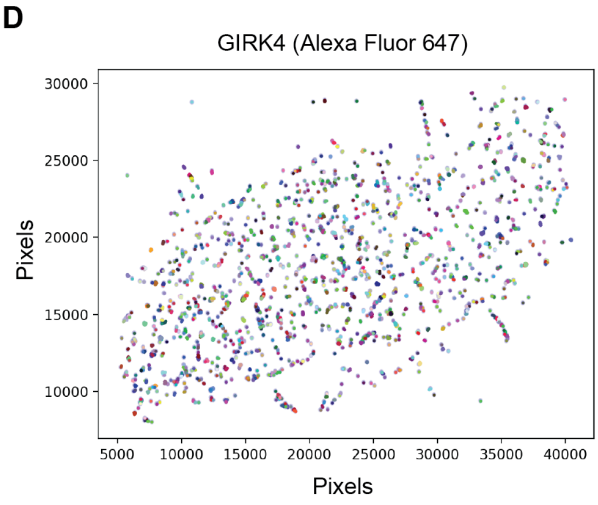
D
GIRK4 (Alexa Fluor 647)
Pixels
Pixels
30000
25000
20000
15000
10000
5000
10000
15000
20000
25000
30000
35000
40000

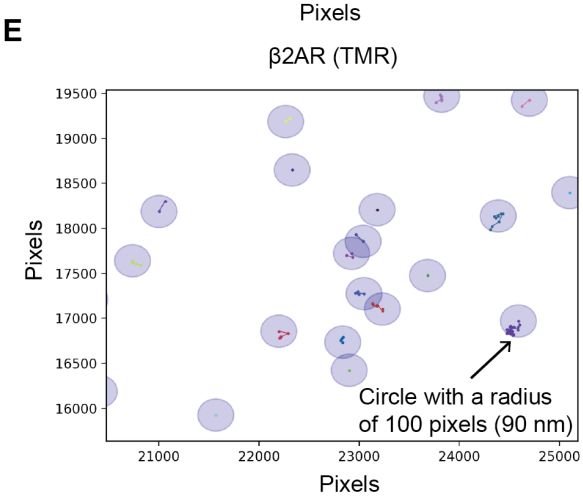
E
β2AR (TMR)
Pixels
Pixels
Circle with a radius of 100 pixels (90 nm)
19500
19000
18500
18000
17500
17000
16500
16000
21000
22000
23000
24000
25000

3.2 THE PROXIMITY BETWEEN GIRK AND GPCRS DOES NOT EXPLAIN SIGNALING SPECIFICITY

Next, I set out to test whether the proximity between GPCRs and GIRK channels explains signaling specificity. If the macromolecular supercomplex formation, or co-localization of GIRK channels and M2Rs is required for specific activation of GIRK, then β2ARs should also be able to activate GIRK when they are forced to co-localize. To test the hypothesis, I constructed concatemeric GPCR-GIRK4 constructs (Fig 3.5A). The C-terminus SNAP-tagged GIRK4 was fused to the N-terminus Halo-tagged M2R or β2AR through a flexible linker of ~120 amino acids. Hence the concatemeric constructs contain a Halo tag and a SNAP tag on its N-terminus and C-terminus, respectively. GIRK channels have a tetrameric structure, so in the concatemer experiments a single GIRK4 channel is surrounded by four GPCRs. I first confirmed that the linker in concatemerized constructs does not degrade, causing the GPCR and GIRK channel to fall apart in HEK cells. M2R-GIRK4 and β2AR-GIRK4 concatemers were transiently transfected to HEK cells, and Western-Blot experiments were performed against the Halo or the SNAP tag (Fig 3.5B). I did not observe significant protein degradation, demonstrating the biochemical stability of GPCR-GIRK4 concatemers in HEK cells.

I then transiently transfected M2R-GIRK4 concatemers into HEK cells and performed whole-cell voltage-clamp recordings. I observed significant GIRK4 currents upon ACh stimulation, suggesting that both M2Rs and GIRK4 channels were functional in the concatemerized construct (Fig 3.5C). In contrast, Iso induced no significant GIRK currents in the β2AR-GIRK4 concatemers with or without $G\alpha_s$ overexpressed (Fig 3.5D and 3.5E). As a control, the functionality of β2ARs in the concatemers was confirmed by the cAMP quantification assay (Fig 3.5F). Taken together, these experiments challenge the macromolecular supercomplex hypothesis by showing that β2ARs cannot activate GIRK4 channels when they are forced to co-localize.

Figure 3.5. Effect of artificially enforced GPCR-GIRK co-localization. (A) A schematic representation of GPCR-GIRK concatemer constructs. GIRK was directly fused to the C-terminus of GPCRs. A cleavable signal peptide and a Halo tag were added to the N-terminus of each concatemer. Additionally, a SNAP tag was added to the C-terminus of each concatemer. (B) Western-Blot analysis of GPCR-GIRK concatemer constructs. HEK cells were transiently transfected with either M2R-GIRK or β2AR-GIRK concatemers. The expected size of these concatemers is ~150 kDa. (C)-(E) Representative voltage-clamp recordings of HEK293T cells transiently transfected with M2R-GIRK concatemers, β2AR-GIRK concatemers, or β2AR-GIRK concatemers and $G\alpha_s$. Membrane potential was held at -80 mV. 10 μM ACh or Iso was applied as indicated. (F) Validation of the function of β2AR-GIRK concatemers. HEK293T cells expressing β2AR-GIRK concatemers were treated with 10 μM propranolol (Pro) or isoprennaline (Iso), and intracellular cAMP levels were quantified (N = 3, ± SD).

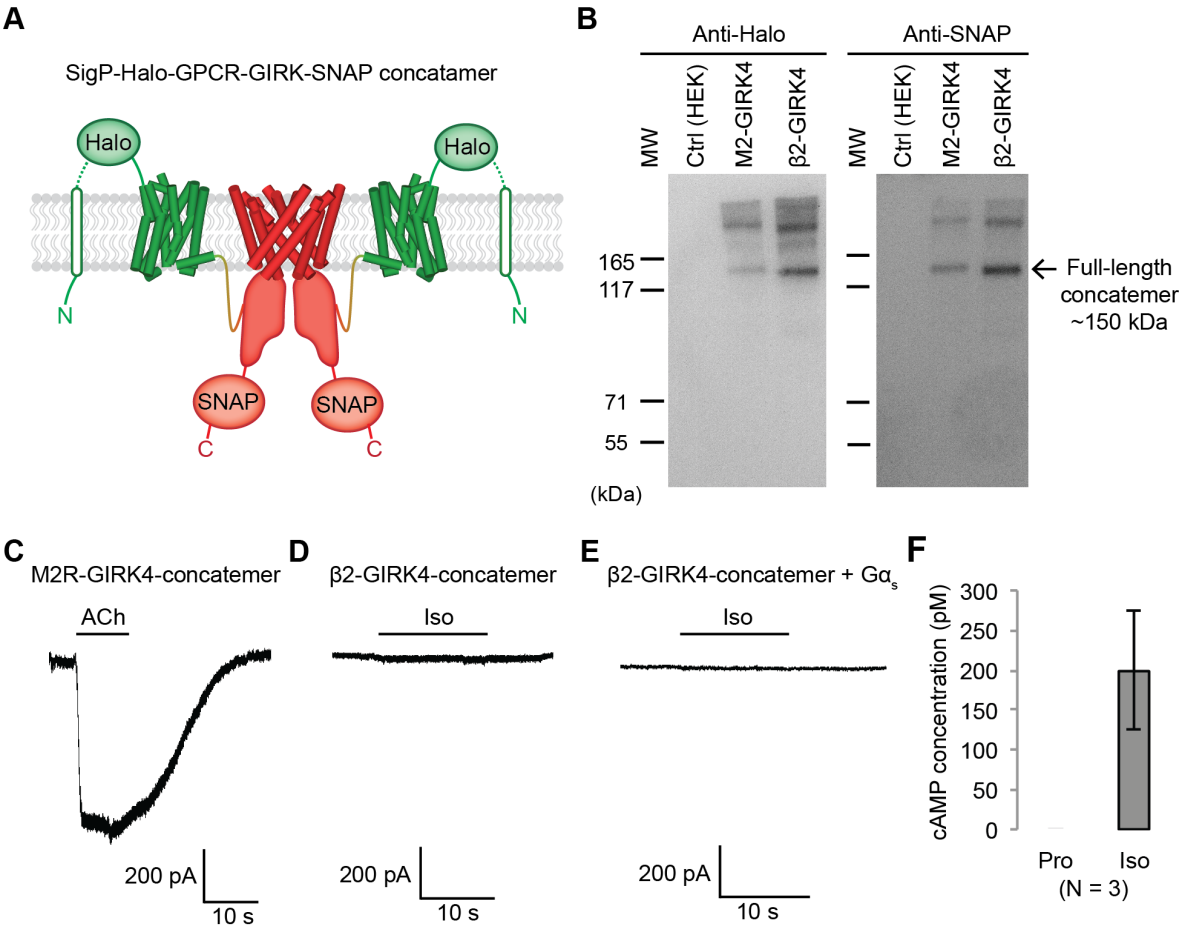
A
SigP-Halo-GPCR-GIRK-SNAP concatamer
Halo
Halo
N
N
SNAP
SNAP
C
C
B
Anti-Halo
Anti-SNAP
MW
Ctrl (HEK)
M2-GIRK4
β2-GIRK4
MW
Ctrl (HEK)
M2-GIRK4
β2-GIRK4
165
117
71
55
(kDa)
Full-length
concatemer
~150 kDa
C
M2R-GIRK4-concatemer
ACh
200 pA
10 s
D
β2-GIRK4-concatemer
Iso
200 pA
10 s
E
β2-GIRK4-concatemer + Gαs
Iso
200 pA
10 s
F
cAMP concentration (pM)
300
250
200
150
100
50
0
Pro
Iso
(N = 3)

3.3 Gα AND G PROTEIN HETEROTRIMERS DO NOT INTERACT WITH GIRK1/4 CHANNELS

It has been demonstrated that $G\alpha_i$ and G protein heterotrimers can directly bind to GIRK channels, functionally regulate the channel, and serve as a bridge between GPCRs and GIRK channels (Clancy et al, 2002; Rubinstein et al, 2007; Geng et al, 2009; Rubinstein et al, 2009; Berlin et al, 2010). However, these experiments were done in heterologous overexpression systems where it is difficult to control the G protein signaling. A previous study from our lab has shown that $G\alpha_{i1}$(GTP) does not functionally interact with GIRK2 channels in the planar lipid bilayer system (Wang et al, 2014). Yet one could still argue that the GIRK1 subunit is required to bind to $G\alpha_i$ and G protein heterotrimers as previously reported (Rubinstein et al, 2009). Therefore, I purified the human full-length GIRK1/4 channel and studies its regulation by $G\alpha_i$ and G protein heterotrimers in the planer lipid bilayer system.

I first examined if $G\alpha_{i1}$(GTP) can regulates the GIRK1/4 channel. Fusion of GIRK1/4 proteoliposomes to the bilayer membrane and subsequent application of $G\alpha_{i1}$(GTPγS) vesicles did not activate the channel (Fig 3.6A). To confirm their presence in the membrane, I demonstrated that the same GIRK1/4 channels could be activated by fusing Gβγ vesicles (Fig 3.6A). I next investigated whether $G\alpha_{i1}$(GTPγS) inhibits the GIRK1/4. In the membrane containing GIRK1/4 channels activated by Gβγ, further application of $G\alpha_{i1}$(GTPγS) vesicles showed little effect on the channel activity (Fig 3.6B).

G protein heterotrimers, $G\alpha_{i3}$(GDP)βγ, have been suggested to couple with GIRK channels via Gβγ prior to GPCR stimulation (Rubinstein et al, 2009). Therefore, I tested whether Gβγ and G protein heterotrimers ($G\alpha_{i3}$(GDP)βγ) compete for binding to GIRK1/4.

Proteoliposomes containing GIRK1/4 channels and low concentration of Gβγ (GIRK1/4:Gβγ = 1 : 0.1, wt:wt) were fused to the bilayer membrane. The channel was partially activated due to low concentration of Gβγ in the membrane (Fig 4.5A). I then fused $G\alpha_{i3}$(GDP)βγ vesicles to the membrane. I observed neither inhibition nor further activation of the channel by $G\alpha_{i3}$(GDP)βγ (Fig 3.6C).

Available structural information excludes the possibility that G protein heterotrimers silently bind to GIRK channels without affecting the channel activity. Our lab has previously demonstrated that four Gβγ are required to open GIRK (Wang et al, 2016). The crystal structure of the GIRK-Gβγ complex showed that four Gβγ bind to the intracellular domain of GIRK channels, leaving little room for G protein heterotrimers to bind to (Fig 3.7) (Whorton and Mackinnon, 2013). As a result, binding of G protein heterotrimers is expected to compete with Gβγ and thus affect GIRK activity, which I did not observe.

Figure 3.6. $G\alpha_{i1}$(GTPγS) and G protein heterotrimer, $G\alpha_{i3}$(GDP)βγ, do not functionally interact with GIRK1/4 channels. The GIRK1/4 currents were plotted according to electrophysiology convention such that negative values represent inward current with respect to channel orientation. The same buffer containing 10 mM K-phosphate (pH 7.4) and 150 mM KCl was used in both chambers, and 2 mM $MgCl_2$ and 32 μM C8-PIP_2 were added to the chamber where the intracellular side of the channel was present. The membranes were held at -50 mV. The grey dashed lines represent the baseline (0 pA). (A) Current recorded from a bilayer with GIRK1/4 channels before and after application of $G\alpha_{i1}$(GTPγS) vesicles followed by application of Gβγ vesicles. (B) Current recorded from a bilayer with GIRK1/4 channels activated by Gβγ (GIRK1/4 : Gβγ = 1 : 2, [wt:wt]) before and after application of $G\alpha_{i1}$(GTPγS) vesicles. Note that the high salt concentration of the vesicle solution (1 M KCl) used to facilitate fusion to the bilayer caused a transient reduction in the GIRK1/4 current. (C) Current recorded from a bilayer with GIRK1/4 channels activated by low concentration of Gβγ (GIRK1/4 : Gβγ = 1 : 0.1, [wt:wt]) before and after application of $G\alpha_{i3}$(GDP)βγ vesicles. Note that the high salt concentration of the vesicle solution (1 M KCl) used to facilitate fusion to the bilayer caused a transient reduction in the GIRK1/4 current.

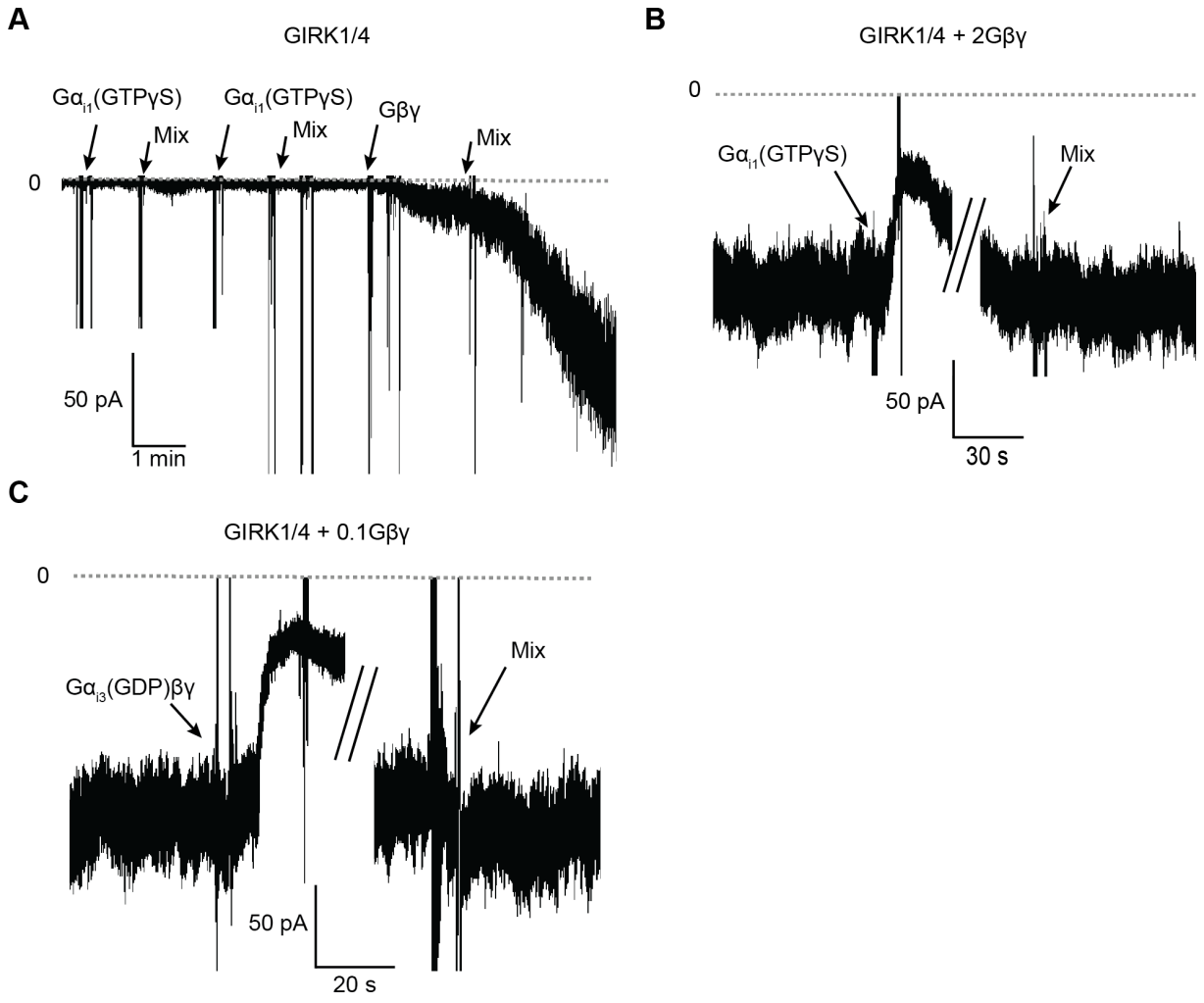
A
GIRK1/4
Gαi1(GTPγS)
Mix
Gαi1(GTPγS)
Mix
Gβγ
Mix
0
50 pA
1 min
B
GIRK1/4 + 2Gβγ
0
Gαi1(GTPγS)
Mix
50 pA
30 s
C
GIRK1/4 + 0.1Gβγ
0
Gαi3(GDP)βγ
Mix
50 pA
20 s

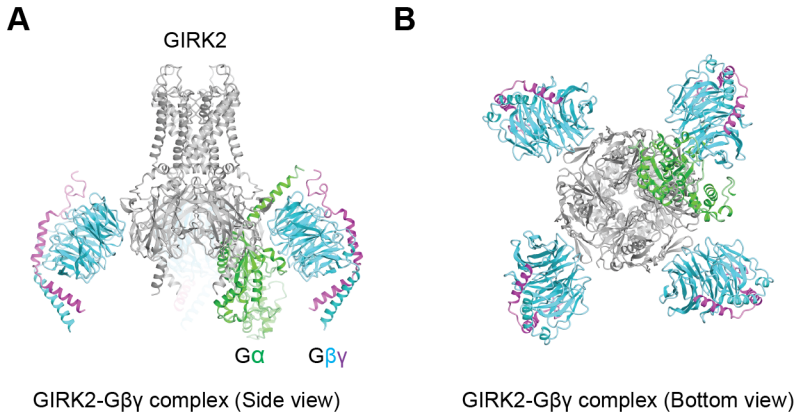

Figure 3.7. G protein heterotrimers cannot bind to GIRK without competing with Gβγ. (A) Side view of the crystal structures of GIRK2-Gβγ complex (PDB: 4KFM) and GDP-bound inhibitory G protein heterotrimer (PDB: 1GP2). The GIRK2 channel is represented as grey. Gα, Gβ, and Gγ are represented as green, cyan, and purple, respectively. Two structures were superimposed according to the position of Gβγ. (B) Bottom view of the crystal structures of GIRK2-Gβγ complex and GDP-bound inhibitory G protein heterotrimer.

CHAPTER 4: MOLECULAR BASIS OF SIGNALING SPECIFICITY BETWEEN GIRK CHANNELS AND GPCRS

As shown in Chapter 2, physiologically there is a signaling specificity between GPCRs and GIRK channels. The most prevailing theory in the field is the macromolecular supercomplex hypothesis. In Chapter 3, I challenged the theory by demonstrating three evidences against the hypothesis. What is the molecular basis behind signaling specificity then? Digby et al suggested that stimulated $G\alpha_s$-coupled receptors might generate insufficient quantities of free $G\beta\gamma$ if $G\alpha_s$(GTP) binds to $G\beta\gamma$ with higher affinity (Digby et al, 2009). Wellner-Kienitz et al suggested that insufficient expression of βARs in cardiac pacemaker cells might be the explanation (Wellner-Kienitz et al, 2001). These studies, although insightful, did not fully explain signaling specificity.

In this chapter, I propose a straightforward new conceptual model of GIRK activation by GPCRs. Using electrophysiological technologies and bioluminescent resonance electron transfer (BRET) assays, I showed that both M2Rs and β2ARs can activate GIRK according to the amount of available G protein heterotrimers. M2Rs activate GIRK with the endogenous level of G protein heterotrimers, however β2ARs require overexpression of G protein heterotrimers.

Quantitative BRET measurements showed that $G\alpha_i$-coupled GPCRs release $G\beta\gamma$ at higher rates than $G\alpha_s$-coupled GPCRs, generating higher $G\beta\gamma$ concentration that activate GIRK and regulate other targets of $G\beta\gamma$. Taken together I conclude that the activity of GIRK channels is simply determined by the efficiency of $G\beta\gamma$ release from GPCRs, and that physiologically only $G\alpha_i$-coupled receptors can provide sufficient amounts of $G\beta\gamma$ to activate GIRK channels. Moreover, our simulation suggested that the higher rate of $G\beta\gamma$ release is attributable to a faster GPCR-G protein association rate in M2Rs compared to β2ARs.

4.1 INFLUENCE OF G PROTEIN LEVELS ON SPECIFICITY

In the experiments described in Chapter 2, activation of GIRK channels by GPCR stimulation was facilitated by endogenous levels of G proteins in the cells (Fig 2.2). I next ask what happens if the levels of G proteins available for mediating activation are altered? Using a cell line in which I established stable expression of GIRK channels and GPCRs, G protein levels were altered using transient transfection. In control experiments endogenous G protein levels support M2R stimulated GIRK channel activation (Fig 4.1A), as was observed in Figure 2.2. Expression of additional $G\alpha_{i1}$ subunits suppressed the level of M2R-stimulated GIRK current, presumably because excess $G\alpha_{i1}$ subunits blunt the normal increase in $G\beta\gamma$ concentration (i.e. $G\alpha_{i1}$ can compete with the channel for available $G\beta\gamma$). Expression of additional $G\alpha_{i1}$ and $G\beta\gamma$ subunits, however, leads to M2R-stimulated GIRK current that exceeds levels mediated by endogenous G proteins alone (Fig 4.1A and C). This latter observation would seem to suggest that increased availability of $G\alpha_i(GDP)\beta\gamma$ substrate (upon which stimulated M2R acts to generate free $G\beta\gamma$) leads to increased $G\beta\gamma$ levels following M2R stimulation. I next ask what happens if sufficiently high levels of $G\alpha_s(GDP)\beta\gamma$ substrate levels are provided, might the β2AR activate GIRK to a detectable extent? Experiments using cells expressing GIRK channels and β2ARs show that excess $G\alpha_s$ and $G\beta\gamma$ subunits give rise to β2AR-stimulated GIRK current (Fig 4.1B and D). This finding suggests that the specificity exhibited by $G\alpha_i$-coupled GPCRs versus $G\alpha_s$-coupled GPCRs is somehow related to differences in the levels of $G\beta\gamma$ that they each are able to generate.

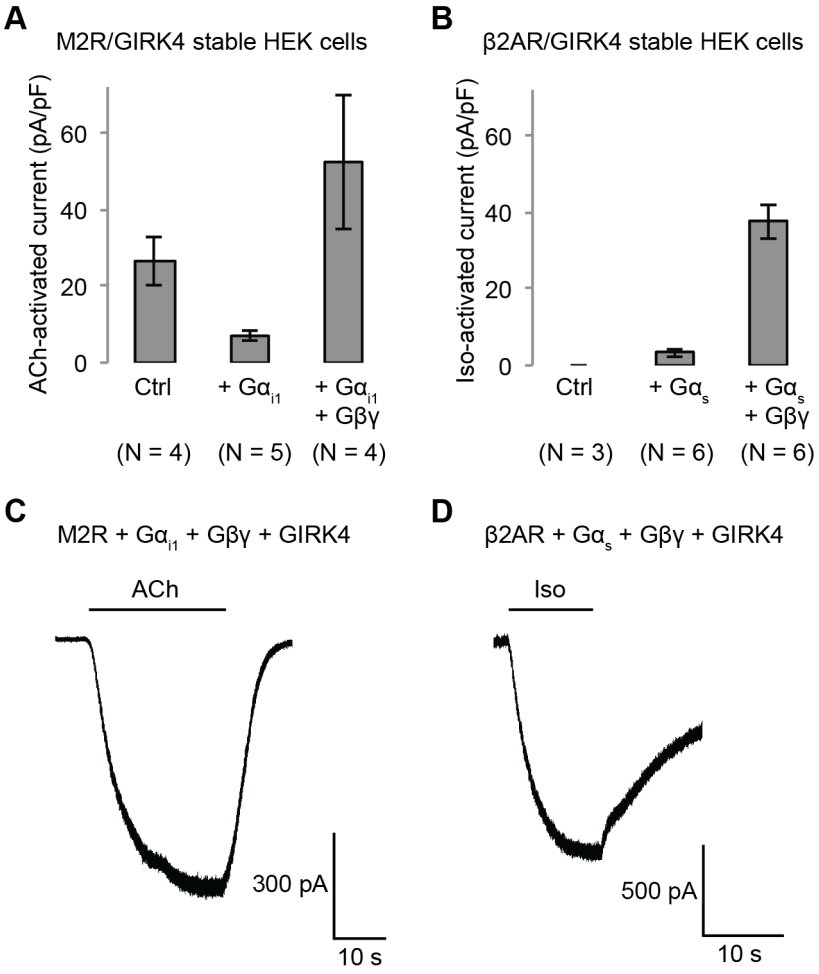

Figure 4.1. Influence of G protein levels on specificity (A) GIRK currents induced by M2R agonist ACh. Cells from a stable HEK293T cell line expressing M2Rs and GIRK channels were transiently transfected with a vector expressing either GFP (Ctrl), $G\alpha_{i1}$, or $G\alpha_{i1}$ and $G\beta\gamma$. 10 μM ACh was applied, and the evoked inward current was normalized to the capacitance of the cell (± SEM). (B) GIRK currents induced by β2AR agonist Iso. Cells from a stable HEK293T cell line expressing β2ARs and GIRK channels were transiently transfected with a control vector expressing either GFP, $G\alpha_s$, or $G\alpha_s$ and $G\beta\gamma$. 10 μM Iso was applied, and the evoked inward current was normalized to the capacitance of the cell (± SEM). (C) A representative voltage-clamp recording of HEK293T cells stably expressing M2Rs and GIRK. The cells were transiently transfected with $G\alpha_{i1}$ and $G\beta\gamma$. (D) A representative voltage- clamp recording of HEK cells stably expressing β2ARs and GIRK. The cells were transiently transfected with $G\alpha_s$ and $G\beta\gamma$.

4.2 DIRECT MEASURE OF THE Gβγ-GIRK INTERACTION

I explored the influence of G protein levels further using a more direct measurement to estimate the Gβγ-GIRK interaction. After fusing the modified yellow fluorescent protein Venus to Gβγ and the bioluminescent protein Nano-Luciferase (NLuc) to GIRK (GIRK4-NLuc) I monitored their proximity by measuring the bioluminescent resonance electron transfer (BRET) ratio (Masuho et al, 2015). The idea is, following GPCR stimulation Gβγ-Venus separates from the GPCR-G protein complex and binds to GIRK4, bringing Venus close to NLuc on the channel and thus increasing the BRET ratio (Fig 4.2A).

Two initial controls were carried out. First, I examined the binding of Gβγ-Venus to the membrane anchored C-terminal PH domain of GRK3 fused to NLuc (masGRK3ct-NLuc), which is known to bind to Gβγ with ~20 nM affinity (Pitcher et al, 1992). This experiment produced a robust increase in the BRET signal following M2R stimulation (Fig 4.2B). Second, I examined the binding of Gβγ-Venus to Kir2.2 fused to NLuc. Kir2.2 is structurally similar to GIRK but does not bind to Gβγ. No change in BRET signal occurred following M2R stimulation (Fig 4.2C). These positive and negative controls imply that the BRET assay may be suitable for monitoring a specific interaction between GIRK and Gβγ subunits released following GPCR stimulation.

HEK cells were transiently transfected with M2Rs, Gβγ-Venus, GIRK4-NLuc, and varying concentrations of $G\alpha_{i1}$. The BRET signal was then monitored over time following ACh stimulation (Fig 4.2D). Even in the absence of additional $G\alpha_{i1,}$ the BRET signal showed a time-dependent increase, consistent with Gβγ-Venus being released from M2Rs and then binding to the GIRK channel. As the amount of $G\alpha_{i1}$ expression was increased the BRET signal increased further, consistent with more Gβγ-Venus being generated as a result of greater $G\alpha_{i1}$(GDP)βγ-

Figure 4.2. Direct measure of the Gβγ-GIRK interaction. (A) A schematic representation of the BRET assay. Upon agonist stimulation of a GPCR, Gβγ-Venus is released. Gβγ-Venus then binds to GIRK-NLuc, which increases the BRET signal. (C) A representative time-resolved BRET ratio curve from HEK293T cells expressing M2Rs, $G\alpha_{i1}$, Gβγ-Venus, and masGRK3ct-NLuc, which is known to interact with Gβγ. (D) A representative time-resolved BRET ratio curve from HEK293T cells expressing M2Rs, $G\alpha_{i1}$, Gβγ-Venus, and Kir2.2-NLuc, another inward-rectifier K^+ channel that is structurally similar to GIRK but does not bind to Gβγ. (D)(E) Representative changes in BRET signal upon stimulation of GPCRs. In (D), HEK293T cells were transfected with M2Rs, Gβγ-Venus, GIRK-NLuc, and increasing amounts of $G\alpha_{i1}$. In (E), HEK293T cells were transfected with β2ARs, Gβγ-Venus, GIRK-NLuc, and increasing amounts of $G\alpha_s$. Agonists were applied at t = 5 sec.

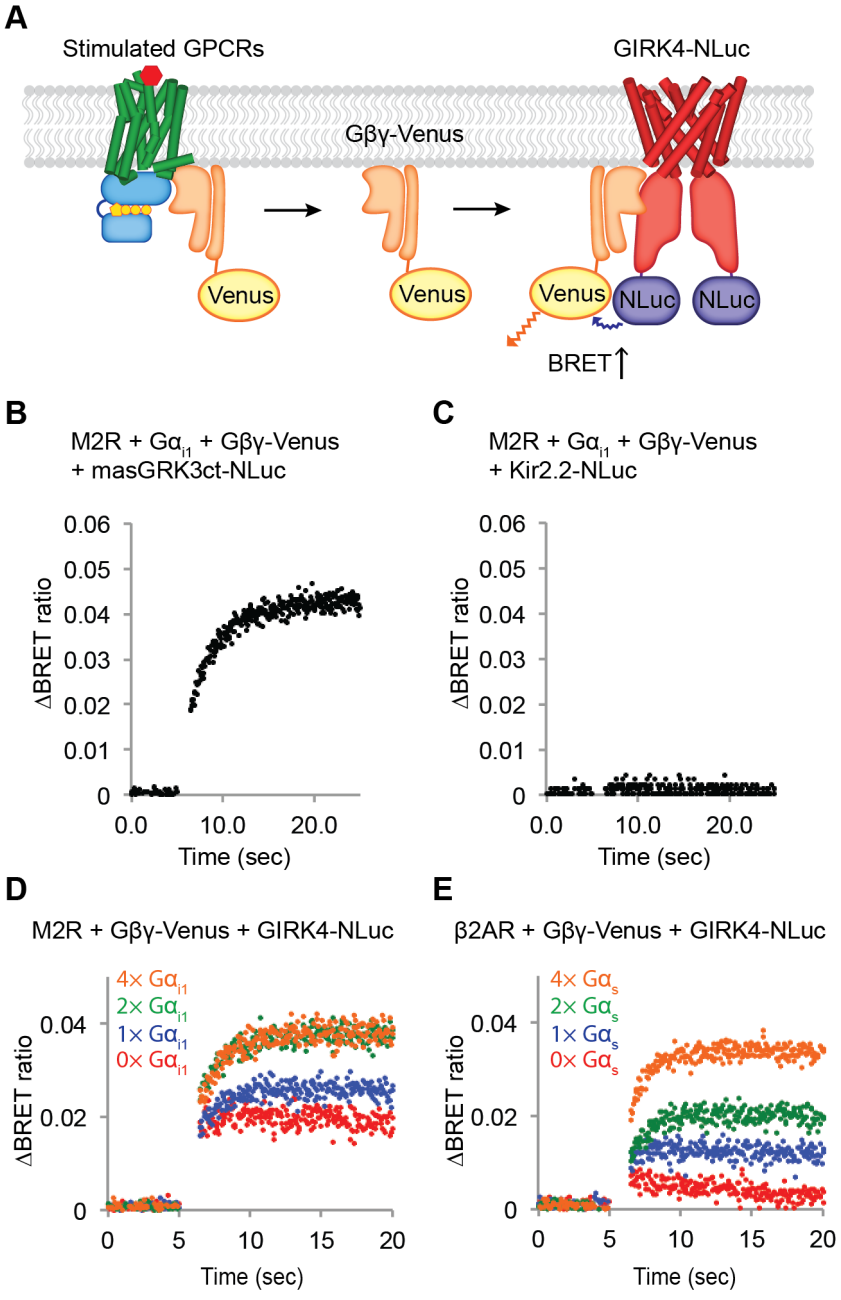
A
Stimulated GPCRs
GIRK4-NLuc
Gβγ-Venus
Venus
Venus
Venus
NLuc
NLuc
BRET
B
M2R + Gαi1 + Gβγ-Venus
+ masGRK3ct-NLuc
ΔBRET ratio
0.06
0.05
0.04
0.03
0.02
0.01
0
0.0
10.0
20.0
Time (sec)
C
M2R + Gαi1 + Gβγ-Venus
+ Kir2.2-NLuc
ΔBRET ratio
0.06
0.05
0.04
0.03
0.02
0.01
0
0.0
10.0
20.0
Time (sec)
D
M2R + Gβγ-Venus + GIRK4-NLuc
4× Gαi1
2× Gαi1
1× Gαi1
0× Gαi1
ΔBRET ratio
0.04
0.02
0
0
5
10
15
20
Time (sec)
E
β2AR + Gβγ-Venus + GIRK4-NLuc
4× Gαs
2× Gαs
1× Gαs
0× Gαs
ΔBRET ratio
0.04
0.02
0
0
5
10
15
20
Time (sec)

Venus substrate availability. Note that this result is not inconsistent with the reduced current generated in Figure 4.1A upon excess $G\alpha_{i1}$ expression because in the BRET experiment (Fig 4.2D) Gβγ-Venus is also over-expressed. As the level of $G\alpha_{i1}$ expression is increased a maximum BRET signal is reached, suggesting that an aspect of this signaling pathway other than $G\alpha_{i1}$ availability eventually becomes limiting. When the same experiment was carried out with the β2AR almost no change in the BRET signal was observed in the absence of $G\alpha_s$ transfection (Fig 4.2E), consistent with the failure of β2AR stimulation (in the absence of $G\alpha_s$ transfection) to activate GIRK channels (Fig 4.1B). In accord with the ability of $G\alpha_s$ and Gβγ overexpression to over-ride specificity and permit β2AR-stimulated GIRK current (Fig 4.1D), the BRET ratio increased with increased expression of $G\alpha_s$ (and Gβγ-Venus) (Fig 4.2E). The electrophysiological and BRET assays are in complete agreement with each other and suggest that specificity in $G\alpha_i$-coupled GPCR signaling results from higher Gβγ concentrations achieved when $G\alpha_i$-coupled receptors are stimulated compared to $G\alpha_s$-coupled receptors.

4.3 GENERALIZATION OF $G\alpha_i$-COUPLED GPCR TARGET SPECIFICITY

If specificity results from higher levels of Gβγ generated when $G\alpha_i$-coupled receptors are stimulated rather than from a specific protein-protein interaction and localization of the receptor with GIRK, then other targets upon which Gβγ acts might also exhibit similar specificity. To test this idea, I carried out experiments using the transient receptor potential melastatin 3 (TRPM3) channel, which is inhibited by direct binding of Gβγ (Fig 4.3A) (Bedheka et al, 2017; Quallo et al, 2017; Dembla et al, 2017). TRPM3 channels and M2Rs were transiently transfected into HEK cells and whole-cell voltage-clamp recordings were performed. TRPM3 channels were first activated by a chemical ligand, pregnenolone sulphate (PS), and then inhibited (85 ± 10%) by

stimulating M2R with Ach (Fig 4.3B and C). Similar experiments with Iso-stimulated β2ARs showed only modest inhibition (17 ± 10%), consistent with some degree of specificity as a result of there being insufficient concentrations of Gβγ generated by the $G\alpha_s$-coupled pathway (Fig 4.3 B and D). As in GIRK experiments, specificity is lost when $G\alpha_s$ and Gβγ are overexpressed (inhibition 73 ± 14%) (Fig 4.3 B, E, and F). These observations further strengthen the idea that $G\alpha_i$-coupled receptors generate higher concentrations of Gβγ in the setting of endogenous G protein concentrations and that these higher Gβγ levels account for Gβγ specificity. These observations also further reject the macromolecular supercomplex hypothesis as a tenable explanation, because similar Gβγ specificity is observed with a completely different protein target of the Gβγ pathway.

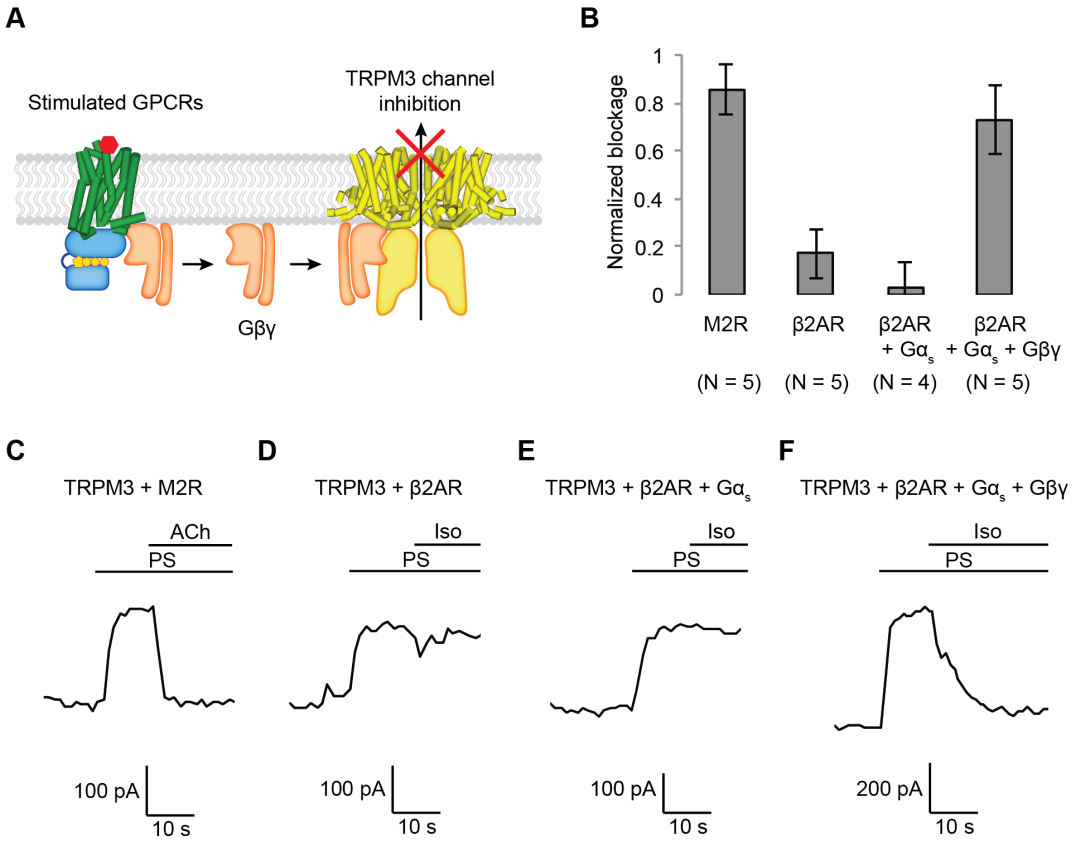

Figure 4.3. Generalization of $G\alpha_i$-coupled GPCR target specificity. (A) A schematic representation of TRPM3 channel inhibition by Gβγ. Upon agonist stimulation, released Gβγ directly binds to and inhibits TRPM3 channels. (B) The amount of current blocked upon GPCR stimulation was normalized to the first peak current (± SEM). (C)-(F) Representative voltage-clamp recordings of HEK293T cells transiently transfected with (C) TRPM3 and M2Rs (D) TRPM3 and β2ARs (E) TRPM3, β2ARs, and $G\alpha_s$, or (F) TRPM3, β2ARs, $G\alpha_s$, and Gβγ. A ramp protocol from -100 mV to +100 mV was applied to the cells every second. The currents at +100 mV were plotted. TRPM3 currents were evoked by 10 μM pregnenolone sulfate (PS). M2Rs and β2ARs were stimulated by 10 μM ACh and Iso, respectively.

4.4 RELATIVE RATES OF Gβγ RELEASE BY $G\alpha_i$ VERSUS $G\alpha_s$-COUPLED GPCRs

By what mechanisms do M2Rs generate higher Gβγ concentrations than β2ARs? If $G\alpha_i$ subunits were more abundant in cells than $G\alpha_s$ subunits then higher rates of Gβγ generation would be expected. This explanation seems unlikely though, because the endogenous levels of $G\alpha_s$ in HEK cells are actually higher than $G\alpha_i$ when we measure levels directly using a Western blot assay in the same cells (Fig 4.4). Higher levels of $G\alpha_s$ in HEK cells were also reported previously on the basis of RNA levels (Atwood et al, 2011).

Alternatively, differences in the affinity of Gβγ for $G\alpha_s$-GTP versus $G\alpha_i$-GTP could potentially account for differences in the levels of free Gβγ generated during β2AR versus M2R stimulation. To test this possibility, I assessed the relative ability of $G\alpha_s$-GTP versus $G\alpha_{i1}$-GTP to bind to Gβγ. Because the affinity of GTP-bound forms of Gα for Gβγ are so low we contrived the experiment shown in Figure 4.5A. GIRK channels and Gβγ were reconstituted into planar lipid bilayers at a mass ratio of ~ 1 : 0.1. In the presence of 8 mM Na^+ and 32 μM C8-PIP_2 a fraction of GIRK channels are activated in the context of limiting Gβγ concentration (Fig 4.6A). Under this condition, sufficiently high concentrations of Gα(GTPγS) can inhibit GIRK activation through competition by binding to Gβγ. Thus, known amounts of $G\alpha_{i1}$(GTPγS) or $G\alpha_s$(GTPγS) were added by replacing the lipid tail with a His_{10} tag and including in the bilayer 3% Ni-NTA lipids. $G\alpha_{i1}$(GTPγS) and $G\alpha_s$(GTPγS) bind to lipid membranes containing Ni-NTA lipids with ~ 500 nM affinity (Fig 4.6B-D). After saturation of Ni-NTA lipids these conditions should yield a Gα(GTPγS) concentration adjacent to the membrane ~ 3 mM (Wang et al, 2016; Touhara et al, 2016). Inhibition of GIRK current was observed, but with no significant difference between $G\alpha_{i1}$(GTPγS) and $G\alpha_s$(GTPγS), suggesting that their affinities for Gβγ are similar (Fig 4.5B-D).

Thus, lower Gβγ concentrations following $G\alpha_s$-coupled receptor stimulation cannot be attributed to sequestration by $G\alpha_s$(GTP).

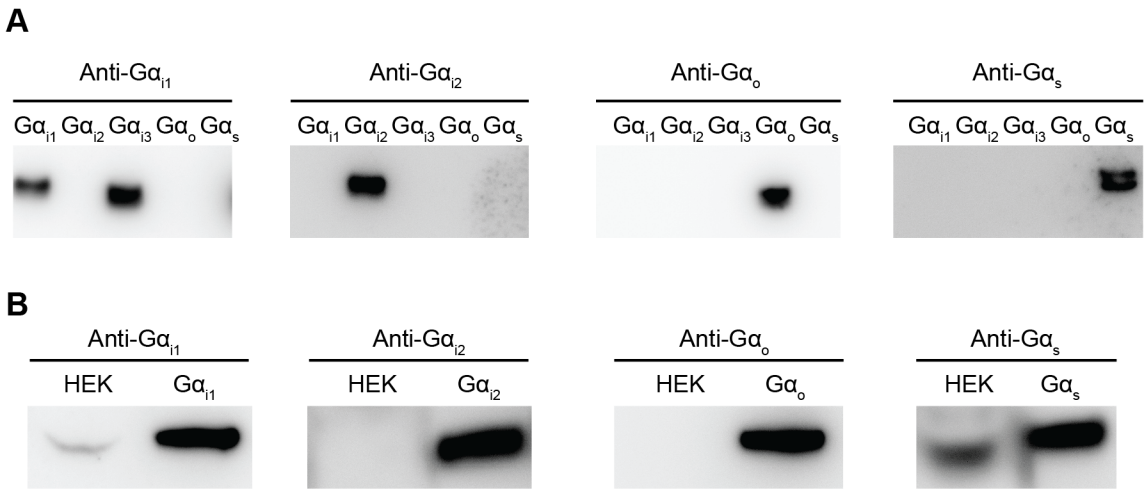

Figure 4.4. Comparison of endogenous Gα levels in HEK293T cells.

(A) Evaluation of antibody specificity. Different Gα proteins were heterologously expressed, purified and analyzed by Western Blot. Anti-$G\alpha_{i1}$ antibody recognizes both $G\alpha_{i1}$ and $G\alpha_{i3}$. Anti-$G\alpha_{i2}$, $G\alpha_o$, and $G\alpha_s$ antibodies specifically recognize their target Gα. (B) Comparison of endogenous Gα levels in HEK293T cells. HEK293T cells were lysed and analyzed by Western Blot. 5 ng of purified Gα was loaded as a reference.

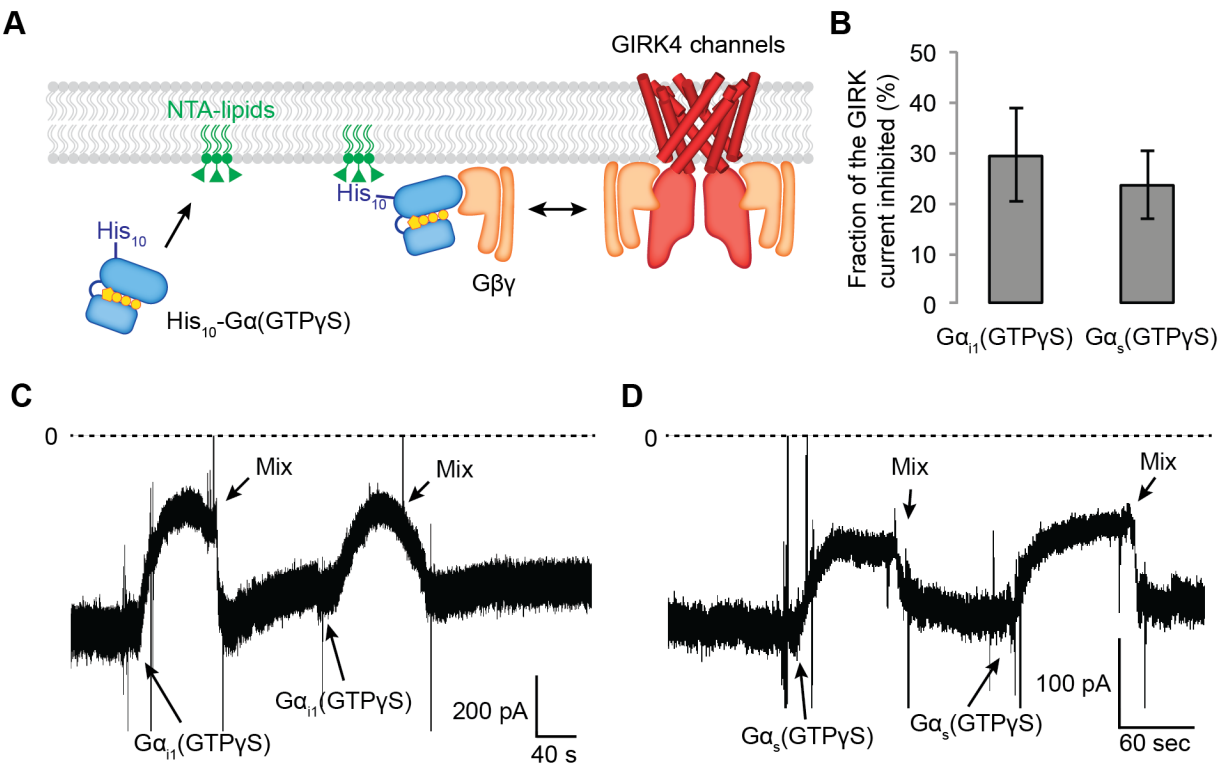

Figure 4.5. $G\alpha_s$(GTPγS) and $G\alpha_{i1}$(GTPγS) do not differentially compete with GIRK channels for Gβγ. (A) A schematic representation of the competition assay between His_{10}-Gα(GTP-γS) and GIRK for Gβγ in a reconstituted planar lipid bilayer system. In these experiments, we controlled the amount of lipid-associated Gα(GTP-γS) to quantitatively evaluate the competition. We first incorporated a fixed amount of Ni-NTA-lipids into the lipid bilayer and applied enough His_{10}-Gα(GTP-γS) to saturate all the available Ni-NTA binding sites (Figure 4.6B-4.6D). Tethered His_{10}-Gα(GTP-γS) could compete with GIRK for Gβγ and therefore inhibits GIRK. (B) Current inhibition by His_{10}-Gα(GTP-γS) was normalized to the initial current levels (N = 3, ± SD). (C)(D) Representative inward GIRK currents from lipid bilayers. GIRK was partially activated by PIP_2, Na^+, and a low concentration of Gβγ. Dashed lines represent the baseline current (0 pA). (C) His_{10}-$G\alpha_{i1}$(GTP-γS) or (D) His_{10}-$G\alpha_s$(GTP-γS) was directly perfused to the bilayer membrane several times followed by mixing the solutions in the bilayer chamber. The transient decrease in the current upon Gα(GTP-γS) application is an artifact due to the absence of Na^+ in His_{10}-Gα(GTP-γS) solution.

Figure 4.6. Purified His_{10}-Gα(GTPγS) binds to the GUV membrane containing Ni-NTA lipids. (A) GIRK channels were partially activated by low amounts of Gβγ. Proteoliposomes containing GIRK and Gβγ at a ratio of 1 : 0.1 (wt : wt) were fused to the planar lipid bilayer membrane. GIRK was then activated by adding 32 μM C8-PIP_2 and 32 mM Na^+ to the bilayer chamber (left trace). Subsequently GIRK was fully activated by fusing Gβγ vesicles (right trace). The ~5 fold increase in the inward GIRK current suggests the partial activation of GIRK channels due to the presence of limiting amounts of Gβγ in the left trace. (B) Typical confocal images of the giant unilamellar vesicle (GUV) equator planes. The corresponding concentration of Alexa Fluor 488-labeled His_{10}-$Gα_{i1}$(GTP-γS) is indicated. (C)(D) Gα(GTP-γS) binding curves to GUVs. The fluorescence intensities measured at different protein concentrations were fitted using a 1:1 binding model.

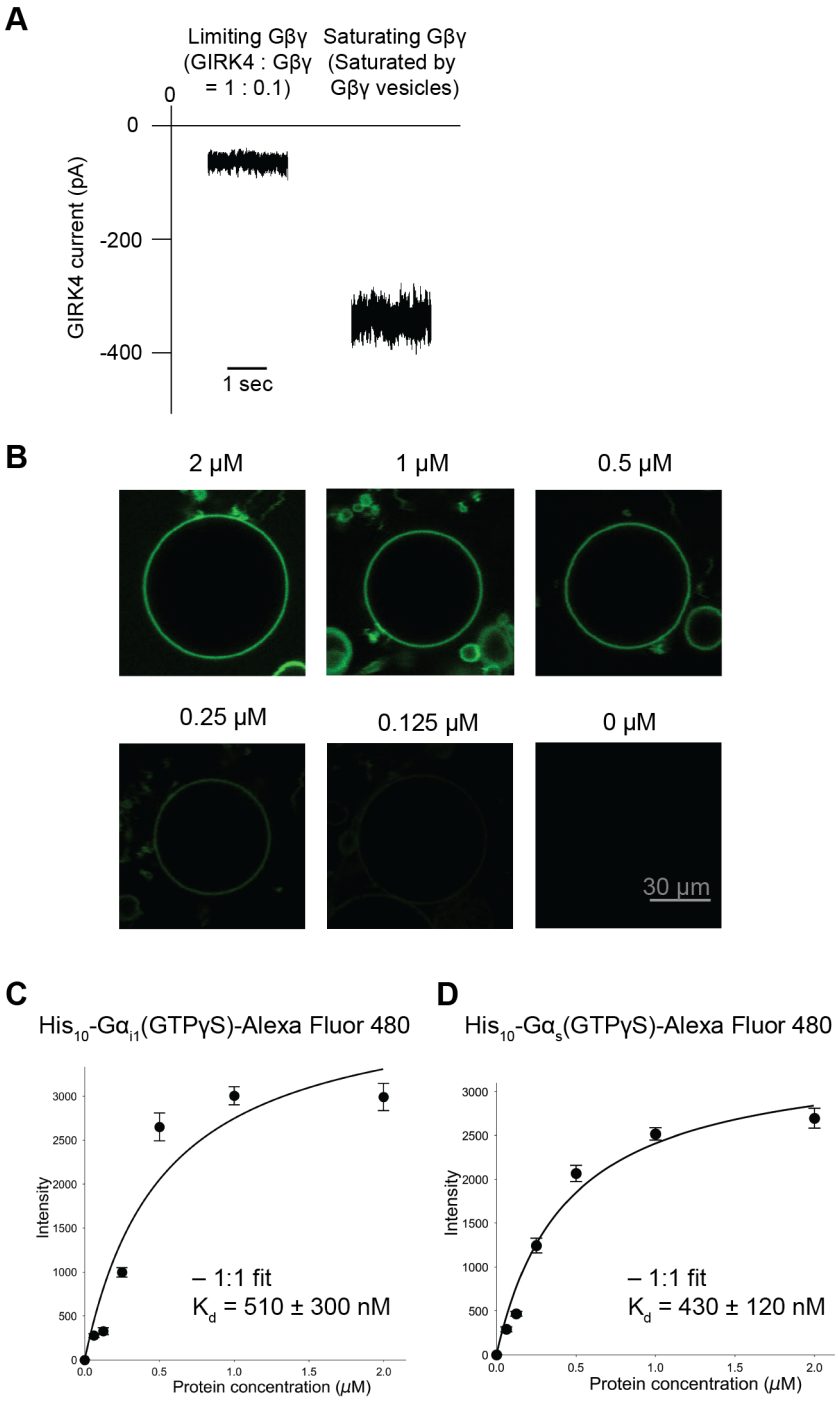
A
Limiting Gβγ (GIRK4 : Gβγ = 1 : 0.1)
Saturating Gβγ (Saturated by Gβγ vesicles)
0
0
-200
-400
GIRK4 current (pA)
1 sec
B
2 μM
1 μM
0.5 μM
0.25 μM
0.125 μM
0 μM
30 μm
C
His10-Gαi1(GTPγS)-Alexa Fluor 480
Intensity
Protein concentration (μM)
– 1:1 fit
Kd = 510 ± 300 nM
D
His10-Gαs(GTPγS)-Alexa Fluor 480
Intensity
Protein concentration (μM)
– 1:1 fit
Kd = 430 ± 120 nM

Next, I tested the possibility that $G\alpha_i$-coupled receptors catalyze intrinsically faster $G\beta\gamma$ release. I developed an assay by attaching Venus to $G\alpha$, NLuc to $G\beta\gamma$, and measured the BRET ratio change to monitor GPCR-mediated dissociation of $G\beta\gamma$-NLuc from $G\alpha$-Venus (Fig 4.7A). I also expressed masGRK3ct in the same cells to sequester $G\beta\gamma$-NLuc once it is released, thus reducing the extent to which $G\beta\gamma$-NLuc will rebind to $G\alpha$-Venus. Two different $G\alpha$-Venus insertion constructs were made – into the αa-αb loop or into the αb-αc loop of $G\alpha$ – to ensure that the observed behavior does not depend on the site of insertion (Fig 4.7B). Prior to GPCR stimulation N-Luc intensity and BRET ratio were nearly constant and approximately similar in magnitude in all experiments (Fig 4.8 and Table 4.1). Following GPCR stimulation the BRET ratio change was minimal for the β2AR but approximately 10-fold greater for M2R. Similar experiments were also carried out with the $G\alpha_i$-coupled dopamine receptor (D2R), which activates GIRK (Fig 4.9A), and the $G\alpha_s$-coupled β1AR, showing again that $G\beta\gamma$-dissociation from $G\alpha$ is much greater for the $G\alpha_i$-coupled receptor (Fig 4.9B and C). I conclude from these experiments that the $G\alpha_i$-coupled receptors M2R and D2R generate more rapid $G\beta\gamma$ release than the $G\alpha_s$-coupled receptors β1AR and β2AR due to a higher intrinsic turnover rate.

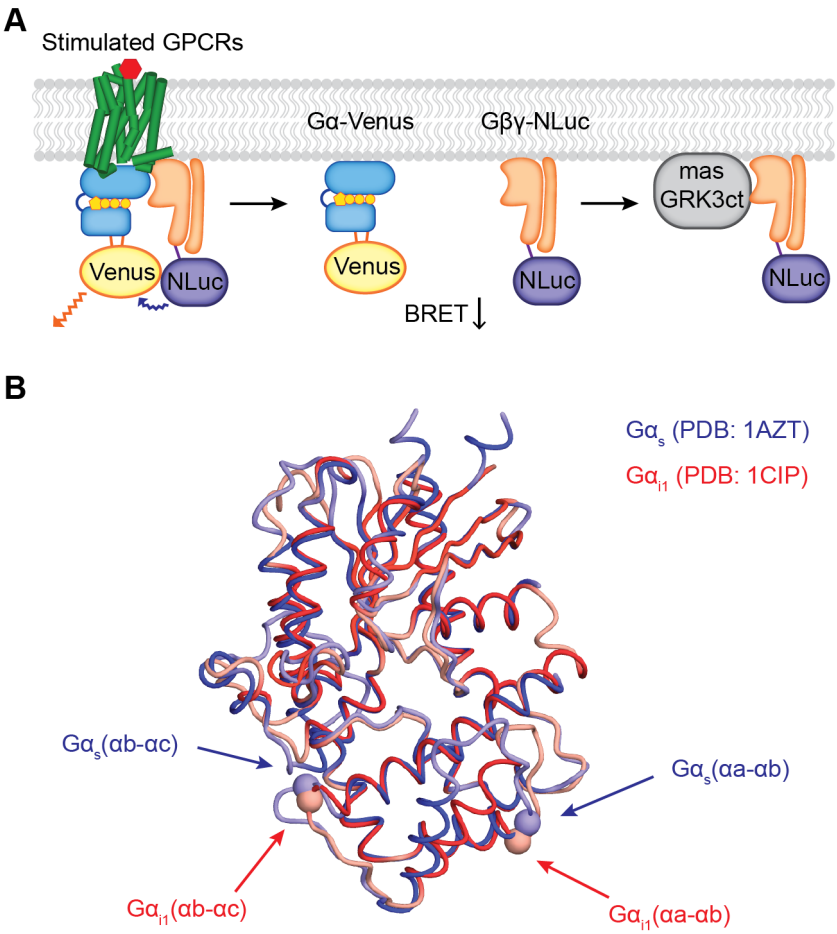

Figure 4.7. Schematic representation of the experimental design used to monitor dissociation of Gα-Venus and Gβγ-NLuc upon agonist stimulation of GPCRs measured by BRET. (A) A schematic representation of the experiment that monitors Gβγ release by BRET. Upon agonist stimulation, GPCRs release Gα and Gβγ. The dissociation of Gα-Venus and Gβγ-NLuc results in a decrease of the BRET signal. Released Gβγ-NLuc was chelated by masGRK3ct, a fusion of the C-terminal PH domain of GRK3 and a myristic acid attachment peptide. (B) Structural comparison between $G\alpha_s$ and $G\alpha_{i1}$. Crystal structures of $G\alpha_s$ (Blue, PDB: 1AZT) and $G\alpha_{i1}$ (Red, PDB: 1GG2) were superimposed. The Venus insertion sites are indicated as arrows. The Cα atoms of residues $G\alpha_s$-113 and 144, and $G\alpha_{i1}$-91 and 121 are represented as spheres.

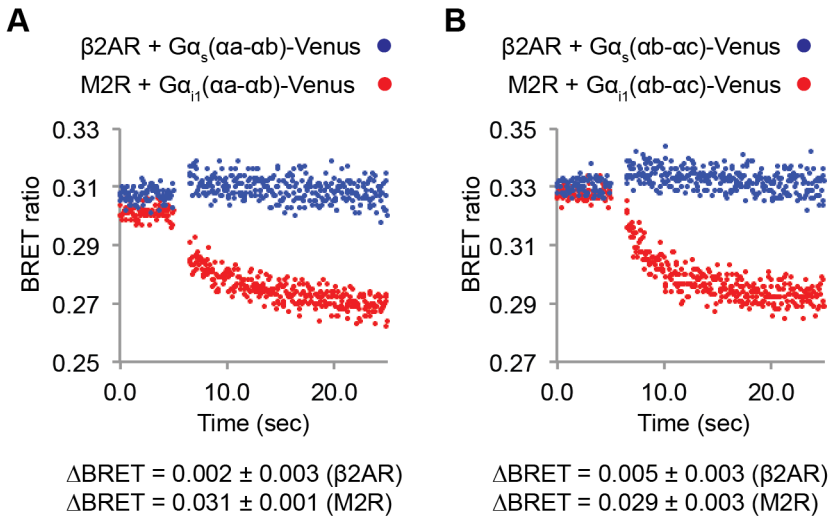

Figure 4.8. M2Rs catalyze release of Gβγ at higher rates compared to β2ARs. (A)(B) Representative time-resolved BRET ratio curves obtained using different GPCRs and different Gα-Venus constructs. HEK cells were co-transfected with GPCRs, Gβγ-NLuc, masGRK3ct, and $G\alpha_{i1}$(αa-αb)-Venus or $G\alpha_{i1}$(αb-αc)-Venus for M2Rs, and $G\alpha_{s}$(αa-αb)-Venus or $G\alpha_{s}$(αb-αc)-Venus for β2ARs. The averaged ΔBRET ratio was shown below each plot (N = 3-4, ± SD).

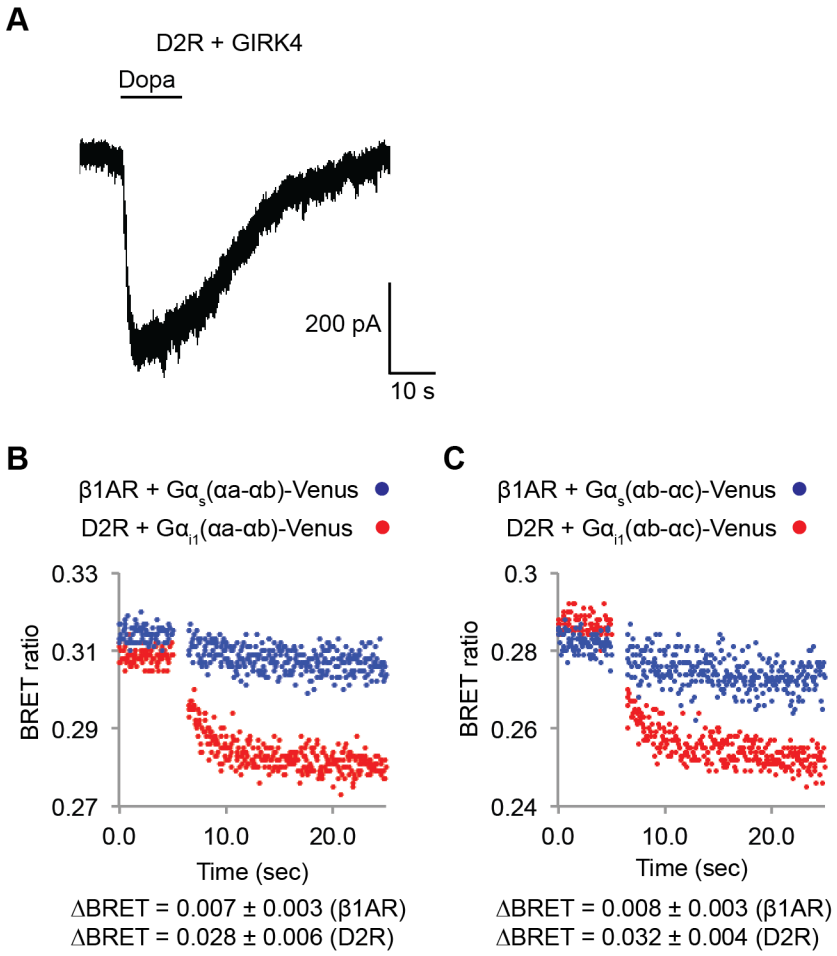

Figure 4.9. D2Rs catalyze release of Gβγ at higher rates compared to β1ARs. (A) D2Rs activate GIRK4 channels in HEK cells. HEK cells were transiently transfected with D2Rs and GIRK4 channels. Whole-cell voltage-clamp recordings were performed. Membrane potential was held at -80 mV in the presence of 100 mM extracellular KCl. 10 μM Dopamine (Dopa) was applied as indicated above the signal. (B)(C) Time-resolved BRET ratio curves obtained using different GPCRs and different Gα-Venus constructs. HEK cells were co-transfected with GPCRs, Gβγ-NLuc, masGRK3ct, and $G\alpha_{i1}$(αa-αb)-Venus or $G\alpha_{i1}$(αb-αc)-Venus for D2Rs, and $G\alpha_s$(αa-αb)-Venus or $G\alpha_s$(αb-αc)-Venus for β1ARs.

Table 4.1. Quantitative-BRET measurements of Gβγ release from different Gα constructs. Averaged Nano-Luc intensity, basal BRET ratio, and ΔBRET ratio were calculated (N = 3-4, ± SD).

	Luc (480)	Basal BRET	ΔBRET
M2R-Gα_{i1}(αa-αb)	1385K ± 36K	0.301 ± 0.003	0.031 ± 0.002
β2AR-Gα_{s}(αa-αb)	1191K ± 280K	0.310 ± 0.007	0.002 ± 0.006
M2R-Gα_{i1}(αb-αc)	808K ± 177K	0.310 ± 0.014	0.029 ± 0.006
β2AR-Gα_{s}(αb-αc)	864K ± 262K	0.311 ± 0.014	0.005 ± 0.005

(N = 4, ± SD)

	Luc (480)	Basal BRET	ΔBRET
D2R-Gα_{i1}(αa-αb)	2329K ± 146K	0.312 ± 0.005	0.028 ± 0.006
β1AR-Gα_{s}(αa-αb)	2451K ± 109K	0.315 ± 0.007	0.007 ± 0.003
D2R-Gα_{i1}(αb-αc)	558K ± 431K	0.287 ± 0.001	0.032 ± 0.004
β1AR-Gα_{s}(αb-αc)	777K ± 34K	0.279 ± 0.004	0.008 ± 0.003

(N = 3, ± SD)

4.5 KINETIC MODEL OF Gβγ SPECIFICITY

Rod and I developed a kinetic model for GIRK activation to test whether we could replicate Gβγ-specificity on the basis of differences in $G\alpha_i$ versus $G\alpha_s$-coupled receptor turnover rates. The model consists of a G protein turnover reaction cycle and a GIRK-Gβγ binding reaction that leads to channel activation (Fig 4.10A). Numerous studies have provided estimates for rate constants in the reaction cycle (Table 4.2) (Breitwieser and Szabo, 1988; Sarvazyan et al, 1998; Sungkaworn et al, 2017). The GIRK-Gβγ binding reaction has been studied in great detail. Dr. Weiwei wang and I have determined the affinity between Gβγ and GIRK (Wang et al, 2016), but his unpublished data suggests that the affinity is most likely ~5 times higher in physiological conditions. These published and unpublished data provides good estimates for k_{56} and k_{65} as well as a cooperativity factor μ (Shea et al, 1997; Wang et al, 2016; Touhara et al, 2016).

The G protein reaction cycle models the conversion of Gα(GDP)βγ (the G protein trimer) into Gα(GTP) and Gβγ in two kinetic transitions. The first transition (k_{12}) describes the formation of a productive complex between the G protein trimer and an active (ligand-bound) GPCR (R*). The second (k_{23}) combines multiple reactions, including GDP/GTP exchange and Gα(GTP) and βγ dissociation. In our experiments, the observation that G protein over-expression increases levels of stimulated Gβγ in cells (Fig 4.1 and 4.3) implies that the k_{12} transition is to some extent rate-limiting under physiological G protein conditions. A single molecule study of the α2 adrenergic receptor (α2AR; a $G\alpha_i$-coupled GPCR) also concluded that complex formation between activated receptor and G protein trimer (i.e. the k_{12} transition) was rate-limiting (Sungkaworn et al, 2017). Furthermore, the same study found that k_{12} for the β2AR was ten times smaller than for the α2AR.

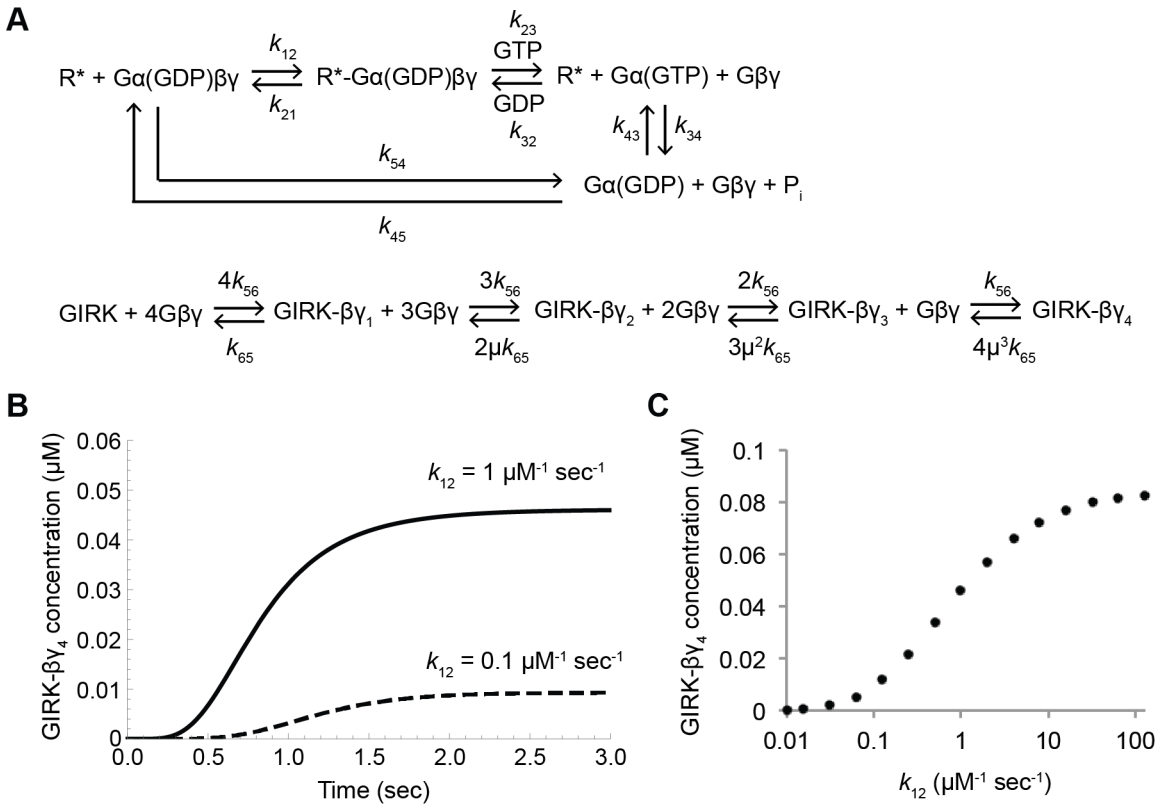

Figure 4.10. Kinetic model of Gβγ specificity. (A) Reaction scheme used to model GPCR activation of GIRK. k_{xy} are the rate constants of the reactions between two G protein states. Rate, equilibrium and cooperativity constants are summarized in Table S2. (B) Calculated GIRK-$\beta\gamma_4$ concentration as a function of time for two different k_{12} magnitudes are shown in black. (C) Calculated steady state GIRK-$\beta\gamma_4$ concentration as a function of k_{12} magnitude.

Table 4.2. Parameters used for the simulation of GIRK activation by GPCRs. k_{12}: The rate of formation of the productive GPCR-G protein complex (Sungkaworn et al, 2017). k_{21}: The rate of dissociation of the productive GPCR-G protein complex (Sungkaworn et al, 2017). k_{23}: The rate of nucleotide exchange and subsequent dissociation of GPCRs, Gα(GTP), and Gβγ (Sungkaworn et al, 2017). k_{32}: The rate of the reverse reaction of nucleotide exchange and dissociation of GPCRs and G proteins. k_{34}: The rate of GTP hydrolysis, based on Breitwieser and Szabo, 1988. k_{43}: The rate of the reverse reaction of GTP hydrolysis. k_{45}: The on-rate between Gα(GDP) and Gβγ, adapted from Sarvazyan et al, 1998. k_{54}: The off-rate between Gα(GDP) and Gβγ, calculated based on k_{45} and K_d = 3 nM (Sarvazyan et al, 1998). k_{56}: The on-rate between the GIRK and Gβγ is diffusion limited (Shea et al, 1997). k_{65}: The off-rate between the GIRK and Gβγ were calculated based on k_{56} and our previous K_d measurement (Wang et al, 2016).

Reaction	Forward-rate	Backward-rate	Note
$R^* + G\alpha(GDP)\beta\gamma \underset{k_{21}}{\overset{k_{12}}{\rightleftarrows}} R^*\text{-}G\alpha(GDP)\beta\gamma$	1 μM^{-1} sec^{-1} (k_{12})	1 sec^{-1} (k_{21})	Sungkaworn et al, 2017
$R^*\text{-}G\alpha(GDP)\beta\gamma \underset{GDP}{\overset{k_{23}}{\overset{GTP}{\rightleftarrows}}} R^* + G\alpha(GTP) + G\beta\gamma$ (k_{32})	1 sec^{-1} (k_{23})	0 M^{-2} sec^{-1} (k_{32})	Sungkaworn et al, 2017
$G\alpha(GTP) \underset{k_{43}}{\overset{k_{34}}{\rightleftarrows}} G\alpha(GDP) + P_i$	2 sec^{-1} (k_{34})	0 M^{-1} sec^{-1} (k_{43})	Breitwieser and Szabo, 1988
$G\alpha(GDP) + G\beta\gamma \underset{k_{54}}{\overset{k_{45}}{\rightleftarrows}} G\alpha(GDP)\beta\gamma$	0.7 × 10^6 M^{-1} sec^{-1} (k_{45})	0.002 sec^{-1} (k_{54})	Sarvazyan et al, 1998
$GIRK\text{-}\beta\gamma_{n-1} + (5\text{-}n)G\beta\gamma \underset{n\mu^{n-1}k_{65}}{\overset{(5-n)k_{56}}{\rightleftarrows}} GIRK\text{-}\beta\gamma_n + (4\text{-}n)G\beta\gamma$ (n = 1-4, μ = 0.3)	(5-n) × 1 × 10^7 M^{-1} sec^{-1} ((5-n) × k_{56})	n × μ^{n-1} × 600 sec^{-1} (n × μ^{n-1} × k_{65})	Wang et al, 2016. Shea et al, 1997.

GPCR density over the entire membrane of atrial cardiac myocytes and in CHO cells is approximately 5 μm^{-2} (Nenasheva et al, 2013). However, G protein signaling occurs within 'hotspots' that we estimate to cover about 10% of the membrane surface (Sungkaworn et al, 2017). Thus, we assume the receptor density to be 50 μm^{-2} within a hotspot and assume an initial $G\alpha(GDP)\beta\gamma$ density of 100 μm^{-2}. When the reaction is switched on (i.e. ligand stimulation) at t = 0 by changing k_{12} from 0 to 0.2 μm^2 $molecule^{-1}$ sec^{-1} (Sungkaworn et al, 2017), $G\beta\gamma$ concentration increases (along with time-dependent concentration changes of other components) and GIRK channels activate to a steady state value within a few seconds following a time course similar to M2R stimulated GIRK currents in SAN cells (Fig 4.11). We note that time courses vary from cell to cell, but that the modeled time course falls within the experimental range.

To model the β2AR receptor we reduced k_{12} ten times, consistent with Sungkaworn et al, leaving all other quantities the same. Lower concentrations of $G\beta\gamma$ are predicted and along with significantly less GIRK activation (Fig 4.10B). Fig 4.10C displays in greater detail calculated GIRK-$(G\beta\gamma)_4$ concentration (i.e. channel activation) as a function of k_{12} magnitude. A steep dependence occurs right around the experimentally determined value for the $G\alpha_i$-coupled receptor turnover rate constant (Sungkaworn et al, 2017). Thus, the model predicts that higher rates of G protein turnover catalyzed by $G\alpha_i$-coupled compared to $G\alpha_s$-coupled GPCRs can account for $G\beta\gamma$ specificity.

Partial agonists by definition activate GPCRs with reduced efficacy compared to full agonists. The effects of two partial agonists, oxotremorine and pilocarpine, on M2R activation of GIRK are shown (Fig 4.12A and B). A study recently concluded that for the β2AR, the distinction between partial and full agonist action lies in the magnitude of k_{12}, its value being smaller for partial agonists (Gregorio et al, 2017). We think this conclusion likely applies to

M2R as well, based on the following observations. When the partial agonists oxotremorine and pilocarpine are used to stimulate M2R, reduced GIRK currents are associated with reduced BRET signals for Gβγ-Venus binding to GIRK-NLuc (blue symbols in Figure 4.12C). Furthermore, when amounts of available $G\alpha_{i1}$ are increased (so that more $G\alpha_{i1}$(GDP)βγ-Venus can form), the partial agonist oxotremorine gives rise to a BRET signal as strong as that of acetylcholine (orange symbols in Figure 4.12C). A similar effect was also observed with pilocarpine, although to a lesser extent. These results are explicable on the basis of the G protein trimer-GPCR on-rate determining the efficacy of different agonists. Thus, k_{12} can explain the difference in agonists versus partial agonists as well as the fundamental difference between M2R and βARs with respect to their ability to activate GIRK channels. In the model we present, k_{12}, is rate limiting under physiological G protein concentrations, and its magnitude determines differential rates of Gβγ generation.

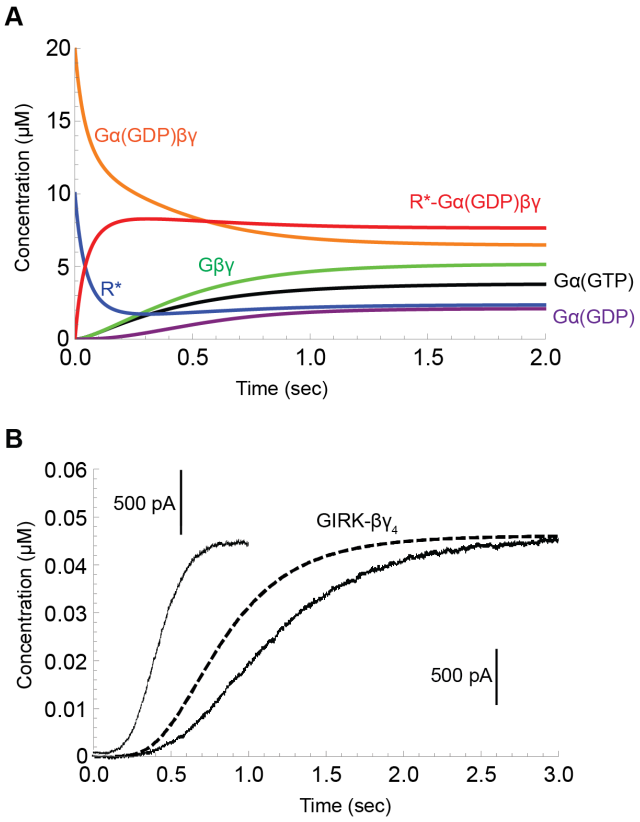

Figure 4.11. The simulation of GPCR-activation of GIRK. (A) Calculated receptor and G protein concentrations as a function of time (k_{12} = 1 μM^{-1} sec^{-1}). (B) ACh-stimulated GIRK currents from two different SAN cells are shown in solid lines. Calculated GIRK-$\beta\gamma_4$ concentration as a function of time is shown in a dashed line.

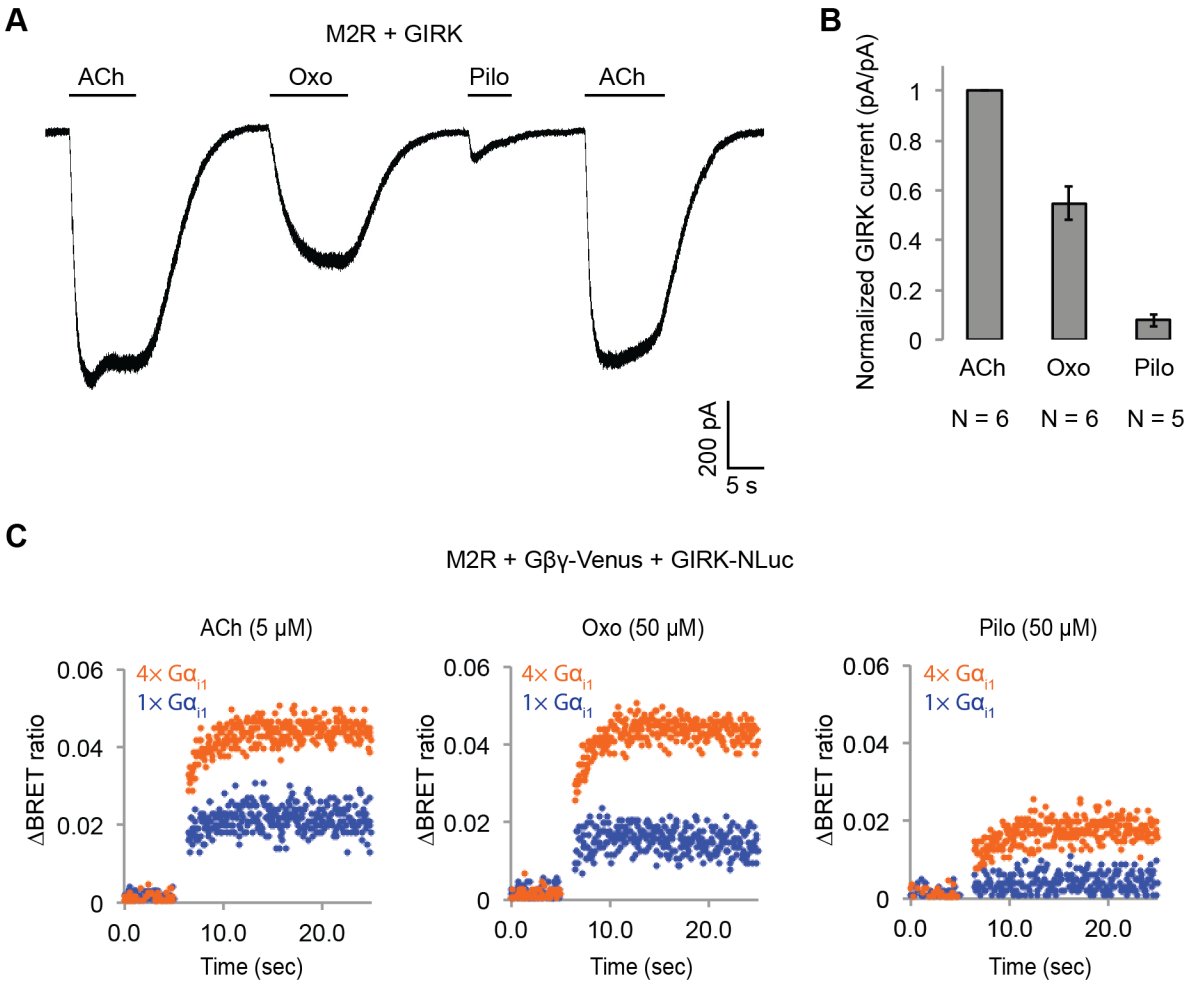

Figure 4.12. Influence of partial agonists to GPCR-activation of GIRK. (A) Muscarinic partial agonists activate GIRK channels to a limited extent. Whole-cell voltage-clamp recordings were performed on stable HEK293T cells expressing M2Rs and GIRK channels. The membrane potential was held at -80 mV. 10 μM ACh, 100 μM Oxotremorine (Oxo), or 100 μM Pilocarpine (Pilo) was applied as indicated. (B) Partial agonist-activated GIRK currents were normalized to ACh-activated GIRK currents (N = 5-6, ± SEM). (C) Representative changes in BRET signal upon stimulation of M2Rs with different agonists. HEK293T cells were transfected with M2Rs, Gβγ-Venus, GIRK-NLuc, and increasing amounts of $G\alpha_{i1}$. 5 μM acetylcholine (ACh), 50 μM oxotremorine (Oxo), or 50 μM pilocarpine (Pilo) was applied at t = 5 sec.

4.6 DISCUSSION AND CONCLUSIONS

The essential conclusion of this study is that M2R catalyzes the generation of Gβγ at a higher rate than β2AR, thus achieving higher concentrations of Gβγ to activate GIRK. The concentrations of $G\alpha_s$(GTP) generated by β2AR are obviously sufficient to stimulate the downstream-amplified $G\alpha_s$ pathway and speed heart rate, but the lower Gβγ levels generated are insufficient to activate GIRK to a great extent. The higher rate of Gβγ generation by M2R likely stems from an intrinsically higher rate of association with G protein trimer (Fig 4.13). This conclusion is most easily appreciated through careful inspection of Figures 4.2D and 4.2E, where it is shown that endogenous levels of Gα (in the presence of expressed Gβγ-Venus to detect Gβγ binding to GIRK) permit Gβγ generation by M2R, but not by β2AR. Furthermore, overexpression of Gα increases the rate of Gβγ generation in both cases, but higher levels of Gα expression are needed for the β2AR to reach its maximum rate. Thus, Gβγ specificity is explicable on the basis of a difference in the rate at which M2R and β2AR associate with G protein trimer, M2R being faster.

When G protein trimer associates with a GPCR, both Gα and receptor undergo a series of conformational changes (Rasmussen et al, 2011; Koehl et al, 2018; Kang et al, 2018; Draper-Joyce et al, 2018; Garcîa-Nafrîa et al, 2018). A chimera Gα subunit containing mostly $G\alpha_{i1}$ amino acids and only 13 C-terminal $G\alpha_s$ amino acids – that engage the receptor – is known to permit βAR activation of GIRK (Leaney et al, 2000). This observation suggests that the Gα conformational change, which involves the main body of the Gα subunit, is more important in determining the rate of G protein trimer-GPCR association.

The hypothesis that Gβγ specificity is based on a macromolecular supercomplex formed between M2R and GIRK seems unlikely as described in Chapter 3. This mechanism fails to

explain why different $G\alpha_i$-coupled GPCRs, such as M2R and D2R in this study, can activate GIRK (Fig 4.1 and Fig 4.9A). It also fails to explain why Gβγ specificity persists when GIRK is simply replaced by TRPM3 as the target in the signaling system (Fig 4.3). Furthermore the fact that most of processes depending on Gβγ downstream signaling are mediated by $G\alpha_i$-coupled GPCRs cannot be explained by the supercomplex hypothesis (Morris and Malbon, 1999; Smrcka, 2008). The simple kinetic explanation for Gβγ specificity based on differences in k_{12} seems consistent with available data.

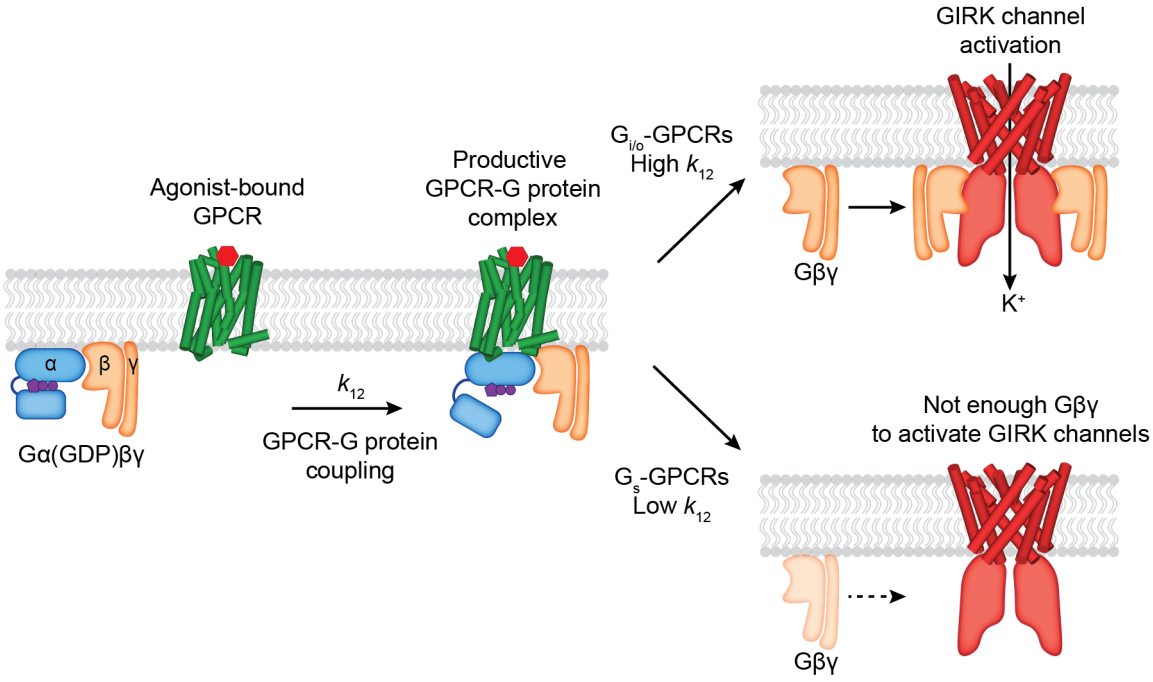

Figure 4.13. Schematic summary of the proposed molecular mechanism of specificity. Resting GPCRs and G protein heterotrimers randomly interact with each other. Upon agonist stimulation, an active GPCR and G protein undergo conformational changes to form a productive GPCR-G protein complex. The rate of this process is defined as k_{12}. In case of $G\alpha_i$-coupled receptors, k_{12} is fast enough to generate sufficient amounts of Gβγ to activate GIRK. In contrast, $G\alpha_s$-coupled receptors cannot activate GIRK due to the lower k_{12}.

CHAPTER 5: THE GIRK1 SUBUNIT POTENTIATES G PROTEIN ACTIVATION OF CARDIAC GIRK1/4 HETERO-TETRAMERS

Mammals express four GIRK channel subunits (GIRK1-4), forming various homo-tetramers and hetero-tetramers. Cardiac GIRK channels are composed of GIRK1 and GIRK4 subunits (Krapavinsky et al, 1995). Since the GIRK1 subunit does not form functional homo-tetramers, GIRK1 and GIRK4 subunits form functional GIRK1/4 hetero-tetramers and GIRK4 homo-tetramers in the heart (Krapavinsky et al, 1995; Chan et al, 1996; Corey and Clapham, 1998). GIRK1 and GIRK4 knockout mice show similar phenotypes in terms of heart rate (Bettahi et al, 2002), suggesting that both subunits perform non-redundant tasks. However, little is known about whether or how GIRK1 influences cardiac GIRK channel behavior. Specifically, what are the functional differences between GIRK1/4 hetero-tetramers and GIRK4 homo-tetramers?

Although GIRK1 and GIRK4 subunits share ~44% sequence identity, one notable difference occurs in the Na^+ binding site. The GIRK1 subunit has an aspartate to asparagine replacement in this Na^+ binding site, presumably rendering it incapable of binding intracellular Na^+ (Ho and Murrell-Lagnado, 1999b). However, it is still unclear what influence this defective Na^+ binding site has on the function of GIRK1/4 hetero-tetramers. Cellular electrophysiological

experiments have not clarified this issue because it is difficult to control the concentration of GIRK ligands inside cells, and it is also not possible to express GIRK1/4 hetero-tetramers without co-expression of GIRK4 homo-tetramers.

In this chapter, I will discuss my work, which addresses these questions by studying Gβγ and Na^+ regulation of GIRK1/4 and GIRK4 channels in the planar lipid bilayer system. First, I was able to purify both GIRK1/4 hetero-tetramers and GIRK4 homo-tetramers, and successfully reconstitute them into planar lipid bilayer membranes. Second, in collaboration with Dr Weiwei Wang, I established a method to quantitatively analyze the relationship between membrane Gβγ concentration and GIRK activity (Wang et al, 2016), and used the method to compare Gβγ activation of GIRK1/4 and GIRK4 channels. I found that the GIRK1 subunit behaves as if it is permanently bound to Na^+, and therefore potentiates Gβγ activation of GIRK1/4 channels. Finally, by investigating Na^+ activation of GIRK channels in cardiac myocytes, I found that cardiac GIRK channels are mostly composed of GIRK1/4 channels (Touhara et al, 2016).

5.1 PURIFICATION AND RECONSTITUTION OF GIRK1/4 HETERO-TETRAMERS

Although the GIRK1 subunit does not form functional homo-tetrameric channels, it does form structural homo-tetramers similar to GIRK4 (Fig 5.1). Therefore, in order to isolate GIRK1/4 hetero-tetramers, GIRK1 and GIRK4 homo-tetramers had to be removed during purification. To remove both homo-tetramers two different tags, a deca-histidine tag and a 1D4 peptide tag, were fused to the GIRK1 and GIRK4 subunits, respectively. Two sequential affinity chromatography steps isolated only GIRK1/4 hetero-tetramer channels containing both tags (Fig 5.2A). Equal bands in all lanes of an SDS-PAGE gel, corresponding to different elution fractions from a gel-filtration column, suggested that the predominant channel species purified contained two GIRK1 and two GIRK4 subunits (Fig 5.2B). This suggestion is based on the different elution times of homo-tetramer GIRK1 and GIRK4 subunits (Fig 5.1). I cannot, however, exclude with certainty the possibility that some channels with 3:1 and/or 1:3 stoichiometry were present in the population of isolated channels. Purified GIRK channels were reconstituted into liposomes and fused with planar lipid bilayer membranes. The channels were activated by fusing lipid-anchored Gβγ-containing vesicles with the membranes and adding the membrane-impermeable, short-chain PIP_2 (C8-PIP_2) to one chamber of the planar bilayer. Although channels and Gβγ insert into the bilayer membrane randomly in both orientations, only channels with their intracellular surface facing the chamber to which PIP_2 was added are activated (Wang et al., 2014). The strong inward-rectification of current as a function of membrane voltage supports the uniform orientation of active channels (Fig 5.2C). In contrast to GIRK1 homo-tetramers, GIRK4 homo-tetramers form functional channels that are activated by GPCR stimulation when expressed in HEK293T cells (Fig 5.1B). To nullify any residual uncertainty that GIRK4 may actually form functional channels in cells by combining with native GIRK1 subunits that may be present, I

purified and reconstituted GIRK4 homo-tetramers and found they produce robust inward-rectifier K^+ currents in planar lipid membranes (Fig 5.2D).

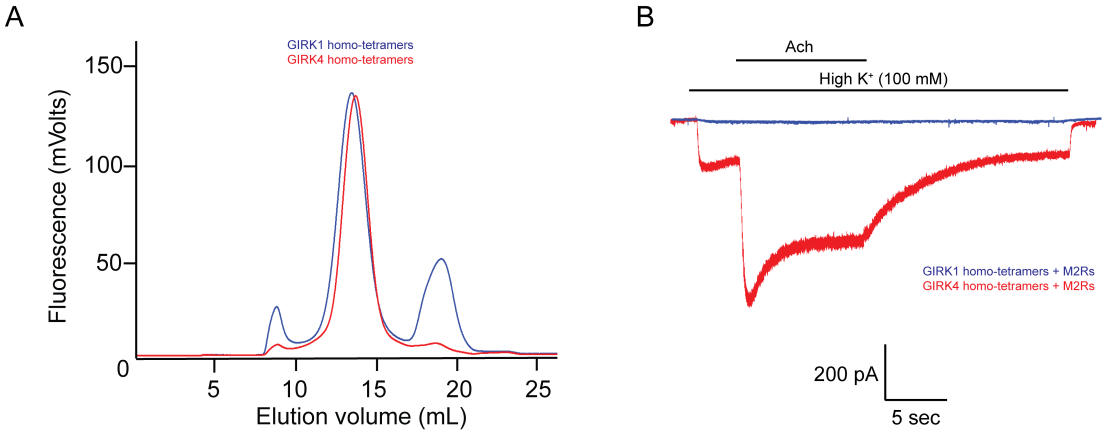

Figure 5.1. The GIRK4 subunit forms functional homo-tetrameric channels, whereas the GIRK1 subunit forms nonfunctional homo-tetramers. (A) HEK293T cells were transiently transfected with the GIRK1 or the GIRK4 subunit fused to GFP, and solubilized cell lysate was analyzed by fluorescent size-exclusion chromatography (Superose 6 10/300 GL). Blue and red elution profiles show GIRK1 homo-tetramers and GIRK4 homo-tetramers, respectively. (B) HEK293T cells were transiently transfected with GIRK1 (blue) or GIRK4 (red), and human M2Rs. Whole-cell voltage clamp recordings were performed. Membrane potential was held at -80 mV, and the extracellular solution was exchanged to high potassium buffer (100 mM KCl) as indicated above the signal, followed by the application of 10 μM acetylcholine.

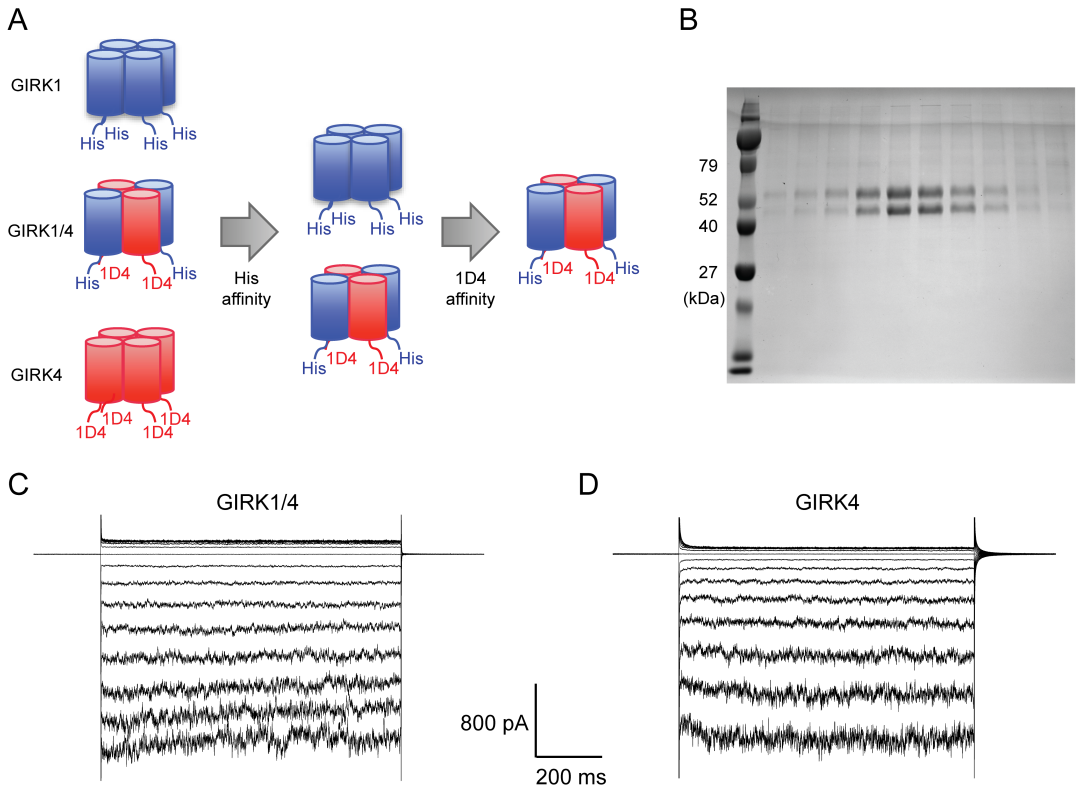

Figure 5.2. Purified cardiac GIRK channels are functional in reconstituted planar lipid bilayer membranes. (A) Schematic of GIRK1/4 hetero-tetramer purification procedure. 1D4-tagged GIRK4 homo-tetramers were removed with Co^{2+} affinity chromatography and His-tagged GIRK1 homo-tetramers were removed with subsequent 1D4 affinity chromatography. (B) Gel-filtration fractions of the GIRK1/4 hetero-tetramer peak were run on 12% SDS- PAGE. GIRK1 and GIRK4 monomers are 56 kDa and 46 kDa, respectively. (C) and (D) The top and bottom chambers are separated by the lipid bilayer formed on a transparency film. The same solution containing 10 mM potassium phosphate buffer pH 7.4 and 150 mM KCl was used in both chambers. Proteoliposomes containing GIRK channels were fused to the bilayer membrane. 32 μM C8-PIP_2 and 2 mM $MgCl_2$ were added to the intracellular side of the chamber, and proteoliposomes containing Gβγ were fused to the membrane, activating GIRK channels. (C) GIRK1/4 hetero-tetramer currents recorded in the lipid bilayer. Membrane potential was held at 0 mV, and 10 mV voltage steps from -80 mV to 80 mV were applied. (D) GIRK4 homo-tetramer currents recorded in the lipid bilayer.

5.2 QUANTITATIVE ANALYSIS OF Gβγ ACTIVATION OF CARDIAC GIRK CHANNELS

To study the dependence of GIRK channel activity on Na^+ and Gβγ concentrations, in collaboration with Dr Weiwei Wang, I developed an assay to measure GIRK activity as a function of membrane-anchored Gβγ concentration. We used lipids with Ni-NTA modified head groups (Ni-NTA-lipids) as illustrated (Fig 5.3A). In this method, bilayer membranes containing specific mole fractions of Ni-NTA-lipids were formed. GIRK channel proteoliposomes, which also contained the same mole fraction of Ni-NTA-lipids as the bilayer membrane, were then fused to the membrane. C8-PIP_2 and 2 μM soluble Gβγ (sGβγ-His_{10}), which contained a deca-histidine-tag instead of its physiological lipid anchor, were applied to the intracellular side of the membrane. At 2 μM concentration sGβγ-His_{10} does not activate GIRK channels directly from solution, however, it saturates (i.e. occupies nearly 100% of) all available Ni-NTA-lipids in the membrane (Wang et al., 2016). These membrane-bound sGβγ-His_{10} molecules are able to activate GIRK channels, which are present in the membrane at a much lower density than Ni-NTA-lipid molecules (Fig 5.3). This method permits the study of GIRK channel activation as a function of the membrane sGβγ-His_{10} density (Gβγ concentration), which is controlled through the predetermined mole fraction of Ni-NTA-lipid molecules in the membrane. In subsequent graphs, Gβγ concentration is quantified as Ni-NTA-lipid mole fraction, but for accounting purposes the stoichiometry of sGβγ-His_{10} to Ni-NTA-lipid is 1:3 (i.e. a single sGβγ-His_{10} molecule binds to 3 Ni-NTA-lipid molecules), meaning the actual sGβγ-His_{10} density on the membrane is one third the density of Ni-NTA-lipid (Wang et al., 2016). In order to compare currents from different membranes that generally contain different numbers of GIRK channels, at the end of each experiment proteolipsomes containing lipid-anchored Gβγ were fused to the

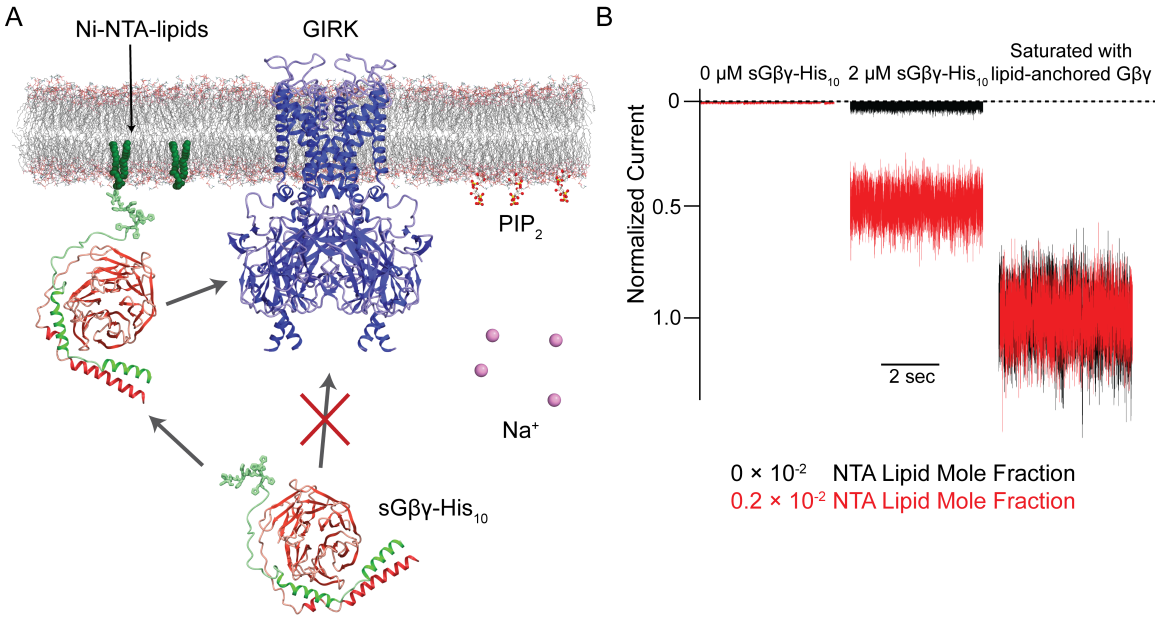

Figure 5.3. Schematic of the Na^+ and Gβγ titration using Ni-NTA-lipids. (A) GIRK channels were incorporated into the membrane containing a known concentration of Ni-NTA-lipids. 32 mM C8-PIP_2 and 2 μM sGβγ-His_{10} were added to the intracellular side of the membrane. Free sGβγ-His_{10} does not activate GIRK channels at the concentration applied, while Ni-NTA-lipids-bound sGβγ-His_{10} mimics lipid-anchored Gβγ and activates GIRK channels. Known concentrations of Na^+ were subsequently added to study the effect of Na^+ concentration on GIRK channel activity in the presence of known concentrations of Gβγ in the membrane. (B) Left and center traces show normalized GIRK4 currents before and after application of 2 μM sGβγ-His_{10} in the presence of 0 (black) or 0.002 (red) mole fraction of Ni-NTA-lipids in the membrane. At the end of each experiment, currents were fully activated by lipid-anchored Gβγ (right signals).

membrane to maximally activate the GIRK channels in the membrane (Fig 5.3B). Current activated at a specific Gβγ concentration (determined by the density of Ni-NTA-lipids) is referred to as normalized current.

Fig 5.4A shows normalized GIRK4 current as a function of Gβγ concentration at 0 mM, 8 mM, and 32 mM Na^+ (Fig 5.4A). GIRK4 current increases as a sigmoid-shaped function, and Na^+ concentration has a prominent effect on Gβγ activation. Specifically, Na^+ increases GIRK4 current at all Gβγ concentrations, but notably, the increase is relatively largest at low Gβγ concentrations where, for example, at 0.001 Ni-NTA mole fraction 32 mM Na^+ increases normalized current almost 20-fold, from 0.018 to 0.34. These data suggest that GIRK4 is similar to the neuronal GIRK channel, GIRK2, in its response to Gβγ and Na^+ (Wang et al., 2016). I therefore applied the same equilibrium gating model used to analyze GIRK2 (Wang et al., 2016). The model has 25 states of ligand occupancy, corresponding to 0 to 4 of each ligand, Gβγ and Na^+, as illustrated (Fig 5.4D). Parameters in the model include an equilibrium dissociation constant K_{db} and cooperativity factor b for Gβγ binding, an equilibrium dissociation constant K_{dn} for Na^+ binding (the cooperativity factor for Na^+ binding is 1), a factor η for the effect that Gβγ and Na^+ have on each other's affinity, and a term θ relating conductivity to ligand occupancy (Table 5.1). The model adequately represents the data with values for the parameters given (Table 5.1). The errors on values for equilibrium dissociation constants and cooperativity factors are larger than those determined for GIRK2 (Wang et al., 2016) because the data set on GIRK4 is smaller. However, the overall conclusion is that GIRK4 is very similar to GIRK2. Through model analysis the data support three conclusions: that 4 Gβγ molecules are required to open the channel (the model yields higher residuals with less than 4), that Gβγ binds cooperatively to GIRK4, and that Na^+ exerts its major effect by increasing the Gβγ affinity for the channel.

Figure 5.4. GIRK channel activity as a function of Na^+ and Gβγ concentrations. (A), (B), and (C) Plots of activity of GIRK4 homo-tetramers (A), GIRK1/4 hetero-tetramers (B), and GIRK1(N217D)/4 hetero-tetramers (C) versus Ni-NTA-lipid mole fraction in the membrane at different Na^+ concentrations. The same buffer (10 mM potassium phosphate pH 8.2, 150 mM KCl) was used in both chambers, and voltage across the lipid bilayer was held at -50 mV. GIRK proteoliposomes were fused to the bilayer membrane containing a known concentration of Ni-NTA-lipids. 2 mM $MgCl_2$ and 32 μM C8-PIP_2 were added to one side of the bilayer chamber and then 2 μM sGβγ-His_{10} was added to the same side of the chamber to activate GIRK channels. 8 mM and 32 mM Na^+ were added to further activate GIRK channels. At the end of each experiment, channels were fully activated by fusing proteoliposomes containing lipid-anchored Gβγ and currents were normalized to the fully activated current (mean ± SEM, n = 3 bilayers). The equilibrium model (D) was used to fit the data (solid curves). K_{db}: Equilibrium dissociation constant between Gβγ and ligand-free GIRK. K_{dn}: Equilibrium dissociation constant between Na^+ and ligand-free GIRK (mM). b: Cooperativity factor for Gβγ binding. η: Cross-cooperativity factor between Gβγ and Na^+ binding. i: The number of Na^+ ions bound to GIRK. For GIRK1/4 hetero-tetramers, the range of i was restricted to the range 2 to 4. j: The number of Gβγ bound to GIRK.

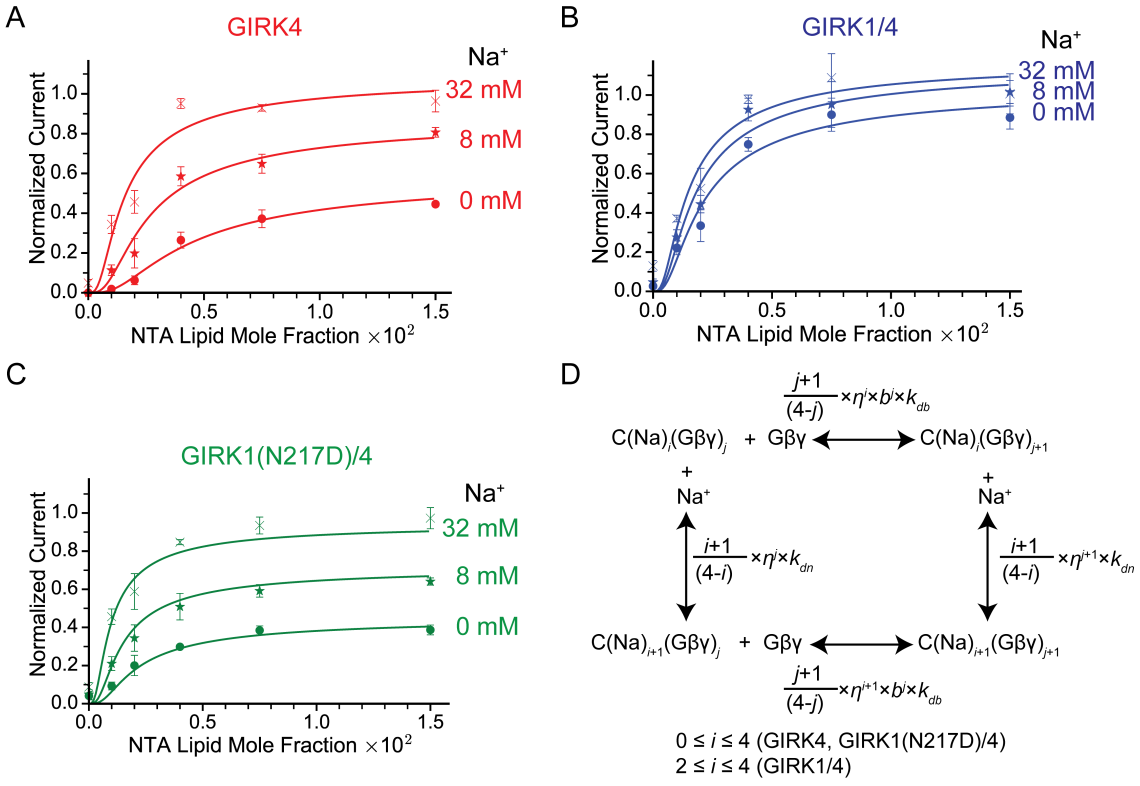
A
GIRK4
Na+
32 mM
8 mM
0 mM
Normalized Current
NTA Lipid Mole Fraction ×10^2
B
GIRK1/4
Na+
32 mM
8 mM
0 mM
Normalized Current
NTA Lipid Mole Fraction ×10^2
C
GIRK1(N217D)/4
Na+
32 mM
8 mM
0 mM
Normalized Current
NTA Lipid Mole Fraction ×10^2
D
C(Na)i(Gβγ)j + Gβγ
C(Na)i(Gβγ)j+1
+ Na+
C(Na)i+1(Gβγ)j + Gβγ
C(Na)i+1(Gβγ)j+1
0 ≤ i ≤ 4 (GIRK4, GIRK1(N217D)/4)
2 ≤ i ≤ 4 (GIRK1/4)

Table 5.1. The fitting parameters for the Na^+ and Gβγ titration. K_{db}: Equilibrium dissociation constant for Gβγ in equilibrium with ligand-free GIRK. K_{dn}: Equilibrium dissociation constant for Na^+ binding to ligand-free GIRK (mM). b: Cooperativity factor for Gβγ binding. μ: Cross-cooperativity factor between Gβγ and Na^+ binding. $\theta_{i,j}$: Normalized activity of i-Na^+ and j-Gβγ-bound GIRK. R^2: Adjusted R-squared. For fitting to GIRK1(N217D)/4 hetero-tetramers, b and $\theta_{4,4}$ were fixed to the same parameters as GIRK1/4 hetero-tetramers.

	The fitting parameters for the Na^+ and Gβγ titration		
	GIRK4	GIRK1/4	GIRK1(N217D)/4
k_{db}	0.004 ± 0.005	0.004 ± 0.006	0.0024 ± 0.0004
k_{dn}	50 ± 40	50 ± 300	50 ± 30
b	0.6 ± 0.3	0.6 ± 0.3	0.6
η	0.7 ± 0.1	0.8 ± 0.4	0.71 ± 0.08
$\theta_{0,4}$	0.6 ± 0.1	-	0.45 ± 0.04
$\theta_{1,4}$	$\theta_{0,4} + (\theta_{4,4} - \theta_{0,4}) \times 1/4$	-	$\theta_{0,4} + (\theta_{4,4} - \theta_{0,4}) \times 1/4$
$\theta_{2,4}$	$\theta_{0,4} + (\theta_{4,4} - \theta_{0,4}) \times 2/4$	1.1 ± 0.1	$\theta_{0,4} + (\theta_{4,4} - \theta_{0,4}) \times 2/4$
$\theta_{3,4}$	$\theta_{0,4} + (\theta_{4,4} - \theta_{0,4}) \times 3/4$	1.2 ± 0.8	$\theta_{0,4} + (\theta_{4,4} - \theta_{0,4}) \times 3/4$
$\theta_{4,4}$	1.2 ± 0.1	1.1 ± 0.8	1.1
R^2	0.96	0.93	0.97

5.3 THE Na^+-INSENSITIVE GIRK1 SUBUNIT POTENTIATES Gβγ ACTIVATION OF THE GIRK1/4

Figure 5.4B shows corresponding data for the GIRK1/4 channel. At all Na^+ concentrations – even in the absence of Na^+ – the response of the GIRK1/4 channel to Gβγ is similar to the GIRK4 channel at higher Na^+ concentrations. Thus, the GIRK1/4 hetero-tetramer channel, compared to the GIRK4 homo-tetramer channel, behaves to a first approximation as if it remains permanently stuck in a Na^+-activated state. That this influence of the GIRK1 subunit is related to its Na^+ binding site is supported by the mutation N217D, which converts the GIRK1 Na^+ binding locus to be more like that of GIRK4 by restoring its Na^+ sensitivity to the hetero-tetramer (Fig 5.4C) (Ho and Murrell-Lagnado, 1999b). To test the idea that Asn217 in GIRK1 mimics a Na^+-bound Asp I fit the GIRK1/4 data to the same model used for the GIRK4 channel, but imposed the condition that two of the four sites are "permanently occupied" by Na^+, with the underlying idea that the two permanently occupied sites represent the GIRK1 subunits. This condition means GIRK1/4 is described by 15 states of ligand occupancy corresponding to 0 to 4 Gβγ and 0 to 2 Na^+. The model encodes this by collapsing the 0, 1 and 2 Na^+-occupied states of the GIRK4 model into a single state with affinity of Gβγ equal to $K_{db}\ \eta^2$ (Table 5.1). This model describes the data for the GIRK1/4 channel accurately with numerical values for K_{db}, K_{dn}, b and η that are indistinguishable from those for the GIRK4 model (Table 5.1). Thus, the properties of the GIRK1/4 channel are consistent quantitatively with the GIRK1 subunits functioning as if they are GIRK4 subunits with Na^+ ions permanently bound to them.

5.4 CARDIAC GIRK CHANNELS ARE MOSTLY COMPSED OF GIRK1/4 CHANNELS

In Figure 5.5 I ask how does intracellular Na^+ affect GPCR-stimulated GIRK currents in mouse embryonic stem cell (mESC)-derived cardiac pacemaker cells. Whole-cell voltage clamp recordings show acetylcholine-activated K^+ currents that are inhibited by tertiapin-Q (TPNQ), a specific GIRK channel blocker (Fig 5.5A). Such recordings were performed with 22 different cells with intracellular solutions containing either 0 mM or 30 mM Na^+. Pacemaker cells showed an average of 32 ± 4 pA of acetylcholine-activated K^+ current in 0 mM Na^+ and 47 ± 6 pA in 30 mM Na^+ (Fig 5.5B). I thus conclude that intracellular Na^+ has essentially no influence on GPCR-stimulated GIRK current in these mESC-derived cardiac cells. This observation is consistent with the data recorded in bilayers if the cardiac cells express predominantly GIRK1/4 hetero-tetramer channels, which are only weakly Na^+ sensitive, and not GIRK4 homo-tetramer channels, which are strongly Na^+ sensitive (Fig 5.4).

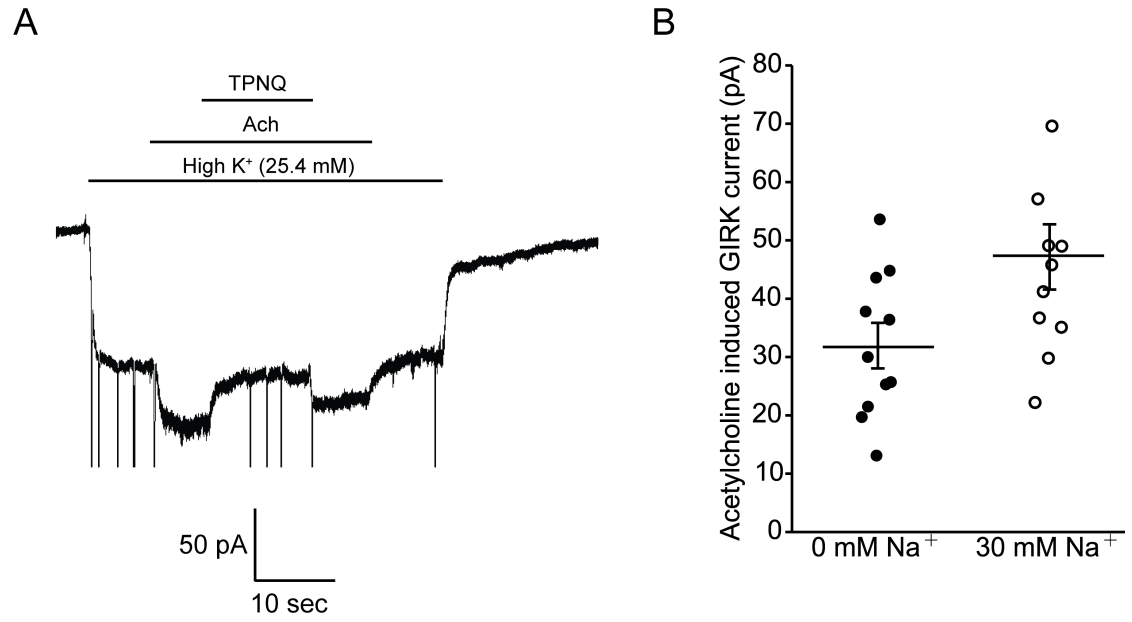

Figure 5.5. Intracellular Na^+ does not significantly activate cardiac GIRK channels. (A) Whole-cell voltage clamp recordings on mESC-derived pacemaker cells. Membrane potential was held at -80 mV and the extracellular solution was exchanged to high potassium buffer (25.4 mM KCl) as indicated above the signal. 10 μM acetylcholine (Ach) was then applied to activate GIRK channels and 100 nM tertiapin Q (TPNQ) was next applied to block cardiac GIRK currents. Acetylcholine-activated GIRK currents were measured by subtracting signals before and after acetylcholine application. (B) Acetylcholine induced GIRK currents were measured with the pipette solution containing 0 mM Na^+ or 30 mM Na^+. Eleven recordings were performed with each pipette and average value was calculated (mean ± SEM, n = 11 cells).

5.5 DISCUSSION AND CONCLUSIONS

In cardiac cells two different subunits, GIRK1 and GIRK4, form G protein gated K^+ channels. Homo-tetramers of GIRK4 and hetero-tetramers of GIRK1 and GIRK4, GIRK1/4, form functional K^+ channels, while homo-tetramers of GIRK1 do not (Krapavinsky et al, 1995; Hedin et al, 1996). It is unclear to what extent GIRK4 homo-tetramers versus GIRK1/4 hetero-tetramers dominate in cardiac cells. It is also unclear to what extent the functional properties of these channels differ because it has not been possible to study GIRK1/4 channels in isolation, the reason being heterologous expression of both subunits naturally gives rise to a mixed population of homo- and hetero-tetramers. To overcome this problem I overexpressed and purified GIRK1/4 hetero-tetramers using sequential affinity columns and also expressed and purified GIRK4 homo-tetramers for comparative analysis. The composition of GIRK1/4 hetero-tetramers is reported to consist mainly of two GIRK1 and two GIRK4 subunits (Silverman et al, 1996; Corey et al, 1998). In this study purified GIRK1/4 hetero- tetramers are also most likely composed of two GIRK1 subunits and two GIRK4 subunits, as estimated from SDS-PAGE of fractions from a gel filtration column (Figure 2B). However, I have no information on the arrangement of subunits within the tetramer either in cells or in our reconstitution experiments.

I observe that GIRK4 homo-tetramers and GIRK1/4 hetero-tetramers exhibit distinctly different properties with respect to their activation by Gβγ and Na^+. It had been shown that the GIRK1 subunit has a defective Na^+ site (Ho and Murrell-Lagnado, 1999b), but the present study establishes the following new conclusions. First, that Na^+ binding to the GIRK4 subunit increases affinity for Gβγ. This effect is encoded in the model by the Gβγ-Na^+ cross interaction term η. Second, the GIRK1 subunit behaves similarly to the GIRK4 subunit with Na^+ permanently bound. Thus, while the GIRK1 subunit is unable to bind Na^+, it causes the channel

to have high affinity for Gβγ even in the absence of Na^+. This effect is encoded in the model by enforcing permanent Na^+ occupancy on the GIRK1 subunits. Taken together, these properties account for the functional differences I observe between GIRK4 and GIRK1/4 channels. GIRK4 channels are less sensitive to G protein stimulation at low Na^+ concentrations (Gβγ binds with lower affinity) and more sensitive at high Na^+ concentrations (Gβγ binds with higher affinity). GIRK1/4 channels on the other hand are very sensitive to Gβγ stimulation at both low and high Na^+ concentrations (Gβγ binds with high affinity independent of Na^+ concentration).

I also find that GPCR-stimulated GIRK currents in mESC-derived cardiac pacemaker cells are nearly independent of intracellular Na^+ concentration. Based on a comparison of these cellular data to the properties of isolated GIRK4 and GIRK1/4 channels in planar lipid bilayers, I conclude that GIRK channels in mESC-derived cardiac channels most likely are predominantly GIRK1/4 hetero-tetramers. We report that GIRK channels in mouse dopamine neurons are very sensitive to intracellular Na^+: in experiments analogous to those in Figure 5.5B, eight fold amplification of GPCR-stimulated GIRK currents was observed (Wang et al., 2016). This degree of Na^+ sensitivity is consistent with neurons expressing GIRK2 homo-tetramers. GIRK2, like GIRK4, encodes an intact Na^+ activation site.

My findings lead us to conclude that the GIRK1 subunit in a GIRK1/4 hetero-tetramer renders the channel relatively insensitive to Na^+ but permanently in a state of high responsiveness to GPCR stimulation. I can only speculate as to why two kinds of GIRK channels exist, ones whose G protein sensitivity is regulated by intracellular Na^+ (i.e. homo-tetramer GIRK4 or GIRK2 channels) and ones whose G protein sensitivity is not much regulated by Na^+ but is always near maximum (i.e. hetero-tetramer GIRK1/4 channels). In neurons, intracellular Na^+ concentration increases during excitation because Na^+ enters the cell through Na^+ channels

during action potentials and through glutamate receptor ion channels in response to excitatory neurotransmitters (Lasser-Ross and Ross, 1992). GIRK2 channels silence neurons in response to inhibitory neurotransmitters, which act through inhibitory GPCRs. The GIRK2 regulation by Na^+ provides a way to modulate the inhibitory response according to the activity level. Such modulation would seem beneficial to a neuron that exhibits a wide range of electrical activity from near silent to high frequency spiking. Cardiac cells on the other hand appear to exhibit less activity-dependent variation in levels of intracellular Na^+ (Harrison et al, 1992). Thus, it seems reasonable that GIRK1/4 channels do not exhibit high Na^+ sensitivity, but instead exhibit a permanent state of cholinergic responsiveness (Ito et al, 1994).

CHAPTER 6: CONCLUSION AND FUTURE DIRECTIONS

In 1921, Otto Loewi discovered that a chemical substance released from the vagus nerve slows the heart beat (Loewi, 1921). Almost 70 years later, the K^+ channel responsible for the parasympathetic slowing of the heart, muscarinic potassium channel was cloned and named GIRK (Kubo et al, 1993). Subsequently it was discovered that Gβγ released from stimulated M2Rs directly binds to and activates GIRK channels (Logothetis et al, 1987; Krapivinsky et al, 1995). Since then extensive research on GIRK channels has identified that not only Gβγ, but also PIP_2 and Na^+ directly bind to and activate GIRK (Huang et al., 1998; Sui et al., 1998; Logothetis and Zhang, 1999; Ho and Murrell-Lagnado, 1999a). However the fundamental question of why GIRK is only activated by $G\alpha_i$-coupled GPCRs like M2Rs remained unanswered. One unsubstantiated hypothesis that explains signaling specificity proposes the existence of a GPCR-G protein-GIRK macromolecular supercomplex mediated by Gα and G protein heterotrimers directly binding to GIRK (Clancy et al, 2005; Rubinstein et al, 2007; Geng et al, 2009; Rubinstein et al, 2009; Berlin et al, 2010). My work challenges this hypothesis as well as providing a better understanding of ligand activation of GIRK channels and redefining the GPCR activation of GIRK channels in both cell biological and biophysical contexts.

First I tested the macromolecular supercomplex hypothesis. I found that protein co-localization is not an underlying mechanism of signaling specificity, and that Gα and G protein

heterotrimers do not directly interact with GIRK channels. I therefore concluded that GIRK channels do not form a macromolecular supercomplex with GPCRs and G proteins. Second I set out to determine the molecular basis behind signaling specificity. I discovered that with physiological amounts of G proteins, only $G\alpha_i$-coupled GPCRs release enough $G\beta\gamma$ to activate GIRK channels, however with overexpressed amounts of G proteins, $G\alpha_s$-coupled GPCRs also activate GIRK. The TRPM3 channel, which is inhibited by direct binding of $G\beta\gamma$, also showed analogous specificity between GPCRs. In addition, I found that $G\alpha_i$-coupled GPCRs catalyze the $G\beta\gamma$ release at a higher rate compared to $G\alpha_s$-coupled GPCRs. Taken together, I propose a new conceptual model of GPCR activation of GIRK, in which GIRK activity is only determined by concentrations of free $G\beta\gamma$. The rate of $G\beta\gamma$ release from $G\alpha_i$-coupled GPCRs is faster than that of $G\alpha_s$-coupled GPCRs, therefore physiologically only $G\alpha_i$-coupled GPCRs can release enough $G\beta\gamma$ to activate GIRK channels. The higher rate of $G\beta\gamma$ release may be attributed to a faster GPCR-G protein association rate in $G\alpha_i$-coupled GPCRs compared to $G\alpha_s$-coupled GPCRs (Fig 4.13).

The other part of my work has provided a more quantitative understanding of $G\beta\gamma$ activation of two cardiac GIRK channels, GIRK1/4 and GIRK4. In collaboration with Dr. Weiwei Wang, I established a method to quantitatively characterize $G\beta\gamma$ activation of GIRK channels in planar lipid bilayer membranes. Using this method, I found that the GIRK1 subunit behaves as if it is permanently bound to Na^+, thereby increasing the affinity of $G\beta\gamma$ to GIRK1/4 channels. This is the first quantitative comparison of ligand regulation of hetero-tetrameric and homo-tetrameric GIRK channels.

Four fundamental unanswered questions arise from the work presented in this thesis. First, why is the rate of $G\beta\gamma$ release faster in $G\alpha_i$-coupled GPCRs compared with $G\alpha_s$-

coupled GPCRs?. I proposed that the rate of formation of the productive GPCR-G protein complex, the rate-limiting step of G protein activation, is faster for $G\alpha_i$-coupled GPCRs compared to $G\alpha_s$-coupled GPCRs. This is consistent with a recent study where the on-rate of $G\alpha_{i1}$ to α2ARs is ~10 times faster than that of $G\alpha_s$ to β2ARs (Sungkaworn et al, 2017). When G protein trimer associates with a GPCR, both Gα and receptor undergo a series of conformational changes (Rasmussen et al, 2011). A chimera Gα subunit containing mostly $G\alpha_{i1}$ amino acids and only 13 C-terminal $G\alpha_s$ amino acids – that engage the receptor – is known to permit βAR activation of GIRK (Leaney et al, 2000). This observation suggests that the Gα conformational change, which involves the main body of the Gα subunit, is more important in determining the rate of G protein trimer-GPCR association. On the other hand, recent cryo-EM structures of $G\alpha_i$-coupled GPCRs in complex with inhibitory G protein trimers showed that $G\alpha_i$-coupled GPCRs require less conformational change to accommodate G protein trimers compared to $G\alpha_s$-coupled GPCRs, which might also be contributing to the faster association rate of $G\alpha_i$-coupled GPCRs and G proteins (Rasmussen et al, 2011, Carpenter et al, 2016; Zhang et al, 2017; Liang et al, 2017; Koehl et al, 2018; Kang et al, 2018; Draper-Joyce et al, 2018; Garcîa-Nafrîa et al, 2018). However, a systematic comparison of the on-rate of different GPCRs to G proteins will be required to address the question of whether $G\alpha_i$-coupled GPCRs associate with G proteins faster than $G\alpha_s$-coupled GPCRs do in general. The G protein on-rates to different GPCRs may be determined by two experiments. First, single-molecule tracking analysis of different GPCRs and G proteins in living cells. Second, GIRK activity, which I demonstrated is determined by the Gβγ concentration in the membrane, could be monitored to compare the rate of Gβγ release from different GPCRs if the quantity of GPCRs and G proteins can be controlled.

Second, there remains a discrepancy between our estimates of the Gβγ concentration

required to activate GIRK and the physiological concentration of Gβγ released from GPCRs (Nenasheva et al, 2013; Wang et al, 2016). It is possible that the affinity of Gβγ to GIRK in living cells is higher than our estimates in the lipid bilayer membrane. Again, the single-molecule tracking analysis of GIRK and Gβγ may be needed to address this question. It is also possible that there are hot spots in the membrane where GPCRs cluster. Due to technical limitations, I could not tell whether GPCRs cluster in my STORM analysis. However, two recent papers from Sungkaworn et al., and Yanagawa et al. demonstrated that membrane proteins could form clusters in the membrane. According to these papers, both $G\alpha_i$ and $G\alpha_s$-coupled GPCRs and G proteins form submicron clusters in the membrane, and remained confined inside the clusters. If that is the case, local Gβγ concentration could be high enough to activate GIRK. Therefore, we think that while localization of GPCRs, G proteins, and GIRK channels into a macromolecular supercomplex (i.e. corresponding to distances of 10 nm) is not the explanation for signaling specificity, crowding of these components into patches ranging from a few hundred nm to a micron is likely important, not for signaling specificity, but to reach the activation threshold for a signal. This idea could be tested if there is a way to control the membrane protein clustering in living cells. My prediction is that if we completely disrupt the clustering, GPCRs would marginally activate GIRK. In addition, my colleagues are attempting to combine the planar lipid bilayer system and a high-resolution fluorescent microscope. If we could reconstitute GPCRs, G proteins, and GIRK channels into the "bilayer-microscope" system, we may be able to correlate the protein density and GIRK activity.

Third, is GPCR-GIRK signaling specificity important in other tissues? My thesis focuses on cardiac subtypes of GPCRs and GIRK channels. However GIRK channels are also present in other tissues such as brain and testis (Lesage et al, 1994; Inanobe et al, 1999). The function of

GIRK channels in testis is unknown. In brain, GIRK1-3 are expressed and known to form various homo- and hetero-tetramers. Neuronal GIRK channels are predominantly extrasynaptic but are also found in the postsynaptic densities (Luján et al, 2009). They are mainly activated by $G\alpha_i$-coupled $GABA_B$ and dopamine D2 receptors but not by $G\alpha_s$-coupled dopamine D1 receptors (Karschin et al, 1996; Lüscher and Slesinger, 2011). In this thesis I showed that M2Rs releases $G\beta\gamma$ at a faster rate than βARs, and this higher rate likely extends to other $G\alpha_i$-coupled GPCRs and therefore likely applies to the neuronal GPCR-GIRK signaling pathway.

Fourth, what is the stoichiometry and arrangement of GIRK1/4 hetero-tetramers? The composition of GIRK1/4 hetero-tetramers is reported to consist mainly of two GIRK1 and two GIRK4 subunits (Silverman et al, 1996; Corey et al, 1998). However it is still unclear whether their arrangement is 1-1-4-4, 1-4-1-4, or a mixture of both. Several hetero-tetrameric K^+ channels such as KCNQ2/3 and Kv1.1/1.4 have been identified over the past years (Wang et al, 1998; Manganas and Trimmer, 2000), but their stoichiometry and arrangements are also unclear, and no atomic structure of hetero-tetrameric K^+ channels is available. Atomic structure determination of GIRK1/4 hetero-tetramers may answer a couple of interesting questions. First, the structure would indicate the arrangement of GIRK1 and GIRK4 subunits and provide information about molecular interactions between the two distinct subunits. Second, it may explain why GIRK1 homo-tetramers are not functional. It has been demonstrated that the homo-tetramer of human GIRK1 with a point mutation (F137S) is functional and can conduct K^+ (Vivaudou et al., 1997). This phenylalanine residue is located in the pore helix, and may push the pore helix toward the selective filter inhibiting K^+ permeation. Structural information will be required to test this hypothesis.

MATERIALS AND METHODS

METHODS FOR CHAPTER 2

Animals

C57BL/6J (Jackson Labs) male and female adult mice (≥ 10 weeks old) were used. Animals were kept in cages with a 12 : 12 h light/dark cycle and unrestricted access to food and water. All experimental procedures were carried out according to a protocol approved by the Institutional Animal Care and Use Committee (IACUC) of The Rockefeller University (Protocol #16864).

Sinoatrial node (SAN) isolation.

Adult mice (≥ 10 weeks old) were anesthetized with 90-150 mg/kg Ketamine and 7.5-16 mg/kg Xylazine IP (Sigma-Aldrich). After 5-10 min, when mice stopped responding to tail/toe pinches they were secured in the supine position by gently fixing their forepaws and hindpaws to a pinnable work surface on an animal surgery tray. SAN isolation was performed according to a published procedure (Sharpe et al, 2016). A midline skin incision was made from the mid abdomen to the diaphragm with a surgical scissor. The heart was exposed after cutting the diaphragm and holding the sternum with curved serrated forceps. The heart was lifted and dissected out of the thoracic cavity as near as possible to the dorsal thoracic wall. The isolated

heart was transferred to a petri dish containing Tyrode's solution (140 mM NaCl, 5.4 mM KCl, 1.2 mM KH_2PO_4, 1 mM $MgCl_2$, 2 mM $CaCl_2$, 5.5 mM D-glucose, 1 mg/mL BSA, 5 mM HEPES-NaOH [pH 7.4]), and quickly washed several times to remove residual blood. The heart was excised and the ventricles were removed. The atria were transferred to a silicone dissection dish and pinned through the inferior and superior vena cavae and the right and left atrial appendages. The interatrial septum was exposed by opening the anterior wall. Next, the right atrial appendage was removed and the SAN was isolated by cutting along the cristae terminals.

The isolated SAN was transferred to low-Ca^{2+}/Mg^{2+} Tyrode's solution (140 mM NaCl, 5.4 mM KCl, 1.2 mM KH_2PO_4, 0.5 mM $MgCl_2$, 0.2 mM $CaCl_2$, 5.5 mM D-glucose, 50 mM Taurine, 1 mg/mL BSA, 5 mM HEPES-NaOH [pH 7.4]) and incubated for 5 min at 37°C. Next the SAN was washed with low-Ca^{2+}/Mg^{2+} Tyrode's solution twice, transferred to low-Ca^{2+}/Mg^{2+} Tyrode's solution with enzymes (0.5 mg/mL Elastase [Worthington], 1.0 mg/mL Type II Collagenase [Worthington], and 0.5 mg/mL Protease xiv [Sigma-Aldrich]), and incubated for 15-20 min at 37°C. Digested tissue was transferred to Kraftbrühe (KB) medium (100 mM K-glutamate, 10 mM K-aspartate, 25 mM KCl, 10 mM KH_2PO_4, 2 mM $MgSO_4$, 20 mM Taurine, 5 mM Creatine, 0.5 mM EGTA, 20 mM D-glucose, 1 mg/mL BSA, 5 mM HEPES-KOH [pH 7.2]), and gently washed. The tissue was washed two more times with KB medium and cells were dissociated by constant trituration at approximately 0.5-1 Hz for 5-10 min. $CaCl_2$ solution was added stepwise (200 μM, 400 μM, 600 μM, and 1 mM) every 5 min to reach to a final concentration of 1 mM. Subsequently an equal volume of Tyrode's solution was gradually added to the KB solution with dissociated cells. Finally, dissociated cells were centrifuged for 3 min at 150 g, resuspended in Tyrode's solution, and plated onto PDL/Laminin pre-coated glass bottom dishes for ~1 h prior to electrophysiological recordings.

Whole-cell voltage clamp recordings on SAN cells.

Whole-cell voltage clamp recordings were performed with an Axopatch 200B amplifier in whole-cell mode. The analog current signal was low-pass filtered at 1 kHz (Bessel) and digitized at 20 kHz with a Digidata 1440A digitizer. Digitized data were recorded using the software pClamp. Patch electrodes (resistance 2.0-4.0 MΩ) were pulled on a Sutter P-97 puller (Sutter Instrument Company, Novato, CA) from 1.5 mm outer diameter filamented borosilicate glass. Spontaneous action potential recordings were performed using the amphotericin perforated-patch technique in current-clamp mode without current injection. For voltage-clamp recordings membrane potential was held at -80 mV throughout the experiments and the extracellular solution was exchanged with local perfusion with a 100 μm diameter perfusion pencil positioned adjacent to the cell. The bath solution contained 140 mM NaCl, 5.4 mM KCl, 1 mM $CaCl_2$, 1 mM $MgCl_2$, 10 mM D-glucose, 10 mM HEPES-NaOH (pH 7.4) (~290 mOsm). For the voltage-clamp recordings, the extracellular solution was exchanged to high K^+ solution containing 130 mM NaCl, 15.4 mM KCl, 1 mM $CaCl_2$, 1 mM $MgCl_2$, 10 mM D-glucose, 10 mM HEPES-NaOH (pH7.4) (~290 mOsm). The pipette solution contained 9 mM NaCl, 140 mM K-gluconate, 2 mM $MgCl_2$, 1.5 mM EGTA-K, 10 mM HEPES-KOH (pH7.4), 3 mM MgATP, 0.05 mM Na_2GTP, 200 μM Amphotericin-B (Sigma-Aldrich) (~310 mOsm).

Whole-cell voltage clamp recordings on HEK or CHO cells expressing GIRK channels.

Human M2R, β2AR, D2R, and mouse β1AR were cloned into a pCEH vector for mammalian expression. A serotonin 5-HT cleavable signal peptide and a SNAP tag were inserted into the N-terminus of each receptor (Sero-SNAP-GPCR). The C-terminal GFP-tagged GIRK4 (GIRK4-GFP) was cloned into a pCEH vector. Human G proteins ($G\alpha_{i1}$, $G\alpha_s$, and $G\beta_1$-IRES-$G\gamma_2$) were

also cloned into a pCEH vector. Sero-SNAP-GPCR and GIRK4-GFP were transiently transfected to HEK293T or CHO cells, and cells were incubated at 37°C for 20-24 h. Stable HEK293 cell lines expressing Sero-Halo-GPCR and GIRK4-SNAP were seeded at 0.4 million cells/mL, and expression was induced with 1 μg/mL of doxycycline. At the same time, G proteins were transiently transfected and cells were incubated at 37°C for 20-24 h. Cells were then dissociated and plated on PDL/Laminin-pre-coated glass coverslips for electrophysiological recordings. Whole-cell voltage clamp recordings were performed with the same setup, pipettes, and perfusion system as described above. The low potassium extracellular solution contained 150 mM NaCl, 5.4 mM KCl, 2 mM $CaCl_2$, 1 mM $MgCl_2$, 10 mM D-glucose, 10 mM HEPES-NaOH (pH 7.4) (~290 mOsm). The extracellular solution was exchanged to high K^+ solution containing 53 mM NaCl, 100 mM KCl, 1 mM $CaCl_2$, 1 mM $MgCl_2$, 10 mM D-glucose, 10 mM HEPES-NaOH (pH7.4) (~290 mOsm). The pipette solution contained 9 mM NaCl, 140 mM K-gluconate, 2 mM $MgCl_2$, 1.5 mM EGTA-K, 10 mM HEPES-KOH (pH7.4), 3 mM MgATP, 0.05 mM Na_2GTP (~310 mOsm).

Whole-cell voltage clamp recordings on Sf9 cell.

The human M2R, β2AR, mouse β1AR, and human GIRK4 were cloned into a pFB vector for insect cell expression. A PreScission protease cleavage site, an enhanced green fluorescent protein (eGFP) and a deca-histidine tag were placed at the C-terminus of each construct. Sf9 cells were co-infected with P3 baculovirus with GPCRs and GIRK4 and incubated at 27°C for 40-48 h. Whole-cell voltage clamp recordings were performed with the same system, pipettes, and perfusion system as described above. The low potassium extracellular solution contained 135 mM NaCl, 10 mM KCl, 4 mM $CaCl_2$, 5 mM $MgCl_2$, 10 mM MES-KOH (pH 6.4) (~320

mOsm). The high potassium extracellular solution contained 45 mM NaCl, 100 mM KCl, 4 mM $CaCl_2$, 5 mM $MgCl_2$, 10 mM HEPES-KOH (pH6.4) (~300 mOsm). The pipette solution contained 85 mM KCl, 60 mM KF, 1 mM $MgCl_2$, 5 mM EGTA-K, 10 mM HEPES-KOH (pH7.2), 3 mM MgATP, 0.05 mM Na_2GTP (~320 mOsm).

cAMP quantification assay.

HEK293T cells transfected with βARs were cultured in 12-well plates for 20-24 h. Sf9 cells infected with P3 baculovirus of βARs were cultured in 12-well plates for 40-48 h. Cells were treated with either 10 μM isoprenaline or propranolol for 10 min and washed twice with PBS + 500 μM isobutylmethylxanthine (IBMX). Cells were collected in 200 μL PBS + IBMX, exposed to four freeze-thaw cycles, and centrifuged (14,000 rpm) for 10 min at 4°C. The supernatant was analyzed for cAMP content according to the manufacturer's protocol (cAMP ELISA Detection Kit, GeneScript).

Confocal microscopy of HEK293T cells

HEK293T cells were transiently transfected with SNAP-M2R or SNAP-β2AR. After overnight incubation at 37°C, the cells were treated with 3 μM SNAP-Surface 488 (NEB) in DMEM/FBS for 30 min to stain the SNAP-tagged receptors. Cells were then washed several times with PBS, fixed with 4% paraformaldehyde, and imaged under a ZEISS inverted LSM 880 NLO laser scanning confocal microscope with an oil immersion 40× objective (numerical aperture 1.40). Microscope and software settings were kept the same for all images acquired. The fluorophore was excited with a white light laser of 488 nm.

METHODS FOR CHAPTER 3

Establishment of the stable HEK cell lines

A SNAP tag was fused to the C-terminus of the full-length GIRK4 channel. A serotonin 5-HT signal peptide and a Halo tag were fused to the N-terminus of human full-length M2R or β2AR. Both GIRK4-SNAP and Halo-M2R or Halo-β2AR were cloned into the pcDNA5/FRT/TO vector. An internal ribosome entry site (IRES) sequence was inserted between SNAP-GIRK4 and Halo-GPCR to allow for their simultaneous expression under the same promoter. Stable HEK293T cell lines were produced using the Flp-In T-REx-293 System according to the manufacturer's protocol (ThermoFisher).

Whole-cell voltage clamp recordings on HEK cells

0.4 million cells/mL of stable HEK cells were plated to tissue culture dishes. After overnight incubation, cells were treated with 0-1000 ng/mL doxycycline (Dox, Sigma-Aldrich), a tetracycline analogue, to induce expression of GIRK4-SNAP and Sero-Halo-GPCR, and were incubated at 37C° for 20-24 h. Full-length human GIRK4 was fused to the C-terminus of full-length human M2R or β2AR. A serotonin 5-HT cleavable signal peptide and a Halo tag were fused to the N-terminus of each concatemer. Additionally, a SNAP tag was fused to the C-terminus of each concatemer. Concatemers were transiently transfected and cells were incubated at 37°C for 20-24 h. Cells were then dissociated and plated on PDL/Laminin-pre-coated glass coverslips for electrophysiological recordings. Whole-cell voltage clamp recordings were performed with the same system, pipettes, perfusion system, and solutions as described above.

cAMP quantification assay

β2AR-GIRK4 stable cells were treated with 1000 ng/mL Dox for 20-24 h to induce protein expression. For GPCR-GIRK concatemers, β2AR-GIRK4 concatemers were transiently transfected to HEK293T cells, and incubated for 20-24 h. Then cAMP quantification assay was performed as described above.

Western-Blot

HEK293T cells transiently transfected with GPCR-GIRK4 concatemers were centrifuged and mixed with an equal volume of loading buffer containing 4% SDS and 10% β-mercaptoethanol. Samples were then run using standard SDS-PAGE procedures on Invitrogen NuPAGE 4-12% Bis-Tris gels and transferred onto PVDF membranes. Western Blot was performed using an anti-SNAP-tag (NEB) or anti-HaloTag (Promega).

Confocal imaging

GIRK4-GPCR stable HEK cells were treated with 0-500 ng/mL Dox for 20-24 h. Cells were then dissociated and re-plated onto PDL-coated glass bottom dishes. After 4 h, GIRK4-SNAP and Sero-Halo-GPCR were labeled using 3 μM SNAP-Surface Alexa Fluor 488 (NEB) and 3 μM HaloTag-TMR ligand (Promega) for 30 min in DMEM + 10% FBS (Thermo Fisher). Stained cells were washed with DMEM/FBS two times, incubated in DMEM/FBS for 30 min, and further washed with DMEM/FBS for three times. Subsequently cells were washed with PBS, and fixed with 4% paraformaldehyde (PFA) for 10 min at room temperature. Stained and fixed stable cells were then imaged with a ZEISS inverted LSM 880 NLO laser scanning confocal microscope with an oil immersion 100× objective (numerical aperture 1.40). Fluorophores were

excited with a white light laser positioned at 488 nm or 594 nm. Microscope and software settings were the same for all images acquired.

STORM analysis

M2R-GIRK4 or β2AR-GIRK4 stable HEK cells were treated with 6 ng/mL Dox for 20-24 h. This concentration of Dox induced modest but high enough M2R-expression to activate GIRK4 channels (Fig 3.2). GFP and $G\alpha_{i1}$ were cloned into pCEH vector, and transiently transfected to M2R-GIRK4 stable cells upon Dox induction. After incubation, cells were re-plated to PDL-coated glass bottom dishes (ibidi) and incubated for 4 h. Then Sero-Halo-GPCRs were labeled with 2 μM HaloTag-TMR (Promega) in DMEM/10% FBS for 1 h. Cells were then washed with DMEM/FBS three times, incubated in DMEM/FBS for 30 min, and further washed with PBS for two times. Subsequently cells were fixed with 4% PFA in PBS for 10 min, permeabilized with 0.1% Triton X-100 in PBS for 10 min, and blocked with PBS + 1% BSA for 30 min. Then GIRK4-SNAP was labeled with 2 μM SNAP-Surface Alexa Fluor 647 (NEB) in PBS + 1% BSA for 30 min, and washed with PBS for four times.

Subsequently STORM analysis was performed. Buffers were exchanged to the STORM buffer (50 mM Tris-HCl [pH 8.0], 10 mM NaCl, 10% D-glucose, 0.8 mg/mL glucose oxidase [Sigma-Aldrich], 40 μg/mL catalase [Roche Applied Science], and 140 mM β-mercaptoethanol [Sigma-Aldrich]). We used a Nikon TiE inverted microscope with Andor Neo sCMOS camera and an oil immersion 100× objective (Apo TIRF, numerical aperture 1.49). 561 nm and 647 nm laser lines (MLB400B, Agilent Technologies) were used to excite TMR and Alexa Fluor 647, respectively. Under constant illumination, the dyes started in the fluorescent state, switched to the dark state and spontaneously recovered to a fluorescent state multiple times before

photobleaching. For each sample, a movie of 1000 frames for TMR was recorded with the speed of 105 ms per frame, and subsequently another movie of 1000 frames for Alexa Fluor 647 was recorded. The cut-off photon counts were 300 for TMR, and 500 for Alexa Fluor 647.

Raw STORM data containing the coordinate and intensity of all blinking events was extracted and analyzed. The coordinates of GPCRs and GIRK4 channels were determined as follows. The dyes in the fluorescent state were observed in the first frame, and they were assigned as distinct dyes (Fig 3.4A, red stars in the Frame 1). In the subsequent frame, the dyes switched to the dark state, and at the same time different dyes switched to the fluorescent states from the dark state (Fig 3.4A, Frame 2). The distances between a new dye in the fluorescent state (Fig 3.4A, the red star in the Frame 2) and dyes observed in the previous frames (Fig 3.4A, green stars in the Frame 2) were calculated. If a new dye in the fluorescent state was outside 100 pixels (90 nm) from any of previously observed dyes, it was regarded as a new distinct dye (Fig 3.4A, the red star in the Frame 2). In contrast, if a new dye in the fluorescent state was within 100 pixels from a previously observed dye (Fig 3.4A, a red star in the Frame 3), they were regarded as the same dye. Then the coordinate of the dye was replaced by that of the new event in the fluorescent state (Fig 3.4A, Frame 4). Note that if a new dye in the fluorescent state was within 100 pixels from multiple previously observed dyes, the closest one was chosen. These procedures continued for 1000 frames. Schematic representation of the coordinate determination procedure is summarized in Figure 3.4A. A representative STORM image is shown in Figure 3.4B. The results of coordinate determination of β2ARs and GIRK4 channels are shown in Figure 3.4C and 3.4D, respectively. The red region in Figure 3.4C is magnified and shown in Figure 3.4E.

The degree of co-localization of GPCRs and GIRK4 channels was compared by calculating the fraction of GPCRs within 100 nm (111 pixels) from GIRK4 channels (i.e. The number of GPCRs within 100 nm from any of the identified GIRK4 divided by the total number of identified GPCRs).

Expression and purification

Human full-length GIRK1 and GIRK4 were cloned into a pEG BacMam (Goehring et al, 2014). At the C-terminus of the GIRK1 construct, PreScission protease (PPX) cleavage site, an enhanced green fluorescent protein (eGFP), and a deca-histidine tag were placed for purification. A 1D4 peptide tag was placed instead of a deca-histidine tag for the GIRK4 construct. For overexpression and protein purification, HEK293S GnTI$^-$ cells were grown in suspension, transduced with P3 BacMam virus of the GIRK1-His and the GIRK4-1D4 in 1 : 1 ratio, and incubated at 37C°. At 8-12 h post-transduction, 10 mM sodium butyrate were added to the culture, and cells were harvested 60h post-transduction. Cells were harvested by centrifugation, frozen in liquid N_2, and stored at -80C° until needed. Frozen cells were solubilized in 50 mM HEPES (pH 7.35), 150 mM KCl, 4% (w/v) n-decyl-β-D-maltopyranoside (DM), and the protease inhibitor cocktail (0.1 mg/mL pepstatin, 1 mg/mL leupeptin, 1 mg/mL aprotinin, 0.1 mg/mL soy trypsin inhibitor, 1 mM benzamidine, and 1 mM phenylmethylsulfonyl fluoride). After 2 h of solubilization, lysed cells were centrifuged, and supernatant was incubated with the Talon metal affinity resin (Clontech Laboratories, Inc. Mountain View, CA) for 1 h at 4C° with gentle mixing. The resin was washed in batch with 5 column volume (cv) of buffer A (50 mM HEPES [pH 7.0], 150 mM KCl, 0.4% [w/v] DM), then loaded onto a column and further washed with 5 cv buffer A + 10 mM imidazole. The column was then eluted with buffer A + 200 mM

imidazole. Peak fraction was collected, and incubated with the 1D4 affinity resin for 1 h at 4C° with gentle mixing. The resin was loaded onto a column and washed with buffer A. 5 mM DTT and 1 mM EDTA were added, and eGFP and affinity tags were cut with PreScission protease overnight at 4C°. The cleaved protein was then concentrated to run on Superose 6 10/300 GL gel filtration column in 20 mM Tris-HCl (pH 7.5), 150 mM KCl, 0.2% (w/v) DM, 20 mM DTT, and 1 mM EDTA.

Human lipid-anchored $G\alpha_{i3}(GDP)\beta\gamma$ was expressed in High Five (Invitrogen, Carlsbad, CA) insect cells by co-infecting baculovirus bearing $G\alpha_{i3}$, $G\beta_1$, and a deca-histidine-tagged YFP-PPX-$G\gamma_2$. After 48 h, the cells were harvested by centrifugation and stored at -80 C° until needed. Frozen pellets were added to buffer B (300 mM NaCl, 50 mM HEPES [pH 8.0] + 10 μM GDP) + protease inhibitor cocktails, and sonicated for 1 min. Lysed cells were then centrifuged at 35,000 g for 30 min to pellet the membranes. Membranes were resuspended in the same buffer using a dounce homogenizer. Na-cholate was added to a final concentration of 1%, and the solution was stirred for 1 h. The solubilized membranes were spundown again at 35,000 g for 30 min to pellet insoluble material. The supernatant was then incubated with Talon resin (Clontech) for 1 h. Talon resin was washed with 5 cv of buffer B + 1% Na-cholate, and 10 cv of buffer B + 1% Na-cholate + 20 mM imidazole. $G\alpha_{i3}$ subunits were then eluted by dissociating the heterotrimer with aluminum tetrafluoride AlF_4^- as previously described (Wang et al, 2014). Gβγ subunit was purified as previously described (Wang et al, 2014). Purified $G\alpha_{i3}$ and Gβγ were then mixed (2:1 [wt:wt] = $G\alpha_{i3}$:Gβγ) and loaded onto a Superdex 200 10/300 gel filtration column in the bilayer buffer (10 mM potassium phosphate [pH 7.4] and 150 mM KCl).

Human lipid-anchored Gβγ, and Gα(GTPγS) were purified as described before (Wang et al, 2014).

Reconstitution of proteoliposomes

All lipids were purchased from Avanti Polar Lipids (Alabaster, AL). Proteoliposomes were reconstituted as described before (Wang et al, 2014). In brief, 20 mg/mL of the lipid mixture (3:1 [wt:wt] = 1-palmitoyl-2-oleyl-sn-glycero-3-phosphoethanolamine [POPE] : 1-palmitoyl-2-oleyl-sn-glycero-3-phospho-[1'-rac-glycerol] [POPG]) was dispersed by sonication and solubilized with 20 mM DM.

Purified GIRK1/4 channels were combined with lipid mixture to make the GIRK1/4:lipid (wt:wt) ratio of 1:10. Then protein-lipid mixtures were diluted into the reconstitution buffer (10 mM potassium phosphate [pH 7.4], 150 mM KCl, 1 mM EDTA, and 3 mM DTT) to make 1 mg/mL (GIRK) and 10 mg/mL (lipid mixture). Detergent was removed by dialysis against the reconstitution buffer at 4C° for 4 days. For co-reconstitution of GIRK1/4 channels and Gβγ, purified GIRK1/4 channels, Gβγ, and lipids were mixed to make the GIRK1/4 : Gβγ : lipid (wt:wt:wt) ratio of 1 : 2 : 10 or 1 : 0.1 : 10.

Gβγ, Gα(GTPγS), and $G\alpha_{i3}$(GDP)βγ proteoliposomes were prepared as described before (Wang et al, 2014). In brief, G proteins were mixed with lipids to make G protein : lipid (wt:wt) raito of 1 : 10, and protein-lipid mixture were dialyzed against the reconstitution buffer at 4C° for 4 days.

Planar lipid bilayer recordings

Bilayer experiments were performed as described before (Wang et al, 2014). In brief, 20 mg/mL of a lipid solution in decane composed of 2:1:1 (wt:wt:wt) of 1,2-dioleoyl-sn-glycero-3-phosphoetanolamine (DOPE), 1-palmitoyl-2-oleyl-sn-glycero-3-phosphocholine (POPC), and 1-palmitoyl-2-oleoyl-sn-glycero-3-phospho-L-serine (POPS) was painted over a ~120 μm hole on

a piece of transparency film. The same buffer (10 mM potassium phosphate [pH 7.4] and 150 mM KCl) was used in both chambers. Voltage across the lipid bilayer was clamped with an Axopatch 200B amplifier (Molecular Devices, Sunnyvale, CA) in whole-cell mode. The analog current signal was low-pass filtered at 1kHz (Bessel) and digitized at 20 kHz with Digidata 1440A digitizer (Molecular Devices). Digitized data were recorded on a computer using the software pClamp (Molecular Devices).

METHODS FOR CHAPTER 4

Whole-cell voltage clamp recordings on HEK cells expressing GIRK channels.

Human $G\alpha_s$, $G\alpha_{i1}$, and $G\beta_1$-IRES-$G\gamma_2$ are cloned into a pCEH vecgtor. Stable cell lines expressing Sero-SNAP-M2R and GIRK4-Halo, or Sero-SNAP-β2AR and GIRK4-Halo was transiently transfected with G proteins, and at the same time protein expression was induced with 1000 ng/mL Dox. After 24 h incubation, cells were dissociated and plated on PDL/Laminin-pre-coated glass coverslips for electrophysiological recordings. Whole-cell voltage clamp recordings were performed with the same setup, pipettes, and perfusion system as described above. The low potassium extracellular solution contained 150 mM NaCl, 5.4 mM KCl, 2 mM $CaCl_2$, 1 mM $MgCl_2$, 10 mM D-glucose, 10 mM HEPES-NaOH (pH 7.4) (~290 mOsm). The extracellular solution was exchanged to high K^+ solution containing 53 mM NaCl, 100 mM KCl, 1 mM $CaCl_2$, 1 mM $MgCl_2$, 10 mM D-glucose, 10 mM HEPES-NaOH (pH7.4) (~290 mOsm). The pipette solution contained 9 mM NaCl, 140 mM K-gluconate, 2 mM $MgCl_2$, 1.5 mM EGTA-K, 10 mM HEPES-KOH (pH7.4), 3 mM MgATP, 0.05 mM Na_2GTP (~310 mOsm).

Whole-cell voltage clamp recordings on HEK cells expressing TRPM3 channels.

Mouse TRPM3α2 was cloned into a pEG BacMam vector. A PreScission protease cleavage site, an enhanced green fluorescent protein (eGFP), and 1D4 peptide tag were placed at the C-terminus of the TRPM3 construct. TRPM3-eGFP, Sero-SNAP-GPCR, and G proteins were transiently transfected to HEK293T cells and cells were incubated at 30°C for 48-72 h. Cells were then dissociated and plated on PDL/Laminin-pre-coated glass coverslips for electrophysiological recordings. Whole-cell voltage clamp recordings were performed as described above. The currents were recorded using a ramp protocol from -100 mV to +100 mV, applied every second, and the currents at +100 mV were plotted. TRPM3 currents were evoked by 10 μM pregnenolone sulfate (PS) (Tocris).

BRET sample preparation.

pCEH plasmids encoding Sero-SNAP-M2R, Sero-SNAP-β2AR, Sero-SNAP-β1AR, and Sero-SNAP-D2R were used in BRET experiments. For Gα-Venus constructs, Venus was inserted to either the αa-αb loop (between residues 91 and 92 for $G\alpha_{i1}$ and 113 and 114 for $G\alpha_s$) or the αb-αc loop (between residues 121 and 122 for $G\alpha_{i1}$ and 144 and 145 for $G\alpha_s$) with flanking SGGGS linkers. Human $G\alpha_{i1}$, $G\alpha_s$, $G\alpha_{i1}$(αa-αb)-Venus, $G\alpha_{i1}$(αb-αc)-Venus, $G\alpha_s$(αa-αb)-Venus, and $G\alpha_s$(αb-αc)-Venus were cloned into a pCEH vector. Venus 156-239-$G\beta_1$ and Venus 1-155-$G\gamma_2$ were cloned into a pCEH-IRES vector to allow for expression of Gβγ-Venus from a single plasmid. Nano Luciferase-$G\beta_1$ (NLuc-$G\beta_1$) and $G\gamma_2$ were cloned into a pCEH-IRES vector to allow for expression of Gβγ-NLuc from a single plasmid. masGRK3ct, masGRK3ct-NLuc, GIRK4-NLuc, and Kir2.2-NLuc were also cloned into a pCEH vector.

For the BRET measurements between Gβγ-Venus and GIRK4-NLuc, 0.35 million HEK293T cells were plated in each well of 12-well plates and incubated overnight at 37°C. After overnight incubation, cells were transfected with Sero-SNAP-GPCR (90 ng), Gβγ-Venus (90 ng), GIRK4-NLuc (90 ng) and different amounts of Gα (90 ng × 0, 1, 2, and 4) using Lipofectamine 2000 (ThermoFisher). Transfected cells were incubated for 20-24 h at 37°C and then used for BRET measurements. GIRK4-NLuc was replaced by masGRK3ct-NLuc or Kir2.2-NLuc for control samples.

For BRET measurements between Gα-Venus and Gβγ-NLuc, HEK293T cells were transfected with Sero-SNAP-GPCR (90 ng), Gβγ-NLuc (90 ng), masGRK3ct (90 ng), and Gα-Venus (90-450 ng), and incubated for 20-24 h at 30°C or 37°C. The measured light emitted by Gβγ-NLuc is proportional to the amount of Gβγ-NLuc in the sample, and the measured light emitted by Gα-Venus is proportional to the amount of G protein trimers in the sample. By having equal intensities for Gβγ-NLuc and Gα-Venus (i.e. NLuc intensity and basal BRET ratio), the rate of Gβγ release can be compared and contrasted for different GPCRs (Table S1). Therefore, samples of each GPCR were prepared with different transfected Gα-Venus-DNA amounts (90-450 ng) to carry out these experiments.

BRET measurements.

After 20-24 h incubation, transfected HEK293T cells were washed with PBS twice and detached by incubation in PBS + 5 mM EDTA for 5 min at room temperature. Cells were harvested by centrifugation at 300 g for 3 min and resuspended into 350 μL BRET buffer (PBS supplemented with 0.5 mM $MgCl_2$ and 0.1% D-glucose). 25 μL of the suspension containing ~70,000 cells was transferred to each well in a 96-well flat-bottom white microplate (Greiner CELLSTAR). The

NLuc substrate (Promega) was diluted into the BRET buffer according to the manufacturer's protocol, and 25 μL of diluted NLuc substrate were added to the cells in 96-well plates. BRET measurements were made with a microplate reader (Synergy Neo, BioTek) equipped with two emission photomultiplier tubes. The BRET signal was determined by calculating the ratio of the light emitted by Venus (535 nm with a 30 nm band width) to the light emitted by NLuc (475 nm with a 30 nm bandwidth).

Western-Blot

HEK293T cells were centrifuged and mixed with an equal volume of loading buffer containing 4% SDS and 10% β-mercaptoethanol. Samples were then run using standard SDS-PAGE procedures on Invitrogen NuPAGE 4-12% Bis-Tris gels and transferred onto PVDF membranes. Western Blot was performed using an anti-$G\alpha_{i1}$ (abcam, ab140125), anti-$G\alpha_{i2}$ (abcam, ab157204), anti-$G\alpha_{o}$ (Santa Cruz Biotechnology, sc-13532), or anti-$G\alpha_{s}$ (Santa Cruz Biotechnology, sc-383).

Expression and purification.

Human full-length GIRK4 was cloned into a pEG BacMam vector (Goehring et al, 2014). A PreScission protease cleavage site, an enhanced green fluorescent protein (eGFP) and a 1D4 peptide tag were placed for purification at the C-terminus of the GIRK4 construct. For overexpression and protein purification, HEK293S GnTI^{-} cells were grown in suspension, infected with P3 BacMam virus of the GIRK4-1D4 and incubated at 37°C. At 8-12 h post-infection, 10 mM sodium butyrate was added to the culture, and cells were harvested 60 h post-transduction. Cells were harvested by centrifugation, frozen in liquid N_2, and stored at -80°C

until needed. Frozen cells were solubilized in 50 mM HEPES (pH 7.35), 150 mM KCl, 4% (w/v) n-decyl-β-D-maltopyranoside (DM), and the protease inhibitor cocktail (0.1 mg/mL pepstatin, 1 mg/mL leupeptin, 1 mg/mL aprotinin, 0.1 mg/mL soy trypsin inhibitor, 1 mM benzamidine, and 1 mM phenylmethylsulfonyl fluoride). Aftre 2 h of solubilization, lysed cells were centrifuged at 36,000 g for 30 min and the supernatant was incubated with 1D4 affinity resin for 1 h at 4°C with gentle mixing. The resin was loaded onto a column and washed with buffer A (50 mM HEPES [pH 7.0], 150 mM KCl, 0.4% [w/v] DM). 5 mM DTT and 1 mM EDTA were added, and eGFP and affinity tags were cut with PreScission protease overnight at 4°C. The cleaved protein was then concentrated and run on a Superose 6 10/300 GL gel filtration column in 20 mM Tris-HCl (pH 7.5), 150 mM KCl, 0.2% (w/v) DM, 20 mM DTT, and 1 mM EDTA.

Human lipid-anchored Gβγ, and soluble Gβγ were purified as described previously (Wang et al, 2014).

Human full-length $G\alpha_{i1}$ $G\alpha_{i2}$, $G\alpha_{i3}$, $G\alpha_{o}$, and $G\alpha_{s}$ were cloned into a pET28a vector. A PreScission protease cleavage (PPX) site followed by a deca-histidine tag was fused to the N-terminus of Gα. The His_{10}-PPX-Gα-pET28a vector was transformed into BL21(DE3) *E. coli* cells and transformants were cultured in LB medium containing 50 μg/L of kanamycin at 37°C for 4 h. Isopropyl-thio-β-D-galactopyranoside was added to a final concentration of 0.5 mM to induce protein expression. Following an additional incubation at 25°C for 12 h, the cells were harvested by centrifugation and resuspended in buffer B (200 mM HEPES-NaOH [pH 7.5], 300 mM NaCl, 2 mM $MgCl_2$, and 10 μM MgGDP) and a protease inhibitor cocktail. Cell extracts were obtained by sonication followed by centrifugation at 36,000 g for 30 min. The supernatant was incubated with Talon metal affinity resin (Clontech) for 1 h at 4°C with gentle mixing. The resin was washed in batch with 5 column volumes of buffer B, then loaded onto a column and

further washed with 10 column volumes of buffer B + 20 mM imidazole. The column was then eluted with buffer B + 200 mM imidazole.

For Western Blotting analysis, the eluted protein was concentrated and run on a Superdex 200 10/300 GL gel filtration column in 10 mM potassium phosphate (pH 7.4), 150 mM KCl, 2 mM $MgCl_2$, and 10 μM GDP.

For the planar lipid bilayer experiment, the eluted protein was concentrated and run on a Superdex 200 10/300 GL gel filtration column in 10 mM potassium phosphate (pH 7.4), 150 mM KCl, and 2 mM $MgCl_2$. 1 mM GTP-γS was then added to ~1 mg/mL purified proteins and incubated at 37°C for 30 min to produce His_{10}-PPX-Gα(GTP-γS). Residual amounts of His_{10}-PPX-Gα(GDP) affect the results of the subsequent bilayer experiment described below. Therefore purified His_{10}-PPX-Gα(GTP-γS) was mixed with soluble Gβγ at a ratio of 4 : 1 (molar : molar) to chelate all the possibly contaminating His_{10}-PPX-Gα(GDP). This low concentration of Gβγ does not affect GIRK activity.

Reconstitution of proteoliposomes.

Reconstitution of GIRK channels and G proteins were performed as described above.

Planar lipid bilayer recordings.

Bilayer membranes were made as previously described (Wang et al, 2016). In brief, 1,2-dioleoyl-sn-glycero-3-phosphoetanolamine (DOPE) and 1-palmitoyl-2-oleyl-sn-glycero-3-phosphocholine (POPC) were mixed at a 1 : 1 ratio (wt : wt) and doped with 3% DGS-NTA (mole fraction). A lipid solution at 20 mg/mL was then prepared using decane. This solution was painted over a ~120 μm hole on a piece of transparency film to form a lipid bilayer. The same

recording buffer (10 mM potassium phosphate [pH 7.4], 150 mM KCl, and 2 mM $MgCl_2$) was used in both chambers. Voltage across the lipid bilayer was clamped using an Axopatch 200B amplifier (Molecular Devices, Sunnyvale, CA) in whole-cell mode. The analog current signal was low-pass filtered at 1 kHz (Bessel) and digitized at 20 kHz with a Digidata 1440A digitizer (Molecular Devices). Digitized data were recorded using the software pClamp (Molecular Devices).

After forming a lipid bilayer, proteoliposomes containing GIRK4 and Gβγ at a ratio of 1 : 0.1 (wt : wt) were applied to the bilayer multiple times until they fused to the bilayer. The channels were then activated by adding 32 μM C8-PIP_2 and 8 mM NaCl to the chamber. GIRK4 channels were partially activated in this condition (Figure S3A). 300 μM GTP-γS and 2 μM soluble Gβγ were added to the chamber to chelate possible contamination of His_{10}-Gα(GDP). This low concentration of added Gβγ does not affect GIRK activity. 500 μM $NiSO_4$ was added directly to the bilayer twice to charge DGS-NTA lipids with Ni^{2+}. A solution of 30 μM His_{10}-Gα(GTP-γS) supplemented with 32 μM C8-PIP_2 was then perfused directly to the bilayer membrane several times until no further blockage was observed. Given the affinity of His_{10}-Gα(GTP-γS) to the bilayer containing 3% DGS-NTA lipids is ~0.5 μM, 30 μM His_{10}-Gα(GTP-γS) was used to saturate DGS-NTA lipids in the bilayer (Figure S3B-S3D). The transient current decrease upon addition of His_{10}-Gα(GTP-γS) is due to the absence of Na^+ (Figure 5C and 5D).

Confocal microscopy of giant unilamellar vesicles (GUVs)

DOPE : POPC 1 : 1 (wt : wt) lipid mixture with 3% DGS-NTA lipids was used to produce GUVs. GUVs were prepared according to a published protocol (Martinac et al, 2010). In short, the lipid mixture was dried under a stream of argon. 2 μL of water was added to dried lipids to

hydrate the lipids. After 3 min, 1 mL of 0.4 M sucrose solution was added. The lipid solution was then moved to a water bath and incubated at 42°C for 3 h to form GUVs. To monitor the interaction between GUVs and His_{10}-Gα(GTP-γS), Alexa Fluor 488 labeled His_{10}-Gα(GTP-γS) was prepared in a buffer containing 10 mM potassium phosphate pH 7.4, 150 mM KCl, 2 mM $MgCl_2$, and 2 nM $NiSO_4$. This protein solution was then mixed with 1/50 volume of GUVs. The equator plane of GUVs was imaged using a ZEISS inverted LSM 880 NLO laser scanning confocal microscope with an oil immersion 100× objective (numerical aperture 1.40). Microscope and software settings were kept the same for all images acquired. The fluorophore was excited with a white light laser of 488 nm. The fluorescence intensity at the edge of the GUVs was measured using the Zeiss ZEN 2 software.

Kinetic simulation

Mass balance equations were derived based on the model (Figure 7A). Rate constants used in the simulation are presented and referenced in Table S2. The set of first order differential equations was solved using the NDSolve function in Mathematica (Wolfram).

METHODS FOR CHAPTER 5

Expression and Purification

GIRK1/4 channels and GIRK4 channels were purified as described above.

Proteoliposome reconstitution

All lipids were purchased from Avanti Polar Lipids (Alabaster, AL). Proteoliposomes were reconstituted as described (Wang et al., 2016). In brief, 20 mg/mL of the lipid mixture (3:1

[wt:wt] = 1-palmitoyl-2-oleyl-sn-glycero-3-phosphoethanolamine [POPE] : 1-palmitoyl-2-oleyl-sn-glycero-3-phospho-[1'-rac-glycerol] [POPG]) was dispersed by sonication and solubilized with 20 mM DM. In the Na^+ and Gβγ titration experiment, 0-0.015 (mole fraction) of 1,2-dioleoyl-sn-glycero-3-[(N-(5-amino-1-carboxypentyl)iminodiacetic acid)succinyl] (nickel salt) (DOGS-NTA) were further added to the lipid mixture.

Purified GIRK channels were combined with the lipid mixture in a GIRK : lipid (wt:wt) ratio of 1:10. Protein-lipid mixtures were then diluted into the reconstitution buffer (10 mM potassium phosphate [pH 7.4], 150 mM KCl, 1 mM EDTA, and 3 mM DTT) to 1 mg/mL (GIRK) and 10 mg/mL (lipid mixture). Detergent was removed by dialysis against the reconstitution buffer at 4C° for 4 days. Gβγ proteoliposomes were prepared as described (Wang et al., 2014).

Planar lipid bilayer recordings

Bilayer experiments were performed as described (Wang et al., 2016). In brief, 20 mg/mL of a lipid solution in decane composed of 2:1:1 (wt:wt:wt) of 1,2-dioleoyl-sn-glycero-3-phosphoetanolamine (DOPE), 1-palmitoyl-2-oleyl-sn-glycero-3-phosphocholine (POPC), and 1-palmitoyl-2-oleoyl-sn-glycero-3-phospho-L-serine (POPS) was painted over a ~120 μm hole on a piece of transparency film. For the Na^+ and Gβγ titration experiments, 0-0.015 (mole fraction) of DGS-NTA was added to a lipid solution in decane composed of 1:1(wt:wt) of DOPE and POPC, and the lipid mixture was painted over a transparency film. The same buffer (10 mM potassium phosphate pH 7.4 or pH 8.2 for the Na^+ and Gβγ titration experiment, 150 mM KCl) was used in both chambers. Recordings were performed as described above.

Whole-cell voltage clamp recordings on HEK cells

Human M2R was cloned into the pIRES-mCherry vector for mammalian cell expression. HEK293T cells were transiently transfected with GIRK1-His_{10}-pEG BacMam or GIRK4-1D4-pEG BacMam, and M2R-pIRES-mCherry were incubated at 37C° for 24-36 h. Cells were dissociated and plated on PDL-coated glass coverslips for electrophysiological recordings. Whole-cell voltage clamp recordings were performed as described above.

Differentiation of mouse embryonic stem cells

W4 (129sv) ES cell line was cultured in 2i/LIF medium (Auerbach et al, 2000; Ying et al, 2008). All ES culture reagents were purchased from Thermo Fisher Scientific (Waltham, MA) except for 2i and LIF (EMD Millipore, Billerica, MA). ESCs were differentiated into spontaneously beating cardiomyocytes with the hanging drop method (Maltsev et al, 1993). Embryoid bodies (EBs) were formed in hanging drops of ~20 μL from ~1000 cells in differentiation medium (GMEM, 10% ES-FBS, 2 mM L-glutamine, 1 mM sodium pyruvate, 1x non-essential amino acids, 0.1 mM 2-mercaptoethanol) and were cultivated in hanging drops for 5 days. Single EBs were transferred into gelatin-coated 48-well plates, and observed daily. Spontaneously contracting EBs were observed around day 8.

Preparation of single pacemaker cells

Contracting regions of day 16-18 EBs were dissected with micro knives, and collected into the solution containing (in mM): 120 NaCl, 5.4 KCl, 5 $MgSO_4$, 20 Glucose, 10 HEPES-NaOH (pH 6.9), 20 Taurine. Collected cells were digested with 50 μM $CaCl_2$ + 1 mg/mL type-II collagenase (Sigma-Aldrich, St. Louis, MO) for 30 min, and plated on 12 mm PDL-coated glass coverslips.

Electrophysiological recordings were performed 24-48 h after the dissociation. On average approximately three beating cells were identified per coverslip.

Whole-cell voltage clamp recordings on pacemaker cells

Whole-cell voltage clamp recordings were performed with the same setup, pipettes, and perfusion system as described above. After the whole-cell configuration was formed, membrane potential was held at -80 mV in low potassium extracellular solution for about 3 min to equilibrate the intracellular solution with the pipette solution. The low potassium extracellular solution contained (in mM): 140 NaCl, 5.4 KCl, 2 $CaCl_2$, 1 $MgCl_2$, 10 D-glucose, 10 HEPES-NaOH (pH 7.4) (~300 mOsm). The high potassium extracellular solution contained (in mM): 120 NaCl, 25.4 KCl, 2 $CaCl_2$, 1 $MgCl_2$, 10 D-glucose, 10 HEPES-NaOH (pH7.4) and 10 μM acetylcholine and 100 nM TPNQ were added (~300 mOsm). 0 mM Na^+ pipette solution contained (in mM): 100 K-PO_4, 30 NMDG-Cl, 10 EGTA-K, 2 $MgCl_2$, 10 HEPES-KOH (pH7.0) (~315 mOsm). 30 mM Na^+ pipette solution contained (in mM): 100 K-PO_4, 30 NaCl, 10 EGTA-K, 2 $MgCl_2$, 10 HEPES-KOH (pH7.0) (~315 mOsm). 0.25 mM Na-GTP and 3 mM Mg-ATP were supplemented to pipette solutions just before the experiments.

APPENDIX I

This Appendix contains the Python code for the STORM analysis described in Chapter 3.

```
### This function reads a csv file containing 1. The number of frame. 2,3. X and Y coordinates.
and 4. Photon counts of blinking events.###

def read_localization_file(csv_file):
    f = open(csv_file, 'r')
    csv_reader = csv.reader(f, delimiter = ',')

    data = []

    for row in csv_reader:
        row = [float(x) for x in row]
        # Remove blinking events whose photon counts are less than a cutoff value.
        if (row[3] >= cutoff and row[0] <= 1000):
            data.append(row)
        else:
            pass
    f.close()

    return data

### Select a region of interest in a STORM image ###
def refine_data(data):
    new_data = []
    for i in data:
        if (xmin < i[1] and i[1] < xmax and ymin < i[2] and i[2] < ymax):
            new_data.append(i)
        else:
            pass
    return new_data

question1 = input('ROI? y or n: ')
xmin, xmax, ymin, ymax = 0, 0, 0, 0
if question1 == 'y':
    xmin, xmax, ymin, ymax = map(float, input("Enter xmin, xmax, ymin, ymax:
").split(',')[:4])
    data = refine_data(data)
    sta.update({'Refined data size': len(data)})
    sta.update({'x,y range': [xmin, xmax, ymin, ymax]})
    print('Post-refine data size: ', len(data))
```

```
else:
    pass

### This function calculates the distance between two coordinates ###
def dist(x1, y1, x2, y2):
    f = math.sqrt((x1-x2)**2+(y1-y2)**2)
    return f

### This function identifies GPCR/GIRK molecules ###
# Identify colonies from all images #
def identify_colonies(data):
    results =[]
    for i in data:
        if i[0] == 1.0:
            results.append(i)
        else:
            dist_set = []
            for j in results:
                value = dist(i[1],i[2],j[-3],j[-2])
                dist_set.append(value)

            if min(dist_set) <= float(distance):
                results[dist_set.index(min(dist_set))].extend(i)
                print(i)
            else:
                results.append(i)
                print(i)
    # Remove colony i j = [[1.0]]
    removed = 0
    for j in results:
        if (len(j) == 4 and j[0] == 1.0):
            removed += 1
            print(j)
            results.remove(j)
        else:
            pass
    print('Removed [1.0]: ', removed)

    return results
```

APPENDIX II

This Appendix contains the Mathematica code for the simulation of GPCR activation of GIRK in Chapter 4.

```
Clear[k12]
Clear[k21]
Clear[k23]
Clear[k32]
Clear[k34]
Clear[k43]
Clear[k45]
Clear[k54]
Clear[k56]
Clear[k65]
Clear[μ]
Clear[r]
Clear[αgdpβγ]
Clear[rαgdpβγ]
Clear[αgtp]
Clear[αgdp]
Clear[βγ]
Clear[girk]
Clear[girkβγ]
Clear[girk2βγ]
Clear[girk3βγ]
Clear[girk4βγ]
k12 = 1 * 10^6; (*on-rate 0.2 um2 molecule-1 sec-1 =
 1*10^6 M-1 sec-1 according to the TIRF paper*)
k21 = 1;(*1 sec-1 according to the TIRF paper*)
k23 = 1;(*The rate of the R*-Gα(GTP)βγ dissociation. 1 sec-
 1 according to the TIRF paper*)
k32 = 0;(*uM-2 sec-1 *)
k34 = 2 * 1;(*GTP hydrolysis rate = 2 sec-1. Breitwieser and Szabo, 1988.*)
k43 = 0;(*GDP never goes back to GTP*)
k45 = 0.7 * 10^6;(*M-1 sec-1, from Sarvazyan et al, 1998, Kd = 2.9 nM, Gai1*)
k54 = 0.002 * 1;(*Calculate based on Kd and kon*)
k56 = 1 * 10^7;(*Affinity of the first binding of Gbg to GIRK =
 1.9 mM. On-rate is diffusion-limited*)
k65 = 19 000 * (0.63)^4 * 1 / 5;
(*Off-rate is calculated based on Kd and on-rate. Four Na+ are bound → 0.63^4*)
μ = 0.3;(*Cooperativity factor for each successive Gβγ binding*)
(*5 molecules um-2 = 1 uM*)
```

```
sol =
 NDSolve[
  {r'[t] == -k12 (r[t]) (αgdpβγ[t]) + k21 (rαgdpβγ[t]) + k23 (rαgdpβγ[t]) -
     k32 (r[t]) (αgtp[t]) (βγ[t]),
   αgdpβγ'[t] == -k12 (r[t]) (αgdpβγ[t]) + k21 (rαgdpβγ[t]) + k45 (αgdp[t]) (βγ[t]) -
     k54 (αgdpβγ[t]),
   rαgdpβγ'[t] == +k12 (r[t]) (αgdpβγ[t]) - k21 (rαgdpβγ[t]) - k23 (rαgdpβγ[t]) +
     k32 (r[t]) (αgtp[t]) (βγ[t]),
   αgtp'[t] == -k34 (αgtp[t]) + k43 (αgdp[t]) + k23 (rαgdpβγ[t]) - k32 (r[t]) (αgtp[t]) (βγ[t]),
   αgdp'[t] == +k34 (αgtp[t]) - k43 (αgdp[t]) + k54 (αgdpβγ[t]) - k45 (αgdp[t]) (βγ[t]),
   βγ'[t] == +k23 (rαgdpβγ[t]) - k32 (r[t]) (αgtp[t]) (βγ[t]) + k54 (αgdpβγ[t]) -
     k45 (αgdp[t]) (βγ[t]) + k65 (girkβγ[t]) - 4 * k56 (girk[t]) (βγ[t]) +
     2 * μ * k65 (girk2βγ[t]) - 3 * k56 (girkβγ[t]) (βγ[t]) + 3 * μ^2 * k65 (girk3βγ[t]) -
     2 * k56 (girk2βγ[t]) (βγ[t]) + 4 * μ^3 * k65 (girk4βγ[t]) - k56 (girk3βγ[t]) (βγ[t]),
   girk'[t] == k65 (girkβγ[t]) - 4 * k56 (girk[t]) (βγ[t]),
   girkβγ'[t] == -k65 (girkβγ[t]) + 4 * k56 (girk[t]) (βγ[t]) - 3 * k56 (girkβγ[t]) (βγ[t]) +
     2 * μ * k65 (girk2βγ[t]),
   girk2βγ'[t] == -2 * μ * k65 (girk2βγ[t]) + 3 * k56 (girkβγ[t]) (βγ[t]) -
     2 * k56 (girk2βγ[t]) (βγ[t]) + 3 * μ^2 * k65 (girk3βγ[t]),
   girk3βγ'[t] == -3 * μ^2 * k65 (girk3βγ[t]) + 2 * k56 (girk2βγ[t]) (βγ[t]) -
     k56 (girk3βγ[t]) (βγ[t]) + 4 * μ^3 * k65 (girk4βγ[t]),
   girk4βγ'[t] == -4 * μ^3 * k65 (girk4βγ[t]) + k56 (girk3βγ[t]) (βγ[t]),
   αgtp[0] == 0, βγ[0] == 0, αgdp[0] == 0, rαgdpβγ[0] == 0, girkβγ[0] == 0, girk2βγ[0] == 0,
   girk3βγ[0] == 0, girk4βγ[0] == 0, girk[0] == 1 * 10^(-6), αgdpβγ[0] == 20 * 10^(-6),
   r[0] == 10 * 10^(-6)}, {αgtp, αgdp, αgdpβγ, βγ, r, rαgdpβγ, girk, girkβγ, girk2βγ,
   girk3βγ, girk4βγ}, {t, 0, 5}, MaxStepSize → 0.001]

Plot[{αgtp[t] /. sol, βγ[t] /. sol, αgdp[t] /. sol, αgdpβγ[t] /. sol, r[t] /. sol,
  girk4βγ[t] /. sol}, {t, 0, 5}, PlotRange → {{0, 2}, {0, 20 * 10^(-6)}},
 PlotStyle → {{Black}, {Green}, {Purple}, {Orange}, {Blue}, {Dashed, Red}},
 BaseStyle → {FontSize → 14, Font → Arial}]

Plot[{girk4βγ[t] /. sol}, {t, 0, 5}, PlotRange → {{0, 3}, {0, 0.06 * 10^(-6)}},
 PlotStyle → {{Black}}, BaseStyle → {FontSize → 14, Font → Arial}]
```

REFERENCES

Albers, R.W., 1967. Biochemical aspects of active transport. *Annual review of biochemistry*, 36, pp.727-756.

Anzola, J., and Rushmer, R., 1956. Cardiac responses to sympathetic stimulation. *Circulation Research*, 4(3):302-307.

Atwood, B.K., et al., 2011. Expression of G protein-coupled receptors and related proteins in HEK293, AtT20, BV2, and N18 cell lines as revealed by microarray analysis. *BMC Genomics*, 12(1):14.

Auerbach, W., et al., 2000. Establishment and chimera analysis of 129/svev- and c57bl/6-derived mouse embryonic stem cell lines. *BioTechniques,* 29:1024–1032.

Bargmann, C.L., 1998. Neurobiology of the Caenorhabditis elegans genome. *Science*, 282(5396):2028-33.

Barry, W.H., and Bridge, J.H., 1993. Intracellular calcium homeostasis in cardiac myocytes. *Circulation*, 87:1806-1815.

Bedheka, D., et al, 2017. Inhibition of transient receptor potential melastatin 3 ion channels by G-protein βγ subunits. *eLife.* 6:e26147.

Bettahi, I., et al., 2002. Contribution of the Kir3.1 subunit to the muscarinic-gated atrial potassium channel I_{KACh}. *The Journal of Biological Chemistry.* 277:48282–48288.

Berlin, S., et al., 2010. G alpha(i) and G betagamma jointly regulate the conformations of a G betagamma effector, the neuronal G protein-activated K^+ channel (GIRK). *The Journal of Biological Chemistry.* 285(9):6179-85.

Bers, D.M., et al., 2003. Intracellular Na^+ regulation in cardiac myocytes. *Cardiovascular Research*, 57(4):897-912.

Brodde, O., and Michel, M.C., 1999. Adrenergic and muscarinic receptors in human the heart. *Pharmacological Reviews*, 41(4):651-689.

Bünemann, et al., 2003. Gi protein activation in intact cells involves subunit rearrangement rather than dissociation. *Proceedings of the National Academy of Sciences of the United States of America.* 100(26):16077–16082.

Breitwieser, G.E., and Szabo, G., 1985. Uncoupling of cardiac muscarinic and beta-adrenergic receptors from ion channels by a guanine nucleotide analogue. *Nature*, 317(6037): 538-540.

Breitwieser, G.E., and Szabo, G., 1988. Mechanism of muscarinic receptor-induced K^+ channel activation as revealed by hydrolysis-resistant GTP analogues. *The Journal of General Physiology*, 91(4):469-493.

Brown H.F., 1979. How does adrenaline accelerate the heart? *Nature*, 280(5719):235-6.

Cabrera-vera, T.M., et al., 2008. Insights into G Protein Structure, Function, and Regulation. *Endocrine Reviews*, 24(6):765-781.

Carpenter, B., et al., 2016. Structure of the adenosine A2A receptor bound to an engineered G protein. *Nature*, 536(7614):104-107.

Chan, K.W., et al., 1996. Control of channel activity through a unique amino acid residue of a G protein-gated inwardly rectifying K^+ channel subunit. *Proceedings of the National Academy of Sciences of the United States of America.* 93:14193–14198.

Clancy, S.M. et al., 2005. Pertussis-toxin-sensitive Galpha subunits selectively bind to C-terminal domain of neuronal GIRK channels: Evidence for a heterotrimeric G-protein-channel complex. *Mol Cell Neurosci*, 28, 375–389.

Corey, S., and Clapham, D.E. 1998. Identification of native atrial G-protein-regulated inwardly rectifying K^+ (GIRK4) channel homomultimers. *The Journal of Biological Chemistry.* 273:27499–27504.

Dembla, S., et al., 2017. Anti-nociceptive action of peripheral mu-opioid receptors by G-beta-gamma protein-mediated inhibition of TRPM3 channels. *eLife*, 6:e26280.

Dempsey, G.J., et al., 2011. Evaluation of fluorophores for optimal performance in localization-based super-resolution imaging. *Nature methods,* 8(12):1027-36.

DiFrancesco, D., 1993. Pacemaker mechanisms in cardiac tissue. *Annual Reviews in Physiology*, 55:455-72.

DiFrancesco, D., and Tortora, P., 1991. Direct activation of cardiac pacemaker channels by intracellular cyclic AMP. *Nature* 351, 145–147.

Digby, G. et al., 2008. Differential dissociation of G protein heterotrimers. *The Journal of Physiology*, 586(14):3325-3335.

Draper-Joyce, C.J., et al, 2018. Structure of the adenosine-bound human adenosine A1 receptor–Gi complex. *Nature*, 558(7711):559-563.

Döring, F., et al., 2002. Inwardly Rectifying K^+ (Kir) channels in *Drosophila*. *The Journal of Biological Chemistry,* 277(28): 25554-25561.

Fowler, C.E., 2007. Evidence for association of $GABA_B$ receptors with Kir3 channels and regulators of G protein signalling (RGS4) proteins. *The Journal of Physiology*, 580.1:51-65.

Garcîa-Nafrîa, J., et al., 2018. Cryo-EM structure of the serotonin 5-HT1B receptor coupled to heterotrimeric Go. *Nature*, 558(7711):620-623.

Geng, X., et al., 2009. Specificity of G-betagamma signaling depends on Galpha subunit coupling with G-protein-sensitive K^+ channels. *Pharmacology*, 84(2):82-90.

Goehring, A., et al., 2014. Screening and large-scale expression of membrane proteins in mammalian cells for structural studies. *Nature Protocols*, 9(11):2574-2585.

Gordon, R., et al., 2015. Autonomic and endocrine control of cardiovascular function. *World Journal of Cardiology*, 7(4): 204-214.

Gregorio, G.G., 2017. Single-molecule analysis of ligand efficacy in β2AR–G-protein activation. *Nature*, 547(7661):68-73.

Harrison, S.M., et al., 1992. The relationship between contraction and intracellular sodium in rat and guinea-pig ventricular myocytes. *The Journal of Physiology.* 449:517–550.

Harvey, R.D., and Belevych, A.E., 2003. Muscarinic regulation of cardiac ion channels. *British Journal of Pharmacology*, 139:1074-1084.

Harvey, R.D., and Hell, J.W., 2013. $Ca_{V1.2}$ signaling complexes in the heart. *Journal of Molecular Cell Cardiology*. 58, 143–152.

Hedin, K.E., et al., 1996. Cloning of a Xenopus laevis inwardly rectifying K^+ channel subunit that permits GIRK1 expression of I_{KACh} currents in oocytes. *Neuron.* 16:423–439

Hein, P. et al., 2006. Gs activation is time-limiting in initiating receptor-mediated signaling. *The Journal of Biological Chemistry*, 281(44), 33345-33351.

Higashijima, T., et al., 1987. The effect of GTP and Mg^{2+} on the GTPase activity and the fluorescent properties of G(o). *The Journal of Biological Chemistry*, 262(2), 757-761.

Hilger, D., et al., 2018. Structure and dynamics of GPCR signaling complexes. *Nature Structural & Molecular Biology*, 25(1):4-12.

Hillenbrand, M., et al., 2015. Comprehensive analysis of heterotrimeric G-protein complex diversity and their interactions with GPCRs in solution. *Proceedings of the National Academy of Sciences of the United States of America*. 112(11):1181-1190.

Ho, I.H., and Murrell-Lagnado, R.D. 1999a. Molecular determinants for sodium-dependent activation of G protein-gated K^+ channels. *The Journal of Biological Chemistry.* 274:8639–8648.

Ho, I.H., Murrell-Lagnado, R.D., 1999b. Molecular mechanism for sodium-dependent activation of G protein-gated K^+ channels. *The Journal of Physiology.* 520:645–651.

Hodgkin, A.L., and Huxley, A.F., 1952. A quantitative description of membrane current and its application to conduction and excitation in nerve. *The Journal of Physiology*, 117:500-544.

Huang, C.L., et al., 1998. Direct activation of inward rectifier potassium channels by PIP2 and its stabilization by Gbetagamma. *Nature*, 391:803–806.

Inanobe, A., et al., 1999. Molecular cloning and characterization of a novel splicing variant of the Kir3.2 subunit predominantly expressed in mouse testis. *The Journal of Physiology*, 521(Pt 1): 19-30.

Irisawa, H., et al., 1993. Cardiac pacemaking in the sinoatrial node. *Physiological Review,* 73: 197-227.

Ito, H., et al., 1994. Background conductance attribute to spontaneous opening of muscarinic K^+ channels in rabbit sino-atrial node cells. *The Journal of Physiology*, 476.1 pp.55-68.

Ivanina, T., et al., 2004. Gαi1 and Gαi3 differentially interact with, and regulate, the G protein-activated K^+ channel. *The Journal of Biological Chemistry*, 279, 17260–17268.

Jones, S.A. et al., 2011. Fast, three-dimensional super-resolution imaging of live cells. *Nature Methods*, 8(6):499-508.

Kang, Y., et al., 2018. Cryo-EM structure of human rhodopsin bound to an inhibitory G protein. *Nature*, 558(7711)553-558.

Karschin, C., et al., IRK(1-3) and GIRK(1-4) inwardly rectifying K^+ channel mRNAs are differentially expressed in the adult rat brain. *The Journal of Neuroscience*, 16(11):3559-3570.

Koehl, A., et al., 2018. Structure of the μ-opioid receptor–Gi protein complex. *Nature*, 558(7711):547-552.

Krapivinsky, G. et al., 1995. Gβγ binds directly to the G protein-gated K^+ channel, I(KACh). *The Journal of Biological Chemistry*, 270(3)pp.29059-29062.

Krapivinsky, G. et a., 1995. The G-protein-gated atrial K^+ channel I_{KACh} is a heteromultimer of two inwardly rectifying K^+-channel proteins. *Nature*, 374(6518):135-141.

Kubo, Y. et al., 1993. Primary structure and functional expression of a rat G-protein-coupled muscarinic potassium channel. *Nature*, 364(6440):802-6.

Lambright, D., et al., 1996. The 2.0 Å crystal structure of a heterotrimeric G protein. Nature, 379(6563):311-319.

Lasser-Ross, N., and Ross, W.N., 1992. Imaging voltage and synaptically activated sodium transients in cerebellar purkinje cells. *Proceedings. Biological Sciences / the Royal Society.* 247:35–39.

Lavine, N., et al., 2002. G Protein-coupled Receptors Form Stable Complexes with Inwardly Rectifying Potassium Channels and Adenylyl Cyclase. *The Journal of Biological Chemistry*, 277(48)pp.46010-46019.

Leaney, J. et al., 2000. The G protein alpha subunit has a key role in determining the specificity of coupling to, but not the activation of, G protein-gated inwardly rectifying K^+ channels. *The Journal of Biological Chemistry*, 275(2)pp.921-929.

Lesage, F., et al., 1994. Cloning provides evidence for a family of inward rectifier and G-protein coupled K^+ channels in the brain. *FEBS Letters*, 353:37-42.

Liang, Y.L., et al, 2017. Phase-plate cryo-EM structure of a class B GPCR–G-protein complex. *Nature*, 546(7656):118-123.

Lim, N.F., et al., 1995. A G Protein-gated K Channel Is Activated via β2-adrenergic Receptors and Gβγ Subunits in *Xenopus* Oocytes. *The Journal of General Physiology*, 105:421-439.

Loewi, O., 1921. Über humorale übertragbarkeit der Herznervenwirkung. *Pflüger's Archiv für die gesamte Physiologie des Menschen und der Tiere*, 189(1):239-242.

Logothetis, D. et al., 1987. The beta gamma subunits of GTPbinding proteins activate the muscarinic K^+ channel in heart. *Nature*, 325(6102):321-326.

Logothetis, D.E., Zhang, H., 1999. Gating of G protein-sensitive inwardly rectifying K^+ channels through phosphatidylin- ositol 4,5-bisphosphate. *The Journal of Physiology.* 520:630

Lozano, R. et al., 2012. Global and regional mortality from 235 causes of death for 20 age groups in 1990 and 2010: a systematic analysis for the Global Burden of Disease Study 2010. *Lancet*, 380: 2095-128.

Luján, R., et al., 2009. New sites of action for GIRK and SK channels. *Nature Reviews Neuroscience*, 10:475-480.

Lüscher and Slesinger, 2011. Emerging concepts for G protein-gated inwardly rectifying potassium (GIRK) channels in health and disease. *Nature Reviews Neuroscience*, 11(5): 301-315.

Maltsev, V.A., et al., 1993. Embryonic stem cells differentiate in vitro into cardiomyocytes representing sinusnodal, atrial and ventricular cell types. *Mechanisms of Development*, 44:41–50.

Manganas, L.N., and Trimmer, J.S., 2000. Subunit composition determines Kv1 potassium channel surface expression. *The Journal of Biological Chemistry*, 275, 29685-29693.

Martinac, B., et al., 2010. Studying Mechanosensitive Ion Channels Using Liposomes. *Methods in Molecular Biology*, 606:31-53.

Masuho, I., et al., 2015. Distinct profiles of functional discrimination among G proteins determine the actions of G protein-coupled receptors. *Science Signaling*, 8(405):ra123.

Morris, A.J., and Malbon, C.C., 1999. Physiological regulation of G protein-linked signaling. *Physiological Reviews*, 79(4):1373-1430.

Nenasheva, T.A., et al, 2013. Abundance, distribution, mobility and oligomeric state of M2 muscarinic acetylcholine receptors in live cardiac muscle. *Journal of Molecular and Cellular Cardiology,* 57 (2013) 129–136.

Noma, A., et al., 1979. Acetylcholine-Induced Potassium Current Fluctuations in the Rabbit Sino-Atrial Node. *Pflügers Arch*, 381:255-262.

Oldham, W.M., and Hamm, H.E., 2006. Structural basis of function in heterotrimeric G proteins. Quarterly *Reviews of Biophysics*, 39(2):117-166.

Oner, S.S., et al., 2010. Receptor-regulated Interaction of Activator of G-protein Signaling-4 and Gαi. *The Journal of Biological Chemistry.* 285:20588–20594.

Peleg, S. et al., 2002. G(alpha)(i) controls the gating of the G protein-activated K(+)channel, GIRK. *Neuron*, 33:87–99.

Pitcher, J.A., et al., 1992. Role of beta gamma subunits of G proteins in targeting the beta-adrenergic receptor kinase to membrane-bound receptors. *Science*, 257(5074):1264-1267.

Quallo, T., et al, 2017. G protein βγ subunits inhibit TRPM3 ion channels in sensory neurons. *eLife*, 6:e26138.

Rasmussen, S.G., et al., 2011. Crystal structure of the β2 adrenergic receptor–Gs protein complex. *Nature*, 477(7366):549-555

Rayner, B., and Weatherall, M., 1959. Acetylcholine and potassium movement in rabbit auricles. *The Journal of Physiology*, 146:392-409.

Riven, I., et al., 2006. GIRK Channel Activation Involves a Local Rearrangement of a Preformed G Protein Channel Complex. *Neuron*, 51:561-573.

Ross, E.M., and Wilkie, T.M., 2000. GTPASE-ACTIVATING PROTEINS FOR HETEROTRIMERIC GP ROTEINS: Regulators of G Protein Signaling (RGS) and RGS-Like Proteins. *Annual Reviews in Biochemistry*, 69:795-827.

Rubinstein, M., et al., 2007. Galphai3 primes the G protein-activated K^+ channels for activation by coexpressed G-betagamma in intact *Xenopus* oocytes. *The Journal of Physiology*, 581(1):17-32.

Rubinstein, M., et al., 2009. Divergent regulation of GIRK1 and GIRK2 subunits of the neuronal G protein gated K^+ channel by G-alpha(i)-GDP and G-betagamma. *The Journal of Physilogy*, 587(14):3473-91.

Sarvazyan et al, 1998. Determinants of $G_{i1}\alpha$ and $\beta\gamma$ binding. *The Journal of Biological Chemistry*, 273(14):7934-7940.

Sakmann, B., et al., 1983. Acetylcholine activation of single muscarinic K^+ channels in isolated pacemaker cells of the mammalian heart. *Nature*, 303(5914):250-3.

Schmitt, N., et al., 2014. Cardiac potassium channel subtypes: New roles in repolarization and arrhythmia. *Physiological Review,* 94: 609-653.

Schreibmayer, W., et al., 1996. Inhibition of an inwardly rectifying K^+ channel by G-protein α-subunits. *Nature*, 380, 624–627.

Sharpe, E.J., et al, 2016. Methods for the Isolation, Culture, and Functional Characterization of Sinoatrial Node Myocytes from Adult Mice. *J. Vis. Exp.*, (116), e54555.

Shea, L.D., et al, 1997. Calculation of Diffusion-Limited Kinetics for the Reactions in Collision Coupling and Receptor Cross-Linking. *Biophysical Journal*, 73(6):2949-2959.

Smrcka, A.V., 2008. G protein $\beta\gamma$ subunits: Central mediators of G protein-coupled receptor signaling. *Cellular and Molecular Life Sciences*, 65(14):2191-2214.

Soejima, M., and Noma, A., 1984. Mode of regulation of the ACh-sensitive K-channel by the muscarinic receptor in rabbit atrial cells. *Pfügers Archiv*, 400(4):424-431.

Sprang, S.R., et al., 2007. Structural Basis of Effector Regulation and Signal Termination in Heterotrimeric G-alpha Proteins. Advances in Protein Chemistry, 74(7):1-65.

Sprang, S.R., 2016. Activation of G Proteins by GTP and the Mechanism of Galpha-Catalyzed GTP Hydrolysis. *Biopolymers*, 105(8):449-462.

Silverman, S.K., et al., 1996. Subunit stoichiometry of a heteromultimeric G protein-coupled inward-rectifier K^+ channel. *The Journal of Biological Chemistry.* 271:30524–30528.

Simonds, W.F., 1999. G protein regulation of adenylate cyclase. *Trends in Pharmacological Sciences*, 20(2):66-73.

Sui, J.L., et al., 1998. Activation of the atrial K_{ACh} channel by the betagamma subunits of G proteins or intracellular Na^+ ions depends on the presence of phosphatidylinositol phosphates. *Proceedings of the National Academy of Sciences of USA*. 95:1307–1312.

Sungkaworn, T. et al., 2017. Single-molecule imaging reveals receptor-G protein interactions at cell surface hotspots. *Nature*, 550(7677):543-547.

Syrovatkina, V., et al., 2017. Regulation, Signaling and Physiological Functions of G-proteins. *The Journal of Molecular Biology*, 428(19):3850-3868.

Taussig, R., et al., 1993. Inhibition of adenylyl cyclase by Gi alpha. *Science*, 261(5118)218-221.

Touhara, K., et al., 1994. Binding of G protein βγ-subunits to pleckstrin homology domains. *The Journal of Biological Chemistry*, 269(14):10217-10220.

Touhara, K.K. et al., 2016. The GIRK1 subunit potentiates G protein activation of cardiac GIRK1/4 hetero-tetramers. *eLife*, 5:e15750.

Vivadou, M., et al., 1997. Probing the G-protein Regulation of GIRK1 and GIRK4, the Two Subunits of the K_{ACh} Channel, Using Functional Homomeric Mutants. *The Journal of Biological Chemistry*, 272(50): 31553-31560.

Wall, W., et al., 1995. The structure of the G protein heterotrimer $G\alpha_iG\beta_1\gamma_2$. *Cell*, 83(6):1047-1058.

Wang, H., et al., 1998. KCNQ2 and KCNQ3 potassium channel subunits: molecular correlates of the M-channel. *Science*, 282(5395): 1890-1893.

Wang, W., et al., 2014. Quantitative analysis of mammalian GIRK2 channel regulation by G proteins, PIP_2 and Na^+ in a reconstituted system. *eLife*, e03671

Wang, W., et al., 2016. Cooperative regulation by G proteins and Na^+ of neuronal GIRK2 K^+ channels. *eLife* 5. doi: 10.7554/eLife.15751.

Wedegaertner, P.B., 1995. Lipid modifications of trimeric G proteins. *The Journal of Biological Chemistry*, 270, 503-506.

Wellner-Kienitz, M., et al., 2001. Overexpression of β1 and β2 Adrenergic Receptors in Rat Atrial Myocytes. *The Journal of Biological Chemistry*, 276(40):37347-37354.

Whorton, M.R. and MacKinnon, R., 2011. Crystal structure of the mammalian GIRK2 K^+ channel and gating regulation by G proteins, PIP_2, and sodium. *Cell*, 147(1):199-208.

Whorton, M.R. and MacKinnon, R., 2013. X-ray structure of the mammalian GIRK2–βγ G-protein complex. *Nature*, 498(7453):190-7.

Wickman, K. et al., 1994. Recombinant G-protein beta gamma-subunits activate the muscarinic-gated atrial potassium channel. *Nature*, 368(6468):255-257.

Yao, X.J., et al., 2008. The effect of ligand efficacy on the formation and stability of a GPCR-G protein complex. *Proceedings of the National Academy of Sciences of the United States of America*. 106(23):9501-9506.

Yanagawa, M., et al., 2017. Single-molecule diffusion-based estimation of GPCR activity. *bioRxiv*, doi.org/10.1101/205161.

Ying, Q.L., et al., 2008. The ground state of embryonic stem cell self-renewal. *Nature*, 453:519–523.

Zhang, Y., et al., 2017. Cryo-EM structure of the activated GLP-1 receptor in complex with a G protein. *Nature*, 546(7657):248-253.